Static fluctuations of a thick 1D interface in the 1+1 Directed Polymer formulation

Elisabeth Agoritsas,[1, *] Vivien Lecomte,[1, 2] and Thierry Giamarchi[1]

[1]*DPMC-MaNEP, University of Geneva, 24 Quai Ernest-Ansermet, 1211 Geneva 4, Switzerland*
[2]*Laboratoire Probabilités et Modèles Aléatoires (CNRS UMR 7599),*
Universités Paris VI et Paris VII, Site Chevaleret,
175 rue du Chevaleret, 75013 Paris, France

(Dated: September 5, 2012)

Experimental realizations of a 1D interface always exhibit a finite microscopic width $\xi > 0$; its existence is erased by thermal fluctuations at sufficiently high temperatures, but turns out to be a crucial ingredient for the description of the interface fluctuations below a characteristic temperature $T_c(\xi)$. Exploiting the exact mapping between the static 1D interface and a 1+1 Directed Polymer (DP) growing in a continuous space, we have studied analytically and numerically both the geometrical and the free-energy fluctuations of a DP at finite temperature T, with a short-range elasticity and submitted to a quenched random-bond Gaussian disorder of *finite* correlation length ξ.

Centering our study on the two-point correlator of the derivative of the disorder free-energy $\bar{R}(t, y)$ as a function of growing 'time' t, we explore several analytical arguments at finite ξ and propose a 'toymodel' in order to characterize the temperature-dependence of the DP endpoint fluctuations. Approximating the full correlator at small endpoint position y by $\bar{R}(t, y) \approx \widetilde{D}_t \cdot \mathcal{R}(y)$, we show on one hand that the amplitude $\widetilde{D}_\infty(T, \xi)$ correctly describes the low- and high-temperature regimes along with the full crossover around $T_c(\xi)$. On the other hand, we discuss the close connection between the temperature-dependent function $\mathcal{R}(y)$ at asymptotically large 'times' and the quenched disorder correlator.

Finally we discuss the consequences of the low-temperature regime for two experimental realizations of KPZ interfaces, namely the static and quasistatic behavior of magnetic domain walls and the high-velocity steady-state dynamics of interfaces in liquid crystals.

CONTENTS

I. INTRODUCTION

Effective one-dimensional (1D) interfaces can be spotted in various experimental contexts, encompassing domain walls (DWs) in ferromagnetic[1–3] or ferroic[4–6] thin films, fractures in brittle materials[7] or paper[8], contact line in wetting experiments[9,10]. The generic framework of the *disordered elastic systems* (DES)[11] has been proven to provide a quite successful modelling for such systems, describing them as point-like elastic strings living in a two-dimensional disordered energy landscape. The competition between the elasticity – the tendency to minimize their distortions – and the disorder – the inhomogeneities of the underlying medium –, blurred by thermal fluctuations at finite temperature, accounts for the resulting metastability and the consequent glassy properties observed in such systems. Moreover the value of the roughness exponent ζ, which characterizes the scaling properties of a self-affine manifold, is fully determined for a given DES once the dimensionality, the type of elasticity and of disorder are chosen, thus promoting the value of ζ to a reliable signature of the disorder universality class to whom a given system might belong.

The specific case of a 1D interface with a short-range elasticity and a random-bond (RB) quenched Gaussian disorder can actually be mapped on other statistical-physics models in the Kardar-Parisi-Zhang (KPZ) universality class[12–14], including in particular the so-called '1+1 Directed Polymer' (DP) which has stimulated an increased activity lately, among both statistical

physicists[15–17] and mathematicians[18,19]. A large variety of results emphasizes the deep connection which exists between the descriptions of a wide range of systems up to random matrices[20,21], such as the Burgers equation in hydrodynamics[22], roughening phenomena and stochastic growth[23], last-passage percolation[24], dynamics of cold atoms[25], and vicious walkers[15,26,27]. A shared feature between those related models is the well-known KPZ exponent $\zeta_{\text{KPZ}} = 2/3$, which characterizes the exact scaling at *asymptotically* large lengthscales or 'times' assuming an *uncorrelated* disorder[20,28–30].

Although of interest regarding the whole KPZ class problems, there are two additional issues which turn out to be relevant for the study of experimental interfaces: on one hand, the characterization of the scaling properties *at finite lengthscales*, with possibly different regimes and crossover lengthscales regarding both the roughness exponent and the amplitude of the geometrical fluctuations; on the other hand, the consequences of the interplay *at finite temperature* between thermal fluctuations and disorder. However, in order to have then a complete realistic description, an additional physical ingredient must be included in the DES model: an experimental realization of interface always exhibits a finite microscopic width $\xi > 0$, which translates equivalently for a point-like interface into a finite disorder correlation length. Above a characteristic temperature $T_c(\xi) > 0$, thermal fluctuations simply erase the existence of such a microscopic width, whereas at sufficiently low temperature it becomes relevant even for the macroscopic properties of the interface. Those two temperature regimes can be hinted by simple scaling arguments[11], which are reflected in the two opposite Functional-Renormalization-Group (FRG) regimes of high-temperature[31] versus zero-temperature fixed-point[32,33]. Their connection has already been addressed analytically in a single computation in a Gaussian-Variational-Method (GVM) approximation[11,34]. Actually its predictions for the low-temperature regime turned out to be potentially accessible and thus physically relevant for ferromagnetic DWs in ultra-thin films[1–3], which are believed to be the experimental realization of precisely the 1D DES considered here.

In this paper, using the exact mapping between the static 1D interface and a 1+1 DP growing in a continuous 2D space, we revisit several analytical arguments initially for an uncorrelated disorder (*i.e.* $\xi = 0$) in order to adapt and possibly generalize them to a correlated disorder (*i.e.* $\xi > 0$). In addition, we address the two issues of finite lengthscales and finite temperature numerically, by measuring both their geometrical and their free-energy fluctuations as a function of lengthscale or DP growing 'time', at finite temperature and in a spatially-correlated random potential. The first motivation is to obtain a numerical confirmation of the GVM predictions for the roughness of a static 1D interface[11,34], at least qualitatively (if not quantitatively, because of arbitrary numerical correcting factors): we actually successfully observe the crossover to the low-temperature regime. The

second motivation, more general, is to test the validity and the coherence of the DP 'rounded' toymodel on the fluctuations of the underlying free-energy, as considered in Refs. 11 and 34, in order to correct some of the GVM artifacts, and to refine its assumptions so it would contain the essential features for the statics and hopefully be useful in order to understand the quasistatic dynamics of 1D interfaces[35-38].

An important preliminary remark concerning our numerical approach is that it is performed directly in the continuous limit of the 1+1 DP, and it uses an exact property of the model – the Statistical Tilt Symmetry (STS) – to focus on the effects of the disorder, dissociated from the pure thermal ones which hide them at small lengthscales.

The plan of the paper is as follows. In Sec. II we define the full model of the static 1D interface in the 1+1 DP formulation, along with the quantities of interest for the characterization of its geometrical and free-energy fluctuations at a given lengthscale r of the 1D interface or 'time' t of the DP. Then in Sec. III we recall the exact properties of the model at asymptotically large 'times' or in its 'linearized' version – obtained by neglecting the KPZ non-linearity –, and use them to justify the construction of a DP 'toymodel'. Extensive scaling arguments are given in order to tackle the opposite low- *versus* high-temperature regimes and their connection, and the underlying scaling assumptions are actually made explicit using saddle-point arguments. In Sec. IV we perform an extensive numerical study of the free-energy and geometrical fluctuations of the full-model, whose results are interpreted from the point of view of our DP toymodel. After a synthetical discussion which yields an effective analytical prediction in Sec. V, we discuss in Sec. VI our results with respect to two experimental systems, namely the domain walls in ultrathin magnetic films and interfaces in liquid crystals and we conclude in Sec. VII.

II. 1+1 DIRECTED-POLYMER FORMULATION OF THE STATIC 1D INTERFACE

A. DES model of a 1D interface

We consider a 1D interface, living in an infinite and continuous 2D space of respectively internal and transverse coordinates $(z, x) \in \mathbb{R}^2$. Restricting the model to the case where the interface has no bubbles nor overhangs, each possible configuration is described by a uni-valued displacement field $u(z) \in \mathbb{R}$ with respect to a flat configuration defined by the z-axis (cf. Fig. 1 left).

In the elastic limit of small distortions and for a short-range elasticity, the energetic cost of elastic distortions are given by the elastic Hamiltonian $\mathcal{H}_{\text{el}}[u] = \frac{c}{2} \int_{\mathbb{R}} dz \, [\nabla_z u(z)]^2$ with c the elastic constant.

Assuming that we have a quenched disorder, accounting typically for a weak collective pinning of the interface by many impurities, the microscopic disorder is described by a random potential $V(z, x)$ with the corresponding energy $\mathcal{H}_{\text{dis}}[u, V] = \int_{\mathbb{R}} dz \, V(z, u(z))$. The disorder average $\overline{\mathcal{O}}$ of an observable at fixed disorder $\mathcal{O}_V$ is then defined with respect to the probability distribution of the disorder configurations $\bar{\mathcal{P}}[V]$, which is assumed to be Gaussian, *i.e.* fully defined by its mean and its two-point disorder correlator:

$$
\begin{aligned}
\overline{V(z, x)} &= 0 \\
\overline{V(z, x) V(z', x')} &= D \cdot \delta(z - z') \cdot R_\xi(x - x')
\end{aligned}
\tag{1}
$$

with D the strength of disorder, which quantifies the typical amplitude of the random potential. The disorder should be statistically translational-invariant in space, and it is actually assumed to be uncorrelated along its internal direction z and correlated on a typical length $\xi > 0$ along its transverse direction x. Finally, we consider the specific case of a random-bond (RB) disorder, *i.e.* with a symmetric function $R_\xi(x)$ decreasing sufficiently fast to encode a short-range disorder and with the chosen normalization $\int_{\mathbb{R}} dx \, R_\xi(x) \equiv 1$.

At equilibrium and for a given disorder configuration, the statistical average over thermal fluctuations $\langle \mathcal{O} \rangle_V$ is then defined with respect to the normalized Boltzmann weight $\mathcal{P}_V[u] \propto e^{-\mathcal{H}[u,V]/T}$ of Hamiltonian $\mathcal{H}[u, V] = \mathcal{H}_{\text{el}}[u] + \mathcal{H}_{\text{dis}}[u, V]$ (the Boltzmann constant is fixed once and for all at $k_B = 1$ so that the temperature has the dimensions of an energy). For a self-averaging disorder, a given observable must be averaged analytically first over thermal fluctuations and secondly over disorder $\overline{\langle \mathcal{O} \rangle}$, recovering in particular a translational invariance in space.

The choice of those different assumptions is explained in detail in Ref. 11. In order to compute the GVM roughness of such a static 1D interface, $R_\xi(x)$ was chosen in Ref. 34 to be a normalized Gaussian function of variance $2\xi^2$, encoding thus the typical width ξ as the single feature of this correlator function (cf. Appendix A).

B. Mapping of the 1D interface on the 1+1 Directed Polymer

The characterization of the geometrical fluctuations of the *static* 1D interface goes through the determination of the probability distribution function (PDF) of the relative displacements $\mathcal{P}(\Delta u(r))$ at a given lengthscale r, with $\Delta u_z(r) \equiv u(z + r) - u(z)$. The contribution of the combined PDF of thermal fluctuations $\mathcal{P}_V[u]$ and of disorder $\bar{\mathcal{P}}[V]$ can be disconnected by focusing directly on the fluctuations of segments of length r on the interface. As defined in Fig. 1, such a segment can be mapped on the trajectory of a directed polymer starting from $(0, 0)$ and growing in 'time' t in the 2D disordered energy landscape described by the random potential $V(t, y)$. The fluctuations of the DP end-point $y(t)$ at a 'time' t, of PDF $\mathcal{P}(t, y)$, encode thus precisely the translational-invariant $\mathcal{P}(\Delta u(r))$ at the lengthscale r.
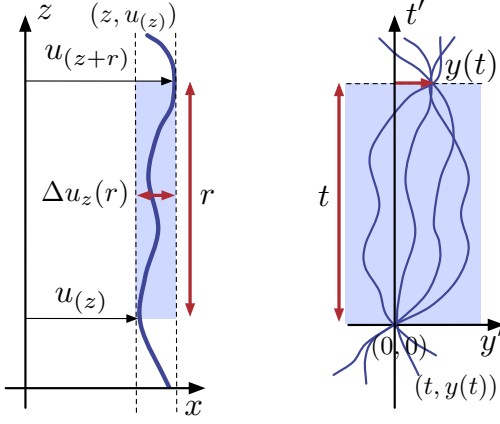
FIG. 1. *Left:* 1D interface configuration of displacement field $u(z)$ with respect to the z-axis; definition of its relative displacement $\Delta u_z(r)$ at a lengthscale r with respect to the internal coordinate z. *Right:* Focus on all the segments of the 1D interface starting from $(0,0)$ and ending at $(t, y(t))$; definition of the DP's end-point position $y(t)$ after a growing 'time' t. The translation table between those two representations is given by $(z, x) \leftrightarrow (t', y')$ for the coordinates, $u(z) \leftrightarrow y(t')$ for the trajectory, $\mathcal{P}(\Delta u(r)) \leftrightarrow \mathcal{P}(t, y)$ for the geometrical PDF and $B(r) = \overline{\langle \Delta u(r)^2 \rangle} \leftrightarrow \overline{\langle y(t)^2 \rangle} = B(t)$ for the roughness function.

The energy of a segment of lengthscale $r \leftrightarrow t_1$, of trajectory $y(t)$ connecting $(0,0)$ to (t_1, y_1), is given by the partial Hamiltonian:

$$\mathcal{H}[y, V; t_1] = \int_0^{t_1} dt \left[\frac{c}{2} (\partial_t y(t))^2 + V(t, y(t)) \right] \quad (2)$$

with the disorder distribution defined by (1). Integrating over the thermal fluctuations at fixed disorder V, the *unnormalized* Boltzmann weight of a DP ending at (t_1, y_1) is then given by

$$W_V(t_1, y_1) = \int_{y(0)=0}^{y(t_1)=y_1} \mathcal{D}y(t) \, e^{-\mathcal{H}[y, V; t_1]/T} \quad (3)$$

with the underlying four DES parameters $\{c, D, T, \xi\}$. The connection between this continuous formulation of the DP, well-known among physicists, and its discretized version on a lattice with the solid-on-solid constrain has recently been properly established[39].

We restrict our study to the case where the polymer is attached in $y = 0$ at initial 'time'. This choice corresponds to the so-called 'sharp-wedge' initial conditions[17] of the KPZ equation as opposed *e.g.* to the 'flat' ones where the initial position would be integrated upon.

C. Geometrical and free-energy fluctuations

We start with the definition of the relevant quantities for the characterization of the geometrical and free-

energy fluctuations, whose numerical study will be presented later on in Sec. IV.

With the following normalization at fixed 'time' t:

$$\bar{W}_V(t) \equiv \int_{-\infty}^{\infty} dy \cdot W_V(t, y) \quad (4)$$

we can define the PDF of the DP end-point, respectively at fixed disorder V and after the disorder average:

$$\mathcal{P}_V(t, y) \equiv \frac{W_V(t, y)}{\bar{W}_V(t)} \, , \; \mathcal{P}(t, y) = \overline{\mathcal{P}_V(t, y)} \quad (5)$$

and use them for the computation of averages for any observable $\mathcal{O}$ which depends on the sole DP end-point position $y(t)$ (and not on its whole trajectory $y(t')$, with $t' \in [0, t]$):

$$\langle \mathcal{O}[y(t)] \rangle_V = \int_{-\infty}^{\infty} dy \cdot \mathcal{O}[y(t)] \cdot \mathcal{P}_V(t, y) \quad (6)$$

$$\overline{\langle \mathcal{O}[y(t)] \rangle} = \int_{-\infty}^{\infty} dy \cdot \mathcal{O}[y(t)] \cdot \mathcal{P}(t, y) \quad (7)$$

and in particular the different moments of the PDF (5):

$$\langle y(t)^k \rangle_V = \int_{-\infty}^{\infty} dy \cdot y(t)^k \cdot \mathcal{P}_V(t, y) \quad (8)$$

$$\overline{\langle y(t)^k \rangle} = \int_{-\infty}^{\infty} dy \cdot y(t)^k \cdot \mathcal{P}(t, y) \quad (9)$$

Actually the PDF $\mathcal{P}(t, y)$ is known to be fairly Gaussian (though the study of its small non-Gaussian deviations encodes relevant physics[23,40–43]), in the sense that

$$\mathcal{P}(t, y) \approx \frac{e^{-y^2/(2B(t))}}{\sqrt{2\pi B(t)}} \quad (10)$$

with its main feature being summarized in its second moment, namely the *roughness function* $B(t)$ and its corresponding roughness exponent $\zeta(t)$:

$$B(t) \equiv \overline{\langle y(t)^2 \rangle} \, , \; \zeta(t) \equiv \frac{1}{2} \frac{\partial \log B(t)}{\partial \log t} \quad (11)$$

a proper exponent ζ being defined only if a powerlaw can be identified on a certain range in t; this is typically the case at large lengthscales, the beginning of this asymptotic regime defining the so-called 'Larkin length'[44] L_c. In absence of disorder, the DP is a Brownian random walk whose PDF $\mathcal{P}_{\text{th}}(t, y)$ is then exactly a Gaussian function of thermal roughness $B_{\text{th}}(t) = \frac{Tt}{c}$. In presence of a short-range RB disorder, there is a crossover from this thermal roughness at small lengthscales to an asymptotic roughness $B_{\text{RM}}(t) \sim t^{4/3}$ in the 'random-manifold' (RM) regime of large lengthscales. A 1D interface is thus a self-affine manifold in these two lengthscales regimes, its geometrical fluctuations being characterized by the scaling $y(t)^2 \sim A(c, D, T, \xi) \, t^{2\zeta}$ with the *diffusive* exponent $\zeta_{\text{th}} = \frac{1}{2}$ at sufficiently small lengthscales (extended

at all lengthscales in absence of disorder), and the *superdiffusive* exponent $\zeta_{\mathrm{RM}} = \frac{2}{3}$ at asymptotically large lengthscales (obtained in Ref. 20, 28–30 assuming $\xi = 0$). Actually the existence of a finite width $\xi > 0$ strongly modifies the scaling of the prefactor $A(c, D, T, \xi)$ and the roughness crossover, with in particular a whole intermediate 'Larkin-modified' lengthscale regime for temperatures below $T_c(\xi) = (\xi c D)^{1/3}$ (cf. Ref. 11 and 34 or Appendix A).

The PDF $\mathcal{P}(t, y)$ and its roughness $B(t)$ are precisely the quantities accessible experimentally via an analysis of a 'snapshot' of an interface configuration (defined as in Fig. 1); however only a single roughness regime has been observed up to now in ferromagnetic DWs, which are believed to be the prototype of our idealized 1D interface (e.g. $\zeta = 0.69 \pm 0.07$ in Ref. 1). From an analytical point of view, additional information can be extracted from the fluctuations of the probability $\mathcal{P}_V(t, y)$ itself, or alternatively from its corresponding pseudo free-energy $F_V(t, y)$ defined at fixed disorder by:

$$\frac{W_V(t, y)}{\overline{W}_{V \equiv 0}(t)} \equiv \exp\left[-\frac{1}{T} F_V(t, y)\right] \tag{12}$$

$$F_V(t, y) = F_{V \equiv 0}(t, y) + \bar{F}_V(t, y) \tag{13}$$

with the following conventions:

$$F_{V \equiv 0}(t, y) = F_{\mathrm{th}}(t, y) + T \log \overline{W}_{V \equiv 0}(t) \tag{14}$$

$$\frac{F_{\mathrm{th}}(t, y)}{T} = \frac{1}{2} \frac{y^2}{B_{\mathrm{th}}(t)} \Leftrightarrow F_{\mathrm{th}}(t, y) = \frac{cy^2}{2t} \tag{15}$$

$$\overline{W}_{V \equiv 0}(t) = \sqrt{2\pi B_{\mathrm{th}}(t)} = \sqrt{2\pi \frac{Tt}{c}} \tag{16}$$

The decomposition of (13) defines the disorder free-energy $\bar{F}_V(t, y)$, which fully encodes the integrated disorder encountered by the DP up to a 'time' t. This contribution can be dissociated from the pure thermal free-energy $F_{\mathrm{th}}(t, y)$ because of the statistical tilt symmetry (STS) of the model, whose different incarnations are discussed in Appendix B. Indeed, with the particular form of the short-range elasticity $\frac{c}{2}(\partial_t y(t))^2$ in (2) and y being a continuous variable, the effective disorder $\bar{F}_V(t, y)$ inherits the statistical translation-invariance of the microscopic disorder $\bar{\mathcal{P}}[V(t, y)]$ defined by (1). Its PDF at fixed 'time' (and similarly any functional of $\bar{F}_V(t, y)$) thus satisfies:

$$\bar{\mathcal{P}}\left[\bar{F}_V(t, y + Y)\right] = \bar{\mathcal{P}}\left[\bar{F}_V(t, y)\right] \tag{17}$$

In order to single out the y-dependent additive contribution of $\bar{F}_V(t, y)$, we also define the random phase $\eta_V(t, y)$ in a kind of 'random-field' formulation of the disorder free-energy:

$$\eta_V(t, y) \equiv \partial_y \bar{F}_V(t, y)$$
$$\bar{F}_V(t, y) = \frac{1}{2}\left(\int_{-\infty}^{y} - \int_{y}^{\infty}\right) dy' \, \eta_V(t, y') + \mathrm{cte}_V(t) \tag{18}$$

where $\mathrm{cte}_V(t)$ is a y-independent constant. Note that the STS implies that $\bar{\mathcal{P}}[\eta_V(t, y + Y)] = \bar{\mathcal{P}}[\eta_V(t, y)]$. We

may assume that the scaling of the distribution $\bar{\mathcal{P}}[\bar{F}, t]$ and $\bar{\mathcal{P}}[\eta, t]$ is in large part controlled by their two-point disorder correlators, on which we focus our interest:

$$\bar{C}(t, |y_1 - y_2|) \equiv \overline{\left[\bar{F}_V(t, y_1) - \bar{F}_V(t, y_2)\right]^2} \tag{19}$$

$$\bar{R}(t, |y_1 - y_2|) \equiv \overline{\eta_V(t, y_1)\eta_V(t, y_2)} \tag{20}$$

which reflect explicitly the translation invariance, and are related by

$$\bar{C}(t, y) = \int_0^y dy_1 \int_0^y dy_2 \cdot \bar{R}(t, |y_1 - y_2|) \tag{21}$$

or alternatively by $\partial_y^2 \bar{C}(t, y) = 2\bar{R}(t, y)$ using their parity.

The connection between the fluctuating disorder free-energy $\bar{F}_V(t, y)$ and the PDF $\mathcal{P}(t, y)$ with its moments $\overline{\langle y(t)^k \rangle}$ can formally be defined as:

$$\overline{\langle y(t)^k \rangle} = \int \mathcal{D}V \, \bar{\mathcal{P}}[V] \frac{\int dy \, y^k \, e^{-F_V(t, y)/T}}{\int dy \, e^{-F_V(t, y)/T}}$$
$$= \int \mathcal{D}\bar{F} \, \bar{\mathcal{P}}[\bar{F}, t] \frac{\int dy \, y^k \, e^{-(F_{\mathrm{th}}(t, y) + \bar{F}_V(t, y))/T}}{\int dy \, e^{-(F_{\mathrm{th}}(t, y) + \bar{F}_V(t, y))/T}} \tag{22}$$

where only the y-dependent part of the pseudo free-energy, *i.e.* the information encoded in the random phase $\eta_V(t, y)$ actually matters. However, even the roughness $B(t)$ cannot be computed straightforwardly through the disorder average, this would require *e.g.* the introduction of replicæ in a GVM framework[34,45,46] (cf. Appendix A).

D. Feynman-Kac evolution equations

Since we work with a one-dimensional object (the 1D interface, likewise the DP), explicit evolution equations can be written down for $W_V(t, y)$, $F_V(t, y)$, $\bar{F}_V(t, y)$ and $\eta_V(t, y)$[29]. We can thus follow the evolution with continuous 'time' or lengthscale t of the effective PDF-related quantities at fixed disorder, and also of the mean values $\overline{\bar{F}_V(t, y)}$ and $\overline{\eta_V(t, y)}$.

However, no such closed equation for the correlators $\bar{C}(t, y)$ and $\bar{R}(t, y)$, the normalized PDF $\mathcal{P}(t, y)$), nor the roughness $B(t)$ of course, are available. This limitation in the lengthscale renormalization of the disorder-average quantities is conceptually similar to the fact that the FRG flow equations[32,33,47,48] of the disorder correlator $R_\xi(x)$ (1) are truncated in a perturbative expansion in $\epsilon = 4 - d$ (with the dimension $d = 1$ for the 1D interface), an exact analytical description at all lengthscales remaining thus unsolved.

At fixed microscopic disorder, in a continuous-time limit and at finite temperature, the so-called 'Feynman-Kac' formula[49–51] for $W_V(t, y)$, is a continuum stochastic heat equation with multiplicative noise[29,39,52,53]:

$$\partial_t \left[\frac{W_V(t, y)}{\overline{W}_{V \equiv 0}(t)}\right] = \left[\frac{T}{2c}\partial_y^2 - \frac{1}{T}V(t, y)\right]\left[\frac{W_V(t, y)}{\overline{W}_{V \equiv 0}(t)}\right] \tag{23}$$

where the normalization $\bar{W}_{V\equiv 0}(t)$ is usually hidden in the functional integration $\int \mathcal{D}y(t)$ of (3). In order to clarify the normalization issues that arise due to the disorder, this last equation is rederived in Appendix C both in continuous and discretized 'time'. In absence of disorder, we recover the standard heat equation:

$$\partial_t \mathcal{P}_{V\equiv 0}(t,y) = \frac{T}{2c}\partial_y^2 \mathcal{P}_{V\equiv 0}(t,y) \tag{24}$$

whose solution at fixed 'time' is the thermal PDF $\mathcal{P}_{V\equiv 0}(t,y) = \mathcal{P}_{\mathrm{th}}(t,y)$, i.e. a Gaussian function of zero mean and variance $B_{\mathrm{th}}(t) = \frac{Tt}{c}$.

Moving in on the pseudo free-energy $F_V(t,y)$ defined by (12) yields a KPZ equation with an additive noise[12,14]:

$$\partial_t F_V(t,y) = \frac{T}{2c}\partial_y^2 F_V(t,y) - \frac{1}{2c}\left[\partial_y F_V(t,y)\right]^2 + V(t,y) \tag{25}$$

So the free-energy landscape seen by the DP end-point is a KPZ growing surface, whose disorder correlation length ξ lies along the *internal* direction of the surface, whereas ξ has been initially defined as a microscopic disorder correlation along the *transverse* direction of the 1D interface or growing DP.

As for the disorder free-energy $\bar{F}_V(t,y)$ (13), it evolves with a tilted KPZ equation:

$$\partial_t \bar{F}_V(t,y) = \frac{T}{2c}\partial_y^2 \bar{F}_V(t,y) - \frac{1}{2c}\left[\partial_y \bar{F}_V(t,y)\right]^2 \\ - \frac{y}{t}\partial_y \bar{F}_V(t,y) + V(t,y) \tag{26}$$

with the new additive term stemming from $-\frac{1}{c}\left[\partial_y F_{\mathrm{th}}(t,y)\right]\left[\partial_y \bar{F}_V(t,y)\right] = -\frac{y}{t}\eta_V(t,y)$. Applying ∂_y it yields finally the evolution equation of the random phase $\eta_V(t,y)$ (18) itself:

$$\partial_t \eta_V(t,y) = \frac{T}{2c}\partial_y^2 \eta_V(t,y) - \frac{1}{2c}\partial_y\left[\eta_V(t,y)\right]^2 \\ - \partial_y\left[\frac{y}{t}\eta_V(t,y)\right] + \partial_y V(t,y) \tag{27}$$

The disorder free-energy and its random phase encode all the information concerning the effects of disorder, so both $\bar{F}_{V\equiv 0}(t,y)$ and $\eta_{V\equiv 0}(t,y)$ are zero. In presence of disorder those quantities are moreover completely hidden at small 'times' by thermal fluctuations:

$$F_V(t,y) \overset{t\to 0}{\approx} F_{V\equiv 0}(t,y) \Rightarrow \bar{F}_V(t,y) \approx 0,\ \eta_V(t,y) \approx 0 \tag{28}$$

whereas they completely dominate the large-lengthscales behavior $(F_V(t,y) \approx \bar{F}_V(t,y) + \mathrm{cte}(t))$, the evolution equation (25) and (26) thus sharing the same statistical steady-state at asymptotically large 'times'. Those disorder-induced quantities can be properly defined at all 'times' (cf. Fig. 2), yielding in particular the following initial conditions:

$$\mathcal{P}_V(t=0,y) = \delta(y) \tag{29}$$
$$\bar{F}_V(t=0,y) \equiv 0 \tag{30}$$
$$\eta_V(t=0,y) \equiv 0 \tag{31}$$
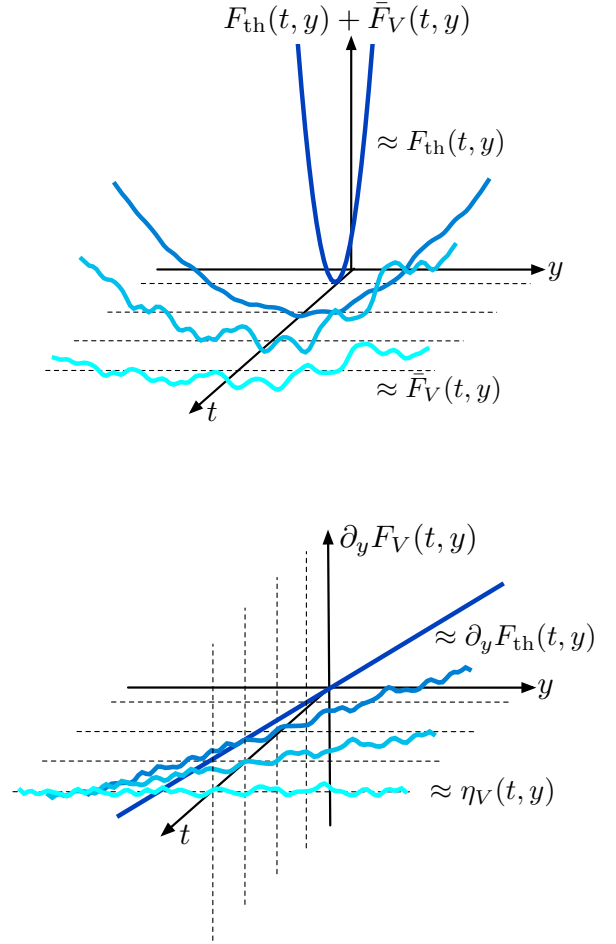
FIG. 2. (Color online) Free-energy landscape seen by the DP end-point as a function of 'time' or lengthscale t. *Top*: Graph of $F_{\mathrm{th}}(t,y) + \bar{F}_V(t,y)$ (imposing $\overline{\bar{F}_V(t,y)} \equiv 0$ for simplification): the thermal parabola $F_{\mathrm{th}}(t,y) = \frac{cy^2}{2t}$ flattens and unveils the disorder fluctuations $\bar{F}_V(t,y)$, which sketches a KPZ surface in its steady state at asymptotically large 'times'. *Bottom*: Alternative point of view with the graph of $\partial_y F_V(t,y) = \frac{cy}{t} + \eta_V(t,y)$, where the random phase is progressively revealed with increasing lengthscale.

Considering at last the evolution of the mean values $\overline{\bar{F}_V(t,y)}$ and $\overline{\eta_V(t,y)}$, at first the translation invariance by STS (17) trivially implies that $\overline{\bar{F}_V(t,y)} = \mathrm{cte}(t)$ (and $\overline{\langle y(t)\rangle} = 0$). Exchanging the disorder average and the partial derivatives $\partial_{y,t}$, on the definition (18) and on (26) respectively, we obtain:

$$\overline{\eta_V(t,y)} = \partial_y \overline{\bar{F}_V(t,y)} = 0 \tag{32}$$
$$\partial_t \overline{\bar{F}_V(t,y)} = -\frac{1}{2c}\overline{[\eta_V(t,y)]^2} = -\frac{1}{2c}\cdot \bar{R}(t, y=0) \tag{33}$$

whereas (27) simply yields the consistency check $\partial_y \bar{R}(t, y=0) = 0$. So the evolution of the mean disorder free-energy is directly given by the sole two-point correlator of $\eta_V(t,y)$ in $y=0$ at a given 'time' t.

As we will discuss at length in the next section, the behavior of $\bar{R}(t,y)$ at small $|y|$ corresponds to the curvature of the disorder free-energy correlator $\bar{C}(t,y)$ around $y=0$ which fully determines the amplitude of the geometrical fluctuations characterized by the roughness prefactor $A(c,D,T,\xi)$. $\bar{R}(t,y)$ has essentially a symmetrical peak centered at $y=0$, whose maximum is well-defined for a finite correlation length ξ but diverges in the limit $\xi \to 0$ (corresponding equivalently to the high-temperature regime). The connection between this regularization at $\xi > 0$ and the evolution of the peak main features, *i.e.* its typical width $\tilde{\xi}_t$ and amplitude $\tilde{D}_t$, will be the two ingredients of the DP toymodel constructed in the next section and tested numerically in Sec. IV.

E. 'Time'-evolution equations for the two-point correlators $\bar{R}(t,y)$ and $\bar{C}(t,y)$

There are no closed equations for $\partial_t \bar{R}(t,y)$ and $\partial_t \bar{C}(t,y)$, but the combination of the Feynman-Kac equations (26)-(27) with the Itō's formula yields nevertheless, as presented in details in Appendix D:

$$\partial_t \bar{R}(t,y) = \frac{T}{c}\partial_y^2 \bar{R}(t,y) - \frac{1}{t}\left\{\bar{R}(t,y) + \partial_y\left[y\bar{R}(t,y)\right]\right\} - \frac{1}{c}\partial_y \bar{R}_3(t,y) - DR_\xi''(y) \tag{34}$$

$$\partial_t \bar{C}(t,y) = \frac{T}{c}\left[\bar{C}''(t,y) - \bar{C}''(t,0)\right] - \frac{y}{t}\bar{C}'(t,y) - \frac{1}{c}\bar{C}_3(t,y) - 2D\left[R_\xi(y) - R_\xi(0)\right] \tag{35}$$

which would be closed but for the presence of the three-point correlators:

$$\bar{R}_3(t,y) \equiv \overline{\eta(t,y)^2 \eta(t,0)} \tag{36}$$

$$\bar{C}_3(t,y) \equiv -2\overline{\left[\bar{F}(t,y) - \bar{F}(t,0)\right]\left[\bar{F}'(t,0)\right]^2} \tag{37}$$

Neglecting the non-linear KPZ term in the evolution equation (26) for $\bar{F}_V(t,y)$ is equivalent to neglecting those three-point contributions. The solution for the corresponding *linearized* correlator $\bar{R}^{\text{lin}}(t,y)$ is given in Appendix E for a generic disorder correlator $R_\xi(y)$. It will be used in the two next sections regarding both analytical arguments and numerical results, in order to discuss on one hand the expected qualitative behavior of the correlator $\bar{R}(t,y)$, and to precise on the other hand the role of the KPZ nonlinearity in the short- *versus* large-'times' and the low- *versus* high-T regimes.

III. EXACT PROPERTIES AND CONSTRUCTION OF A DP TOY-MODEL

In this section we first recall the analytical results for the asymptotically large 'times' DP fluctuations, exact

for an *uncorrelated* disorder ($\xi = 0$), and examine their possible generalization for a *correlated* disorder ($\xi > 0$). Armed with those considerations, we then define our DP toymodel by assuming that the asymptotic scaling in distribution of the disorder free-energy $\bar{F}(t,y)$ is modified only at small displacements $|y| \lesssim \xi$ where $\xi > 0$[34] and remains a valid approximation even at small lengthscales. Using scaling arguments, we explicit the relations between the DP toy-model effective parameters and the 1D interface parameters $\{c,D,T,\xi\}$ in the two limits of low- versus high-temperature, and extrapolate a continuous crossover between those two regimes via the temperature dependence of the GVM Larkin length[34]. We conclude this construction by sketching two saddle-point arguments for the roughness, which use either the large lengthscale t or the zero-temperature limit of $\frac{1}{T}$ as a control parameter in order to accredit our asymptotic assumptions for a short-range correlated disorder ($\xi > 0$).

A. Free-energy fluctuations at asymptotically large 'times'

At infinite 'time' and in an uncorrelated disorder ($\xi = 0$), the distributions $\bar{\mathcal{P}}\left[\bar{F}\right]$ and $\bar{\mathcal{P}}\left[\eta\right]$ are Gaussian and their two-points correlators are exactly known

$$\bar{C}_{\xi=0}(\infty,y) = \tilde{D}_\infty \cdot |y|, \ \bar{R}_{\xi=0}(\infty,y) = \tilde{D}_\infty \cdot \delta(y) \tag{38}$$

with $\tilde{D}_\infty = cD/T$. The Dirac δ-function of $\bar{R}$ encodes the infinite-'time' amnesia of the DP with respect to the remoteness of its initial condition $t=0$, and the absolute value of $\bar{C}$ encodes the scale invariance of this steady state characterized by $\bar{F}(y) \sim y^{1/2}$ in distribution. This steady-state solution of the KPZ equations (25)-(26) for a δ-correlated $V(t,y)$ actually yields the prediction $\zeta_{\text{KPZ}} = 2/3$ for the asymptotic roughness exponent[29] (as discussed later in Sec. III D).

As shown in Appendix F 2, Gaussian distributions with those correlators are steady-state solutions of the Fokker-Planck (FP) equation for $\partial_t \bar{\mathcal{P}}\left[\bar{F},t\right]$ and $\partial_t \bar{\mathcal{P}}\left[\eta,t\right]$ at $\xi = 0$ only *at strictly infinite 'time'*, imposing $\tilde{D}_\infty = cD/T$ and the boundary conditions $\eta_V(t,y)|_{y=\pm\infty} = 0$. The correlator of the random phase (20) then coincides with the transverse correlator of the microscopic disorder (1), up to the overall amplitude $\tilde{D}_\infty$. Note that the KPZ nonlinear term $-\frac{1}{2c}\left[\partial_y \bar{F}_V(t,y)\right]^2$ in (26) plays no role in the determination of this asymptotic amplitude, since its contribution disappears completely with the chosen boundary conditions.

Actually at $\xi = 0$ the distribution of our total free-energy $F_V(t,y)$ itself, given by the KPZ equation with 'narrow-wedge' initial condition, is exactly known at all 'times' in terms of a Fredholm determinant with an Airy kernel[18,54–57]; it is non-Gaussian and at asymptotically large 'times' it tends to the GUE Tracy-Widom distribution[18,58], which eventually yields a Gaussian

function at infinite 'time'. Its second cumulant corresponds to our correlator $\bar{C}(t,y)$ (for $\bar{F}_V(t,y)$) and is exactly known asymptotically as the correlator of an Airy process[59]. It schematically adds saturation 'wings' to the absolute value (38) of $\bar{C}_{\xi=0}(t,y)$, which appear at $y^2 \sim \overline{\langle y(t)^2 \rangle}$, i.e. where the transverse displacement is defined by the roughness $B(t)$ at this lengthscale t (see Ref. 46).

In a correlated disorder (1) with $\xi > 0$, the distributions $\bar{\mathcal{P}}[\bar{F},t]$ and $\bar{\mathcal{P}}[\eta,t]$ are a priori not Gaussian but we can still focus on the two-point correlator $\bar{R}(t,y)$ properties. We know in particular that its integral must be zero at all finite 'times'[46], with the possible exception of strictly infinite 'time'; this actually requires the existence of saturation 'wings' of the asymptotic $\bar{C}_{\xi=0}(t,y)$, which are pushed to $y \to \pm\infty$ at $t \to \infty$.

Inspired by the Fokker-Planck scheme at $\xi = 0$ case, if we assume nevertheless a Gaussian $\bar{\mathcal{P}}_{\mathrm{G}}[\bar{F},t]$ of correlator $\bar{R}(t,y)$, we show in Appendix F3 that at infinite 'time' the correlator

$$\bar{R}^{\mathrm{lin}}(\infty,y) = \widetilde{D}_\infty \cdot R_\xi(y), \quad \widetilde{D}_\infty = \frac{cD}{T} \quad (39)$$

defines a steady-state solution for the linearized FP equation where the KPZ non-linear term $-\frac{1}{2c}\left[\partial_y \bar{F}_V(t,y)\right]^2$ has been neglected, imposing again $\widetilde{D}_\infty = cD/T$ and the boundary condition $\eta_V(t,y)|_{y=\pm\infty} = 0$. Note that $\bar{\mathcal{P}}_{\mathrm{lin}}[\bar{F},t]$ must consistently be Gaussian. Actually the full solution of this linearized correlator at finite 'time' is derived in Appendix E for a generic RB disorder correlator $R_\xi(y)$, yielding the following decomposition:

$$\left(\frac{cD}{T}\right)^{-1} \bar{R}^{\mathrm{lin}}(t,y) = R_\xi(y) - b^{\mathrm{lin}}(t,y) \quad (40)$$

with

$$\begin{aligned}
&b^{\mathrm{lin}}(t,y)\sqrt{B_{\mathrm{th}}(t)} \\
&= -\frac{y}{\sqrt{B_{\mathrm{th}}(t)}} R^{(-1)}_{\xi/\sqrt{B_{\mathrm{th}}(t)}}\left(y/\sqrt{B_{\mathrm{th}}(t)}\right) \\
&\quad + \int_0^\infty dw\, w^2 e^{-w\left[w+y/\sqrt{B_{\mathrm{th}}(t)}\right]} R^{(-1)}_{\xi/\sqrt{B_{\mathrm{th}}(t)}}(w) \\
&\quad + \int_{y/\sqrt{B_{\mathrm{th}}(t)}}^\infty dw\, w^2 e^{-w\left[w-y/\sqrt{B_{\mathrm{th}}(t)}\right]} R^{(-1)}_{\xi/\sqrt{B_{\mathrm{th}}(t)}}(w)
\end{aligned}$$

(41)

where $R^{(-1)}_\xi(y)$ denotes the primitive of the disorder correlator, all the rescaling is purely diffusive with as usual $B_{\mathrm{th}}(t) = \frac{Tt}{c}$ and $\lim_{t\to\infty} b^{\mathrm{lin}}(t,y) = 0$ so that the asymptotic correlator (39) is indeed recovered.

This result suggests the following generic decomposition at finite 'time' for the exact correlator:

$$\bar{R}(t,y) = \widetilde{D}_\infty \cdot \left[\mathcal{R}_\xi(y) - \frac{b_+(t,y)+b_-(t,y)}{2}\right] \quad (42)$$

$$\int_{\mathbb{R}} dy\, \mathcal{R}_\xi(y) \equiv 1 \Rightarrow \int_{\mathbb{R}} dy\, b_\pm(t,y) = 1\, \forall t \quad (43)$$
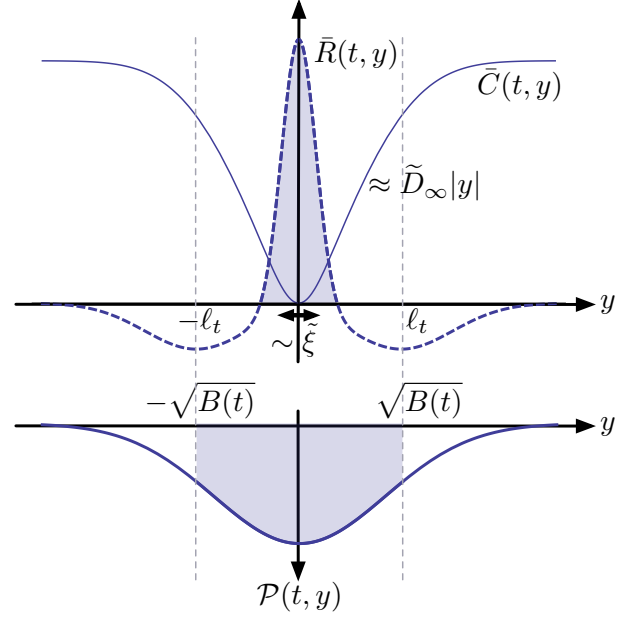
FIG. 3. Top: Schematic graphs of the two-point correlators $\bar{C}(t,y)$ and $\bar{R}(t,y)$ (respectively in full and dashed curves) at fixed 'time' $t > t_{\mathrm{sat}}$, which suggests the generic decomposition (42)-(43); they display the two characteristic lengthscales $\tilde{\xi}$ and ℓ_t in the y-direction; the dashed area below the central peak of $\bar{R}$ corresponds roughly to the saturation amplitude $\widetilde{D}_\infty$ and translates into the slope of the intermediate linear behavior of $\bar{C}$ (since $\partial_y^2 \bar{C}(t,y) = 2\bar{R}(t,y)$ by (21)). Bottom: Corresponding PDF $\mathcal{P}(t,y)$ whose variance is the roughness $B(t)$; the dashed area emphasizes the most probable positions of the DP endpoint, which exclude the large y and thus the 'wings' of $\bar{C}$ or the negative bumps of $\bar{R}$.

suited for the asymptotically large 'times' where we conjecture the function $\mathcal{R}_\xi(y)$ to tend towards the microscopic-disorder transverse correlator $R_\xi(y)$ at high temperature, with distinct corrections $b_\pm(t,y)$ corresponding to the 'wings' in $\bar{C}(t,y)$ and moving to large y with increasing lengthscale t as illustrated in Fig. 3 with $\ell_t \sim \sqrt{B(t)}$ as discussed in Ref. 46.

Finally, the asymptotic amplitude $\widetilde{D}_\infty$ in (42) is predicted to be cD/T in the limit $\xi \to 0$; however this prediction is non-physical in the limit $T \to 0$ so it must break down for temperatures below $T_c(\xi) = (\xi cD)^{1/3}$ as discussed in Ref. 11. We will examine from now on the assumption that for $T < T_c$ the decomposition (42) remains valid but with $\widetilde{D}_\infty = cD/T_c$, justifying it with scaling and saddle-point arguments and testing it numerically. Since the full linearized solution is known explicitly, we know that such a saturation of the asymptotic amplitude can only arise from the KPZ non-linear contribution at 'times' below the Larkin length, before the corrections $b_\pm(t,y)$ separate from the microscopic disorder correlator $R_\xi(y)$.

B. DP Toymodel

We do not know exactly the distributions $\bar{\mathcal{P}}\left[\bar{F}, t\right]$ and $\bar{\mathcal{P}}\left[\eta, t\right]$, or even their correlators $\bar{C}(t,y)$ and $\bar{R}(t,y)$, for a generic disorder transverse correlator (1). As we have just seen, neglecting the KPZ non-linearity in the Feynman-Kac equations, it is however possible to go beyond (39) and actually compute at all 'times' the correlators $\bar{C}^{\text{lin}}(t,y)$ and $\bar{R}^{\text{lin}}(t,y)$, starting from a generic RB correlator $R_\xi(y)$ (cf. (41)); they reconnect of course with the infinite lengthscale limit (39) but their corresponding corrections $b_\pm(t,y)$ encode a pure thermal scaling of the roughness, inherited from the small lengthscales and kept at all lengthscales[46].

Taking an opposite point of view, we have considered a DP toymodel constructed from the asymptotically large 'times' properties of the random-phase η_V. This construction is consistent at least down to the Larkin length L_c (defined after (11) as the lengthscale marking the beginning of the asymptotic powerlaw regime), since by definition of L_c the DP fluctuations display a scale invariance at 'times' $t > L_c$; this construction can actually be pushed to smaller lengthscales, down to a saturation 'time' t_{sat} at high temperatures but as we will argue not at temperatures below $T_c(\xi)$ ($t_{\text{sat}} \leq L_c$).

First we assume that the effective disorder at fixed 'time', $\bar{F}_V(t,y)$ and $\eta_V(t,y)$, have *Gaussian distributions* accordingly to their linearized FP equation. So they are fully described by their two-points correlators (19) and (20) (translational-invariant by the STS (17)) and their mean values $\overline{\eta_V(t,y)} = 0$ and $\overline{\bar{F}_V(t,y)} = -\frac{t}{2c}\bar{R}(t,0)$ by (32) and (33) (which play however no role in the computation of statistical averages).

Secondly we assume that *the random-phase correlator has a stable normalized function* $\mathcal{R}$, all the possible 'time'-dependence being hidden in two effective parameters $\widetilde{D}_t$ and $\tilde{\xi}_t$:

$$\bar{R}(t,y) \approx \widetilde{D}_t \cdot \mathcal{R}_{\tilde{\xi}_t}(y) , \int_{\mathbb{R}} dy \cdot \mathcal{R}_{\tilde{\xi}_t}(y) \equiv 1 \qquad (44)$$

This form generalizes the decomposition (42) but neglecting the corrections $b_\pm(t,y)$. This is a self-consistent approximation since those corrections and the corresponding 'wings' of $\bar{C}(t,y)$ appear at $y^2 \sim B(t)$, and by definition of the roughness it correspond to an improbable position of the DP end-point of decreasing weight $\mathcal{P}(t,y)$ as illustrated in Fig. 3.

Finally we assume that *the function* $\mathcal{R}_{\tilde{\xi}}(y)$ *coincides with the transverse correlator* $R_\xi(y)$ *of the microscopic disorder*, as for the linearized FP equation at infinite 'time' (39). The effective width $\tilde{\xi}_t$ and amplitude $\widetilde{D}_t$ are kept generic though but under the asymptotic constraint

$$\widetilde{D}_\infty(T,\xi) \equiv f(T,\xi) \cdot \frac{cD}{T} \qquad (45)$$

where $f(T,\xi)$ is an interpolating parameter such that we recover the correct $\xi = 0$ limit (38) with $f(T,0) \equiv 1$.

In Ref. 34, we have obtained for this DP toymodel a set of GVM predictions for the roughness and the Larkin length, with $R_\xi(y)$ taken specifically as a Gaussian function of variance $2\xi^2$ (cf. Appendix A). Those predictions are constructed centered on the full-RSB cutoff $u_c(T,\xi)$ of equation (A10). Assuming $\tilde{\xi}_t \approx \xi$ and $\widetilde{D}_t \approx \widetilde{D}_\infty$, the form (45) and the definition $f(T,\xi) \equiv \frac{4}{3}u_c(T,\xi)$ yields a a self-consistent equation for the interpolating parameter:

$$f^6 = 4\pi \left[\frac{T}{T_c(\xi)}\right]^6 (1 - f) , \ T_c(\xi) \equiv (\xi cD)^{1/3} \qquad (46)$$

that connects monotonously the low- and high-temperature scaling of $\widetilde{D}_\infty$ at $f(T_c, \xi) \approx 0.94$:

$$T \ll T_c : f \approx (4\pi)^{1/6} \tfrac{T}{T_c} \Rightarrow \widetilde{D}_\infty(0,\xi) \sim cD/T_c \quad (47)$$

$$T \gg T_c : \qquad f \lesssim 1 \qquad \Rightarrow \widetilde{D}_\infty(T,0) \sim cD/T \quad (48)$$

and hence for the Larkin length (A9) and the asymptotic roughness (A7) beyond L_c:

$$L_c(T,\xi) = 4\pi \cdot \frac{T^5}{cD^2} \cdot f(T,\xi)^{-5} \qquad (49)$$

$$B_{\text{asympt}}(t) \approx \frac{3}{2^{2/3}\pi^{1/3}} \left[\frac{\widetilde{D}_\infty(T,\xi)}{c^2}\right]^{2/3} t^{4/3} \qquad (50)$$

According to these GVM predictions, the amplitude of the geometrical fluctuations $y(t)^2 \sim A(c,D,T,\xi)t^{2\zeta}$ at large lengthscales has a temperature dependence which is damped as sufficiently low T below $T_c(\xi) > 0$, whereas the superdiffusing scaling $\zeta = \frac{2}{3}$ remains unchanged.

For the DP toymodel, there is thus a physically deep connection between the full-RSB cutoff u_c, the amplitude of the random-phase correlator $\bar{R}(t,y)$ at small $|y|$, the Larkin length L_c and the amplitude of the roughness at large lengthscales, this last quantity being typically accessible in experiments.

C. Scaling arguments

Coming back to a full path-integral representation for the roughness and more generally for any average of observables depending exclusively on the DP endpoint, we present thereafter scaling arguments such as sketched in Ref. 11 for the 1D interface model defined in Sec. II A. We also refer to Ref. 60 for a previous approach. Note that we systematically disregard the numerical prefactors in the whole section. Assuming that the random potential V scales in distribution consistently with its two-point transverse correlator $R_\xi(y)$ and that $R_\xi(ay) = a^{-1}R_{\xi/a}(y)$, the rescaling of the spatial coordinates and of the energy yields *exactly* for the roughness:

$$B(r; c, D, T, \xi) = a^2 \bar{B}(r/b; 1, 1, T/\widetilde{E}, \xi/a) \qquad (51)$$

where $\bar{B}$ is the roughness function with *adimensional* parameters, provided the scalings factors satisfy the two

relations involving the Flory exponent $\zeta_F^{1D} = 3/5$:

$$a = (D^{1/3}c^{-2/3}b)^{3/5} \Leftrightarrow b = (D^{-1/5}c^{2/5}a)^{5/3} \quad (52)$$

$$\widetilde{E} \equiv ca^2/b = (cD^2b)^{1/5} = (acD)^{1/3} \quad (53)$$

Fixing one of the scaling factors to a characteristic scale of the model gives three possible choices, each suited for the description of a particular temperature regime (high-T, low-T and their connection), with the *ad hoc* assumptions on the scaling function $\bar{B}(\bar{r}; 1, 1, \bar{T}, \bar{\xi})$. Firstly with respect to the temperature T:

$$\widetilde{E} = T \,, \ b = r_*(T) \equiv \frac{T^5}{cD^2} \,, \ a = \xi_{\text{th}}(T) \equiv \frac{T^3}{cD} \quad (54)$$

$$B(r; c, D, T, \xi) \overset{(T \gg T_c)}{\approx} \xi_{\text{th}}(T)^2 \bar{B}\left(\frac{r}{r_*(T)}; 1, 1, 1, 0\right) (55)$$

catches the high-T scalings if the function $\bar{B}(\bar{r}; 1, 1, 1, 0)$ is properly defined (cf. Sec. III D). Secondly with respect to the finite width or disorder correlation length ξ:

$$a = \xi \,, \ \widetilde{E} = T_c(\xi) \equiv (\xi c D)^{1/3} \,, \ b = r_*(T_c) \quad (56)$$

$$B(r; c, D, T, \xi) \overset{(T \ll T_c)}{\approx} \xi^2 \bar{B}\left(\frac{r}{r_*(T_c)}; 1, 1, 0, 1\right) \quad (57)$$

catches the low-T scalings if the function $\bar{B}(\bar{r}; 1, 1, 0, 1)$ is properly defined (cf. Sec. III D), with $r_*(T_c) = \xi^{5/3}c^{2/3}D^{-1/3}$. Thirdly with respect to the Larkin length $L_c(T, \xi)$, defined as the beginning of the asymptotic 'random-manifold' regime[44]:

$$b = L_c(T, \xi) \equiv r_*(T)/f(T, \xi)^5 \quad (58)$$

$$a = \xi_{\text{eff}}(T, \xi) = \xi_{\text{th}}(T)/f(T, \xi)^3 \quad (59)$$

$$\widetilde{E} = T/f(T, \xi) \quad (60)$$

$$B(r; c, D, T, \xi) = \xi_{\text{eff}}^2 B(r/L_c; 1, 1, f, \xi/\xi_{\text{eff}}) \quad (61)$$

with $f(T, \xi)$ an interpolating function between the high-T and low-T regimes for both the Larkin length and its corresponding effective width:

$$f(T, 0) = 1 \,, \quad f(0, \xi) = T/T_c \quad (62)$$

$$L_c(T, 0) = r_*(T) \,, \quad L_c(0, \xi) = r_*(T_c) \equiv r_0(\xi) \ (63)$$

$$\xi_{\text{eff}}(T, 0) = \xi_{\text{th}}(T) \,, \quad \xi_{\text{eff}}(0, \xi) = \xi \quad (64)$$

We can now focus on the roughness itself, and discuss the consequences of a powerlaw behavior at larges lengthscales, which is known to be governed by the roughness exponent $\zeta_{\text{RM}}^{\text{exact}} = \frac{2}{3}$. A behavior such as

$$\bar{B}_{\text{asympt}}(\bar{r}; 1, 1, \bar{T}, \bar{\xi}) \overset{(\bar{r} \gg 1)}{\approx} \bar{r}^{2\zeta_{\text{RM}}} \quad (65)$$

without any other parameter dependence (this constrain can actually be taken as another definition of the Larkin length (58) for $\bar{r} = r/L_c$) implies for the rescaling (58)-(60):

$$B_{\text{asympt}}(r; c, D, T, \xi) \approx \underbrace{\left[\frac{\xi_{\text{eff}}(T, \xi)}{L_c(T, \xi)^{\zeta_{\text{RM}}}}\right]^2}_{\equiv A(c, D, T, \xi)} r^{2\zeta_{\text{RM}}} \quad (66)$$

An artifact of the GVM framework is that it predicts the Flory exponent of the model for the asymptotic roughness exponent; for the 1D interface $\zeta_F^{1D} = \frac{3}{5}$ whereas for the DP toymodel $\zeta_F^{\text{toy}} = \frac{2}{3} = \zeta_{\text{RM}}^{\text{exact}}$. So either the asymptotic GVM exponent coincides with the Flory exponent of (52) and all the temperature dependence is cancelled in $A(c, D, T, \xi)$, or they do not and the scaling prediction

$$A(c, D, T, \xi) = \left(\frac{D^{3/10}}{c^{3/5}L_c^{1/10}}\right)^{4/3} = \left[\frac{D}{cT}f(T, \xi)\right]^{2/3} \quad (67)$$

matches the GVM result for the DP toymodel (50) with (45). It is important to emphasize that the Flory exponent $\frac{3}{5}$ is imposed by the rescaling procedure of the full model of a 1D interface, whereas the exact RM exponent $\frac{2}{3}$ is the true physical roughness exponent at large lengthscales and is predicted by assuming only that the scaling of the disorder free-energy is dominated by $\bar{F}(t, y)^2 \sim \widetilde{D}_\infty |y|$ as in (38) hence $\zeta_F^{\text{toy}} = \zeta_{\text{RM}}^{\text{exact}}$ (cf. Sec. III D).

If we try boldly the rescaling $b = r$ in order to catch the large lengthscales behavior, we obtain:

$$b = r \,, \ a = (D^{1/3}c^{-2/3}r)^{3/5} \,, \ \widetilde{E} = (cD^2r)^{1/5} \quad (68)$$

$$B(r; c, D, T, \xi) \overset{(r \to \infty)}{\approx} \left(\frac{Dr^3}{c^2}\right)^{2/5} \bar{B}(1; 1, 1, 0, 0) \quad (69)$$

that would predict the asymptotic roughness exponent $\zeta_F^{1D} = \frac{3}{5}$ if the function $\bar{B}(\bar{r}; 1, 1, 0, 0)$ was properly defined, but this is not the case since the two limits $T \to 0$ and $\xi \to 0$ cannot be exchanged or taken simultaneously.

The quantity $f(T, \xi)$ has been introduced here in order to interpolate between the two limits (54) and (56), in the only way compatible with the rescaling procedure (52)-(53). We argue however that $f(T, \xi)$ is the same parameter defined in (45) for $\widetilde{D}_\infty$ in our DP toymodel. Actually all the scalings (54)-(57) are properly recovered in a GVM approximation of the Hamiltonian[34], cf. (A1)-(A4), with the identification $f(T, \xi) \equiv \frac{6}{5}v_c(T, \xi)$ that transforms the equation (A3) for the full-RSB cutoff $v_c(T, \xi)$ into

$$f^6 = \frac{16\pi}{9}\left[\frac{T}{T_c(\xi)}\right]^6 (1 - f) \quad (70)$$

So $f(T, \xi)$ turns out to be the key quantity for the connection of our scaling arguments and the two sets of GVM predictions, centered either on the Hamiltonian or on the pseudo free-energy at a fixed lengthscale, both recalled in Appendix A. The numerical discrepancy between the equations (70) and (46) for $f(T, \xi)$ can be either reabsorbed in the definition $\tilde{\xi}_t \approx \frac{2}{3}\xi$ for the latest, or more safely attributed to the GVM approximation.

D. Saddle-point arguments

In conclusion of this section on analytical results, we present two saddle-point arguments which provide a controlled validation of our different assumptions at $T > 0$

and $\xi > 0$. Firstly we use $\frac{1}{T}$ as a large parameter at low temperature in order to argue the existence of a proper limit for $\bar{B}(\bar{r}; 1, 1, 0, 1)$ in (57) (the high-temperature case (57) is already well controlled); this is not obvious in the usual conventions of mathematicians regarding the DP, see Appendix G. Secondly we revisit the original derivation of the exponent $\zeta_{\mathrm{RM}}^{\mathrm{exact}} = \frac{2}{3}$ by Huse, Henley and Fisher[29] from the point of view of our DP toymodel and using the lengthscale t as large parameter for the saddle point.

1. Zero-temperature roughness of the 1D interface

The low-temperature limit in (57) can be made explicit coming back to the path-integral definition of the roughness and performing the rescaling (56) with $t_*(T) \equiv \frac{T^5}{cD^2}$ as in (54):

$$B(t_1; c, D, T, \xi) = \xi^2 \bar{B}\left(\frac{t_1}{t_*(T_c)}; 1, 1, \frac{T}{T_c}, 1\right) \qquad (71)$$

$$= \xi^2 \frac{\displaystyle\int_{y(0)=0} \mathcal{D}y \, y\left(\frac{t_1}{t_*(T_c)}\right)^2 e^{-\frac{T_c}{T} \int_0^{\frac{t_1}{t_*(T_c)}} dt \left[\frac{1}{2}(\partial_t y)^2 + V_1(t, y(t))\right]}}{\displaystyle\int_{y(0)=0} \mathcal{D}y \, e^{-\frac{T_c}{T} \int_0^{\frac{t_1}{t_*(T_c)}} dt \left[\frac{1}{2}(\partial_t y)^2 + V_1(t, y(t))\right]}} \qquad (72)$$

where $V_1(t, y(t)) \equiv V(t, y(t))|_{D=1, \xi=1}$. In the path integrals, the trajectories $y(t)$ have a fixed starting point $y(0) = 0$ but a free endpoint $y(t_1)$. Since all temperature-dependence has been gathered in a single and large prefactor $\frac{T_c}{T}$, the path integrals are dominated by a *common* optimal trajectory $y^\star(t)$, which, assuming that it exists, does not depend on temperature since it minimizes $\int_0^{t_1/t_*(T_c)} dt \left[\frac{1}{2}(\partial_t y)^2 + V_1(t, y(t))\right]$. The saddle trajectory endpoint is then reached at some optimal endpoint $y_1^\star = y_1^\star\left(\frac{t_1}{t_*(T_c)}, V_1\right)$, common to the numerator and denominator and independent of T. Finally, one obtains from (72) that in (71) $\lim_{T \to 0} \bar{B}\left(\frac{t_1}{t_*(T_c)}; 1, 1, \frac{T}{T_c}, 1\right)$ is finite, being equal to $\overline{y_1^\star\left(\frac{t_1}{t_*(T_c)}, V_1\right)^2}$. So if the optimal path $y^\star$ does exist and if its variance at fixed lengthscale t_1 is finite, the zero-temperature limit is well-defined. See Appendix G for a discussion on this last point.

2. DP toymodel scaling argument, asymptotic roughness and Flory exponent

The scaling arguments of the previous section, established on the full model of a 1D interface, have of course their counterpart for our DP toymodel. The main assumption is that the large 'time' scaling of $\bar{F}(t, y)$ is governed by its infinite-'time' correlator $\bar{C}(t, y) = \widetilde{D}_\infty |y|$ (38) with the amplitude being essentially a constant

$\widetilde{D}_t \approx \widetilde{D}_\infty$ (denoted thereafter simply by $\widetilde{D}$) and similarly $\tilde{\xi}_t \approx \tilde{\xi}$. This ensures that upon the change of variable $y = a\bar{y}$ and $t = b\bar{t}$, the following free-energy is equal in distribution to

$$F_{\mathrm{th}}(t, y) + \bar{F}(t, y) \stackrel{d}{=} \frac{a^2}{b} \frac{c\bar{y}^2}{2\bar{t}} + a^{\frac{1}{2}} \widetilde{D}^{\frac{1}{2}} \bar{F}_1(\bar{t}, \bar{y}) \qquad (73)$$

where $\bar{F}_1(t, y) \equiv \bar{F}(t, y)|_{\widetilde{D}=1, \tilde{\xi}/a}$. The argument of Ref. 29 can then be summarized as follows: the free-energy and roughness fluctuation exponents χ and ζ are respectively defined as $\bar{F}(y) \sim b^\chi \bar{F}(\bar{y})$ and $y \sim b^\zeta$ (which amounts to take $a \sim b^\zeta$). The fact that in distribution $\bar{F}(t, y) \stackrel{d}{\sim} a^{\frac{1}{2}} \bar{F}(\bar{y})$ implies $\chi = \frac{1}{2}\zeta$ while equating the thermal and disorder contributions in (73) leads yields $\chi = 2\zeta - 1$. These two equations fully determine the values of the exponents: $\chi = \frac{1}{3}$ and $\zeta = \frac{2}{3}$. Taking care of the prefactors of those powerlaws, we define the following rescaling procedure:

$$B(t; c, \widetilde{D}, T, \tilde{\xi}) = a^2 \bar{B}(t/b; 1, 1, T/\widetilde{E}, \tilde{\xi}/a) \qquad (74)$$

$$a = (\tilde{D}/c^2)^{1/3} b^{2/3} \Leftrightarrow b = c\widetilde{D}^{-1/2} a^{3/2} \qquad (75)$$

$$\widetilde{E} \equiv ca^2/b = (\widetilde{D}^2 b/c)^{1/3} = \tilde{D}^{-1/2} a^{1/2} \qquad (76)$$

where $\bar{B}$ is the roughness function with *adimensional* parameters, if the scalings factors satisfy the two relations involving the Flory exponent $\zeta_{\mathrm{F}}^{\mathrm{toy}} = 2/3$. To understand how this power counting can describe correctly the large 'time' asymptotics, we chose the rescaling equivalent to (68):

$$b = t, \quad a = (\widetilde{D}/c^2)^{\frac{1}{3}} t^{\frac{2}{3}}, \quad \widetilde{E} = (\widetilde{D}^2 t/c)^{1/3} \qquad (77)$$

which implies from the definition of the roughness $B(t; c, \widetilde{D}, T, \tilde{\xi})$ in (22):

$$B(t; c, \widetilde{D}, T, \tilde{\xi}) = \left[\frac{\widetilde{D}}{c^2}\right]^{\frac{2}{3}} t^{\frac{4}{3}}$$
$$\times \frac{\int d\bar{y} \, \bar{y}^2 \exp\left\{-\frac{1}{T}\left[\frac{\widetilde{D}^2}{c} t\right]^{\frac{1}{3}} \left[\frac{\bar{y}^2}{2} + \bar{F}_1(1, \bar{y})\right]\right\}}{\int d\bar{y} \exp\left\{-\frac{1}{T}\left[\frac{\widetilde{D}^2}{c} t\right]^{\frac{1}{3}} \left[\frac{\bar{y}^2}{2} + \bar{F}_1(1, \bar{y})\right]\right\}} \qquad (78)$$

where the overline denotes the average over the random $\bar{F}_1$. The advantage of our specific choice of the rescaling parameters a and b is that the 'time'-dependence of the exponentials in (78) is then gathered in a single prefactor $t^{\frac{1}{3}}$. For each fixed $\bar{F}_1$, one may thus evaluate the integrals in $\bar{y}$ through the saddle point method in the large t limit. The integrals at the numerator and denominator of (78) are dominated by the same $y^\star[\bar{F}_1]$ which minimizes $\frac{\bar{y}^2}{2} + \bar{F}_1(1, \bar{y})$, ensuring that $y^\star[\bar{F}_1]$ *is independent of* t. We read from (78) that

$$B_{\mathrm{asympt}}(t; c, \widetilde{D}, T, \tilde{\xi}) = \overline{(y^\star[\bar{F}_1])^2} \cdot (\widetilde{D}/c^2)^{\frac{2}{3}} t^{\frac{4}{3}} \qquad (79)$$

i.e. the roughness exponent is $\zeta_{\mathrm{RM}}^{\mathrm{exact}} = \frac{2}{3}$. However all this construction breaks down at the very last when the scaling $\bar{F}(t, y)^2 \sim \widetilde{D}|y|$ ceases to be valid, at small

$|y| \leq \tilde{\xi}$, *i.e.* when the scaling factor $a(t)$ matches with the effective width $\tilde{\xi}$. This yields an alternative definition of the Larkin 'time' t_0 as $a(t_0) \equiv \tilde{\xi}$ or $t_0 = (c^2 \tilde{\xi}^3 / \widetilde{D})^{1/2}$. Coming from the large lengthscales, this asymptotic scaling breaks earlier due to thermal fluctuations, at the Larkin 'time' $t_c \geq t_0$. Identifying t_c and $L_c(\xi, T)$, generalizing $\tilde{\xi} \approx \xi$ to $\xi_{\text{eff}}(T, \xi)$ of (63) and using finally $\widetilde{D} = f(T, \xi) \frac{cD}{T}$ of (45), we recover consistently with (49) and (62) for the Larkin 'time':

$$a(t_c) \equiv \xi_{\text{eff}} \Leftrightarrow t_c = \left(\frac{c^2 \xi_{\text{eff}}^3}{\widetilde{D}} \right)^{1/2} = \frac{T^5}{cD^2} f(T, \xi)^{-5} \quad (80)$$

which has as a lower bound its low-temperature limit

$$t_0 = \xi^{5/3} c^{2/3} D^{-1/3} = r_*(T_c(\xi)) \quad (81)$$

The large-'time' limit makes the scaling assumption $\bar{F}_1(1, \bar{y})^2 \sim |y|$ even more reliable, and the saddle point can be properly taken in this limit, yielding the Flory exponent of the DP toymodel $\zeta_F^{\text{toy}} = \frac{2}{3}$. This was not the case for the 1D interface in (69). Indeed, upon the rescalings (68) we obtain in a path-integral representation:

$$B(t_1; c, D, T, \xi)$$
$$= \left[\frac{Dt_1^3}{c^2} \right]^{\frac{2}{5}} \bar{B} \left(1; 1, 1, \frac{T}{(cD^2 t_1)^{\frac{1}{5}}}, \frac{\xi}{(D^{\frac{1}{3}} c^{-\frac{2}{3}} t_1)^{\frac{3}{5}}} \right) \quad (82)$$

$$= \left[\frac{Dt_1^3}{c^2} \right]^{\frac{2}{5}} \frac{\displaystyle\int_{y(0)=0} \mathcal{D}y \; y(1)^2 \, e^{-\frac{\widetilde{E}}{T} \int_0^1 dt \left[\frac{1}{2}(\partial_t y)^2 + V\left(\frac{t}{t_1}, y(t)\right)\big|_{D=1, \frac{\xi}{a}} \right]}}{\displaystyle\int_{y(0)=0} \mathcal{D}y \; e^{-\frac{\widetilde{E}}{T} \int_0^1 dt \left[\frac{1}{2}(\partial_t y)^2 + V\left(\frac{t}{t_1}, y(t)\right)\big|_{D=1, \frac{\xi}{a}} \right]}}$$
$$(83)$$

with $a = (D^{1/3} c^{-2/3} t_1)^{3/5}$, $\widetilde{E} = (cD^2 t_1)^{1/5}$. The large t_1 asymptotics cannot be taken directly from this expression since it is not in a saddle form and all scales are intertwined, contrarily to the study of the free-energy itself which corresponds to scales integrated up to 'time' t_1.

IV. NUMERICAL STUDY OF THE CONTINUOUS 1+1 DP

In the previous section we have considered several analytical arguments in the context of a finite disorder correlation length $\xi > 0$ and combined them to propose a DP 'toymodel' which assumes essentially that the main physical features of the correlator $\bar{R}(t, y)$ are gathered in $\tilde{\xi}_t$, $\widetilde{D}_t$ and the shape $\mathcal{R}(y)$. In this section devoted to a numerical study of the continuous 1+1 DP, we aim at testing those analytical results and the validity of our DP toymodel.

The Feynman-Kac equations (26)-(27) for $\partial_t \bar{F}_V(t, y)$ and $\partial_t \eta_V(t, y)$ provide the starting point for a numerical

study of the geometrical and free-energy fluctuations of the 1+1 DP, and consequently of the static 1D interface, directly in their continuum formulation. This approach uses an exact property of the model – the statistical tilt symmetry (17) (cf. Appendix B) – to focus on the effects of the disorder, dissociated from the pure thermal ones.

Among the numerical procedures previously used to tackle this problem, we can mention firstly the DP under the solid-on-solid (SOS) constraint[31,46,61] where the polymer lives on a discretized lattice; secondly the semi-continuous 1D interface, discretized along its internal dimension but with each point living in a *continuous* 1D splined random potential[62]; and thirdly the continuous DP that we will present thereafter. Those approaches are of course complementary, especially for the investigation of the large- *versus* small-lengthscales and high- *versus* low-temperature properties, if a suitable translation from the specific numerical parameters to the physical ones $\{c, D, T, \xi\}$ is provided[39,46].

Our procedure is actually based on the continuous analogue of the transfer-matrix method of a DP on a lattice with the SOS constraint, in the sense that it is performed after integration over thermal fluctuations since it follows the partial partition function with the lengthscale (namely the Feynman-Kac equations (25)-(27)), for many individual disorder configurations. The continuous-limit formulation has two advantages: first the discretization issue in numerics is pushed back to a problem of numerical integration of partial differential equations, so even 'small' lengthscales can be studied without discretization artifacts; secondly in the continuous limit the numerical parameters are directly the physical ones of the analytical model.

Thereafter we will first present our numerical procedure, and then discuss the different numerical results obtained, which are respectively the 'time'-evolution of the correlator $\bar{R}(t, y)$ and its parameters $\{\tilde{\xi}_t, \widetilde{D}_t\}$ at fixed temperature, the temperature-dependence of the asymptotic effective correlator $\overline{R}_{\text{sat}}(y)$, the 'time'- and temperature-dependence of $\overline{F}_V(t, y)$, and the temperature-dependence of the roughness $B(t)$. All the numerical parameters are gathered in Appendix H.

A. Numerical recipe

Computing $\bar{F}_V(t, y)$ for individual disorder configurations $V(t, y)$ up to a maximal 'time' t_m, we can measure directly the geometrical and free-energy fluctuations stemming at thermodynamic equilibrium from thermal fluctuations exploring a given random potential. Then averaging these fluctuations over many disorder configurations we have access to the quantities of interest defined in Sec. II C and discussed in the previous sections from an analytical point of view.

a. Finite box and microscopic discretized grid. The Feynman-Kac evolution equations (26)-(27) are defined in a continuous limit with $t > 0$ and $y \in \mathbb{R}$. In

numerics we work necessarily on a microscopic discretized grid in both (t, y) variables and in a finite box $(t, y) \in [0, t_m] \times [-y_m, y_m]$ without periodic boundary conditions. However, in experimental realizations of 1D interfaces we also have some microscopic cut-off in lengthscales, ultimately the crystal parameter, and a macroscopic cut-off due to scarcer statistics at larger lengthscales.

b. *Generation of an individual disorder configuration.* In order to generate individual disorder configurations for a given set of DES parameters, we first define a two-dimensional grid of spacing $\left\{ \xi_t^{\mathrm{grid}}, \xi_y^{\mathrm{grid}} \right\} = \{t_m/L_t, y_m/L_y\}$ (cf. Fig. 4). On each point of the grid we pick a set of random numbers according to a normal distribution of variance D^{grid} (the 'strength of disorder') and the smooth random potential $V(t, y)$ is obtained by interpolating between the grid points with a 2D cubic spline as illustrated in Fig. 22 (*top*). As detailed in Appendix I, its corresponding two-point correlator at fixed 'time' is given by the translation-invariant:

$$\overline{V(t,y)V(t,0)} = D^{\mathrm{eff}} \cdot R_{\xi_y}^{\mathrm{CubicS}}(y) \tag{84}$$

$$D^{\mathrm{eff}} = D \cdot R_{\xi_t}^{\mathrm{CubicS}}(0) = D^{\mathrm{grid}} \xi_y^{\mathrm{grid}} \tag{85}$$

with the function R_ξ^{CubicS} made explicit in (I2)-(I3). The values of those parameters are fixed for all our numerical computations to

$$\xi_t^{\mathrm{grid}} = 1 , \ \xi_y^{\mathrm{grid}} = 2 , \ D^{\mathrm{grid}} = 4 \ \Rightarrow \ D = D^{\mathrm{eff}} = 8 \tag{86}$$

Note that the physical parameter used in analytical arguments is D and not D^{eff}, but they coincide with this particular choice ξ_t^{grid}.

c. *Numerical integration at fixed disorder.* We have chosen to follow the evolution of the disorder free-energy $\bar{F}_V(t, y)$ (26) because among its counterparts $\eta_V(t, y)$ is too noisy, $F_V(t, y)$ includes $F_{\mathrm{th}}(t, y)$ that hides the disorder-induced fluctuations of $\bar{F}_V(t, y)$ except at large 'times', and the exponential in $W_V(t, y) \propto e^{-F_V(t,y)/T}$ suppresses the numerical resolution. Moreover, by subtracting the exact $F_{\mathrm{th}}(t, y)$ for $y \in \mathbb{R}$ directly in the evolution equation, we get rid of the finite-box artifacts that would have arisen in the pure elastic contribution. The numerical integration of the differential equation (26) was performed using a numerical algorithm included in $\mathtt{Mathematica}^{63}$, which adapts the numerical discretization in y at each 'time'-step in order to minimize the numerical errors. The main limitation was that the larger the maximum 'time' t_m, the longer the computation time. Moreover, the lower the temperature the more the numerical solution of the Feynman-Kac equations is sensitive to the spatial variations of the random potential, thus dictating a smaller grid discretization in order to minimize the numerical error and increasing considerably the computation time. The number of disorder configurations that have been considered for a given set of DES parameters is thus a compromise between the convergence of the disorder average and a reasonable computation time (as summarized in Appendix H).

d. *Initial condition.* At short 'times' the free-energy is dominated by its pure thermal contribution (28) which diverges at $t = 0$, so we take as initial condition at $t_0 = 0.1$ the thermal distribution $\mathcal{P}(t_0, y) = \mathcal{P}_{\mathrm{th}}(t_0, y)$ as defined by (24), *i.e.* $\bar{F}_V(t_0, y) \equiv 0$. We assume that at large 'times' the DP has completely forgotten this initial condition, but at short 'times' above t_0 its behavior should carry some artifact for the disorder-induced quantities $\bar{F}_V$ and η_V.

e. *Boundary conditions.* We imposed at each 'time' that $\eta_V(t, \pm y_m) = 0$ *i.e.* $\partial_y \bar{F}_V(t, \pm y_m) = 0$. This is equivalent to the statement that for $|y| \geq y_m$, we have $W_V(t, y) \approx W_{V \equiv 0}(t, y)$ and thus the normalized DP endpoint probability is $\mathcal{P}(t, y) \approx \mathcal{P}_{\mathrm{th}}(t, y) \approx 0$. This boundary condition can be physically correct only for 'times' such that $\sqrt{B(t)} < y_m$, else the DP 'senses' inevitably the boundaries of the finite box. This choice of boundary condition implies for the normalization $\bar{W}_V(t)$ (4) that the contribution for y outside $[-y_m, y_m]$ is exactly known analytically:

$$\frac{1}{2}\bar{W}_V^{\mathrm{num}}(t) = \int_0^{y_m} dy \cdot e^{-\left(F_{\mathrm{th}}(t,y) + \bar{F}_V(t,y)\right)/T} + \mathrm{cte}(t, y_m)$$

$$\mathrm{cte}(t, y_m) = \int_{y_m}^{\infty} dy \cdot e^{-F_{\mathrm{th}}(t,y)/T} , \ F_{\mathrm{th}}(t, y) = \frac{cy^2}{2t} \tag{87}$$

which yields $\mathcal{P}_V(t, y)$ as defined by (5) (cf. Fig. 4).

f. *Recorded data.* We have actually recorded, on a microscopic grid linear in y: on one hand the disorder free-energy $\bar{F}_V(t, y)$ and the random-phase $\eta_V(t, y) \equiv \partial_y \bar{F}_V(t, y)$, with their mean values $\overline{\bar{F}_V(t, 0)}$ and $\overline{\eta_V(t, 0)}$ and their respective two-point correlators $\bar{C}(t, y)$ and $\bar{R}(t, y)$; and on the other hand the PDFs $\mathcal{P}_V(t, y)$ and $\mathcal{P}(t, y)$, their corresponding moments $\overline{\langle y(t)^k \rangle}$ and in particular the roughness $B(t) \equiv \overline{\langle y(t)^2 \rangle}$ with the roughness exponent $\zeta(t)$. We have recorded those quantities using a microscopic grid *linear* in t, and in parallel for the roughness-related quantities we have used a microscopic grid *logarithmic* in t in anticipation of powerlaws determination. Note that the even parity of the correlators has been explicitly used to increase their statistics, so the measured $\bar{C}(t, y)$ and $\bar{R}(t, y)$ are symmetric by construction:

$$\bar{R}(t, y) = \tfrac{1}{2}\overline{[\eta(t, y)\eta(t, 0) + \eta(t, -y)\eta(t, 0)]}$$

$$\bar{C}(t, y) = \tfrac{1}{2}\overline{\left[\bar{F}(t, y) - \bar{F}(t, 0)\right]^2} + \overline{\left[\bar{F}(t, -y) - \bar{F}(t, 0)\right]^2}$$

g. *Fitting functions for $\bar{R}(t, y)$.* The correlator $\bar{R}(t, y)$ is not known exactly at finite 'time', and we have thus only postulated its generic form $\bar{R}(t, y) \approx \widetilde{D}_t \cdot \mathcal{R}_{\tilde{\xi}_t}(y)$ in (42)-(43). Following the DP toymodel assumption (44), we have systematically extracted the typical width $\tilde{\xi}_t$ and amplitude $\widetilde{D}_t$ for three different function $\mathcal{R}_{\tilde{\xi}}(y)$ with the chosen normalization
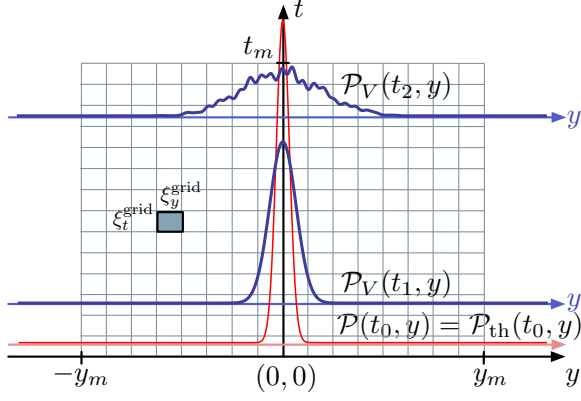
FIG. 4. (Color online) Sketch of the numerical procedure for the 1+1 continuous DP in the finite box $[0, t_m] \times [-y_m, y_m]$ with the initial condition at $t_0 = 0.1$ taken purely thermal $\mathcal{P}(t_0, y) = \mathcal{P}_{\text{th}}(t_0, y)$ (red curve). There are three levels of discretization grids by decreasing scale: the grid for the random potential $\xi_t^{\text{grid}} = 1$ and $\xi_y^{\text{grid}} = 2$ (the grey box on the left side); the linear grids for the recording of data $\Delta t^{\text{lin}} = t_m/80$ and $\Delta y^{\text{lin}} = 2y_m/100$, and the logarithmic grid $t_j^{\text{log}} = t_0 \cdot (t_m/t_0)^{j/80}$ with $j = 0 \ldots 80$; the microscopic grid for the numerical integration adapted in both (t, y)-directions by Mathematica. At a given configuration of disorder $V(t, y)$ as illustrated in Fig. 22, the PDF $\mathcal{P}_V(t, y)$ is computed at increasing 'time' following (26), with the boundary condition $\eta_V(t, \pm y_m) = 0$ and the *ad hoc* normalization (87), as illustrated at $t_0 < t_1 < t_2$ (blue curves).

$\int_{\mathbb{R}} dx \, \mathcal{R}_{\tilde{\xi}}(x) \equiv 1$. Firstly $\mathcal{R}_{\tilde{\xi}}(y)$ is taken to be a Gaussian function, whose single feature is given by its variance $2\tilde{\xi}^2$:

$$\mathcal{R}_{\tilde{\xi}}^{\text{Gauss}}(y) = \frac{e^{-y^2/(4\tilde{\xi}^2)}}{\sqrt{4\pi}\tilde{\xi}} \tag{88}$$

Secondly we add phenomenologically two negative oscillations of the observed correlator, by using a cardinal sinus of period $\tilde{\xi}/\pi$ with a Gaussian envelope function:

$$\mathcal{R}_{\tilde{\xi}}^{\text{SincG}}(y) = e^{-y^2/(4\tilde{\xi}^2)} \cdot \frac{\sin\left[\pi y/\tilde{\xi}\right]}{\pi y \, \text{Erf}(\pi)} \tag{89}$$

And thirdly we consider the same function as the exact two-point correlator of the microscopic random potential $\mathcal{R}_{\tilde{\xi}}^{\text{CubicS}}(y) = R_{\xi}^{\text{CubicS}}(y)$ defined in (I2)-(I3). $\{\tilde{\xi}_t, \widetilde{D}_t\}$ are reliable quantities if they do not depend on the choice of the fitting function, except for a numerical constant between $\mathcal{R}^{\text{Gauss}}$, $\mathcal{R}^{\text{SincG}}$ and $\mathcal{R}^{\text{CubicS}}$. In Appendix I, we have compared the fit of the correlator $\overline{V(t, y)V(0, 0)}$ with respect to $\mathcal{R}^{\text{Gauss}}$, $\mathcal{R}^{\text{SincG}}$ and $\mathcal{R}^{\text{CubicS}}$, and determined the numerical constants for passing from one to the others, as a consistency check of this procedure on this well-controlled correlator.

B. 'Time'-evolution of the effective disorder correlator $\bar{R}(t, y)$ at fixed temperature

In this section we study in detail the 'time'-evolution of the correlator $\bar{R}(t, y)$ measured numerically for three different temperatures $T \in \{0.35, 1, 6\}$, respectively at low-, intermediate- and high-temperature – cf. Appendix H for the complete set of corresponding numerical parameters.

In Fig. 5, we can follow the evolution of the correlator, starting by construction from the thermal condition $\bar{R}(t_0, y) \equiv 0$ at initial 'time' $t_0 = 0.1$. At small 'times' the central peak first increases but quickly saturates, and all the curves start accumulating in the vicinity of $y = 0$ (*left side*). Assuming thus that at sufficiently large 'times' the correlator has reached its presumably stationary form at small y, the saturation correlator $\bar{R}_{\text{sat}}(y)$ can be obtained by averaging the correlator over $t > t_{\text{min}}$ (superimposed black curve in the *right side*). The corresponding saturation correlator $\bar{R}_{\text{sat}}(y)$ can then be fitted with respect to the three fitting functions (*center*), the corresponding values for the fitting parameters $\left\{\tilde{\xi}_{\text{sat}}, \widetilde{D}_{\text{sat}}\right\}$ being listed in Tab. I. Having checked that those results are stable for different values $t_{\text{min}} > 10$, we have chosen arbitrarily $t_{\text{min}} = 25$ for all temperatures in order to be safely above the saturation 'time' t_{sat} which clearly exists but might be shifted by the artificial thermal condition at initial 'time' $t_0 = 0.1$. The negative excursions of $\bar{R}(t, y)$ at large y are treated as noise for the averaged $\bar{R}_{\text{sat}}(y)$, which as an artifact slightly displaces the asymptotic behavior below the abscissa axis.

So we can distinguish two regimes for the correlator $\bar{R}(t, y)$: a short-'time' evolution *a priori* marked by the artificial initial condition, and above a certain 'time' $t_{\text{sat}} \approx 10$ a saturation of the central peak to a given stable function $\bar{R}_{\text{sat}}(y) \approx \widetilde{D}_{\text{sat}} \cdot \mathcal{R}_{\tilde{\xi}_{\text{sat}}}(y)$ which can then be measured numerically provided that we neglect the negative excursions at large y as proposed in our DP toy model (44).

Going one step further and testing different fitting functions for $\mathcal{R}(y)$, we observe graphically that at high-T the exact microscopic disorder correlator $\mathcal{R}^{\text{CubicS}}(y)$ or alternatively its phenomenological counterpart $\mathcal{R}^{\text{SincG}}(y)$ both correctly encompass the features of the whole peak, including its maximum and its negative anti-correlations, but not the negative asymptote which is an expected artifact of the averaging procedure. This behavior could thus be consistent with the decomposition (42)-(43) at high-T and at 'times' $t > t_{\text{sat}}$, and the infinite-'time' limit (39) where the microscopic disorder correlator is recovered. At low-T however $\mathcal{R}^{\text{Gauss}}(y)$ appears to be more suited to capture the central peak and its maximum, although completely skipping the anti-correlations which are obviously inherited from the microscopic disorder correlator but progressively altered when the temperature is lowered.

Assuming that the validity of the decomposition $\bar{R}(t, y) \approx \widetilde{D}_t \cdot \mathcal{R}_{\tilde{\xi}_t}(y)$ could be extended to smaller
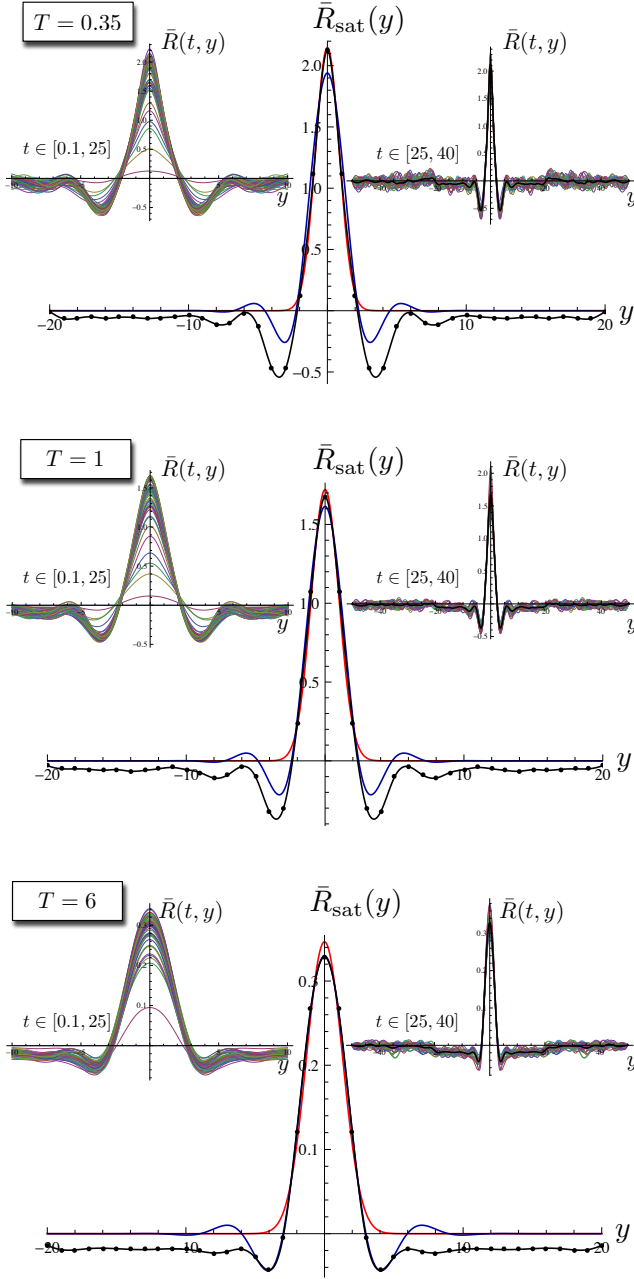
FIG. 5. (Color online) Effective disorder correlator $\bar{R}(t,y)$ measured numerically at fixed temperature $T \in \{0.35, 1, 6\}$. The different 'times' $t \in [0.1, 40]$ are separated in two subsets $[0, t_{\min}]$ (*left*) and $[t_{\min}, 40]$ (*right*) with $t_{\min} = 25$, with a timestep $\Delta t = 0.5$. *Left side* ($y \in [-20, 20]$): Initial development of the central peak, saturation and accumulation of the curves in the vicinity of $y = 0$. *Right side* ($y \in [-40, 40]$): Large 'times' correlators and their average over $t > t_{\min}$ with $t_{\min} = 25$ (superimposed black curve). *Center*: Saturation correlator $\bar{R}_{\text{sat}}(y)$ (black dots) with its Gaussian (88) (red) and 'SincG' (89) (blue) fitting functions, 'CubicS' collapsing exactly on 'SincG' – cf. Tab. I for the explicit values of the fitting parameters.

$(t > t_{\min} = 25)$	$T = 0.35$	$T = 1$	$T = 6$
$\widetilde{D}_{\text{sat}}^{\text{Gauss}}$	4.6 ± 0.2	4.3 ± 0.2	1.13 ± 0.04
$\widetilde{D}_{\text{sat}}^{\text{SincG}}$	4.4 ± 0.2	3.9 ± 0.2	0.99 ± 0.03
$\widetilde{D}_{\text{sat}}^{\text{CubicS}}$	4.37 ± 0.07	3.89 ± 0.05	0.98 ± 0.06
$\widetilde{D}_{\text{sat}}^{\text{SincG}}/\widetilde{D}_{\text{sat}}^{\text{Gauss}}$	0.95	0.91	0.87
$\tilde{\xi}_{\text{sat}}^{\text{Gauss}}$	0.61 ± 0.04	0.70 ± 0.04	0.92 ± 0.04
$\tilde{\xi}_{\text{sat}}^{\text{SincG}}$	2.25 ± 0.07	2.42 ± 0.05	2.99 ± 0.06
$\tilde{\xi}_{\text{sat}}^{\text{CubicS}}$	2.25 ± 0.07	2.40 ± 0.05	2.97 ± 0.06
$\tilde{\xi}_{\text{sat}}^{\text{SincG}}/\tilde{\xi}_{\text{sat}}^{\text{Gauss}}$	3.72	3.45	3.25

TABLE I. Fitting parameters $\{\tilde{\xi}_{\text{sat}}, \widetilde{D}_{\text{sat}}\}$ at $T \in \{0.35, 1, 6\}$, computed from the saturation correlators $\bar{R}_{\text{sat}}(y)$ plotted in Fig. 5 for $t_{\min} = 25$.

'times', we have followed the evolution of the two fitting parameters $\{\tilde{\xi}_t, \widetilde{D}_t\}$, as plotted in Fig. 6-7 for the same fixed temperatures $T \in \{0.35, 1, 6\}$ as in Fig. 5. Even though this assumption *a priori* breaks down for $t < t_{\text{sat}}$, the three fits yield consistent values both for $\widetilde{D}_t$ and $\tilde{\xi}_t$, with reasonable uncertainties even at short-'times'. On one hand we recover for $\widetilde{D}_t$ the two regimes observed for the correlator $\bar{R}(t,y)$, *i.e.* an increase of this amplitude at short 'times' and a saturation beyond t_{sat} as indicated by the straight lines $\widetilde{D}_\infty$ in Fig. 6 (obtained by averaging $\widetilde{D}_t$ over $t > t_{\min} = 25$). On the other hand $\tilde{\xi}_t$ slightly decreases at short 'times' and its saturation seems to appear much sooner, especially at high-T. As a self-consistency check, we can notice that the average of the fitting parameters $\left\{\tilde{\xi}_\infty, \widetilde{D}_\infty\right\}$ have the same values as the fitting parameters of the averaged correlator $\left\{\tilde{\xi}_{\text{sat}}, \widetilde{D}_{\text{sat}}\right\}$ (cf. Tab. I); their estimated errors are actually surprisingly close even though they have distinct origins, stemming respectively from the variance of $\left\{\tilde{\xi}_t, \widetilde{D}_t\right\}$ at $t > t_{\min}$ and from the uncertainty over the fit of $\bar{R}_{\text{sat}}(y)$.

If the function $\mathcal{R}_{\tilde{\xi}_t}(y)$ did coincide exactly with the microscopic disorder correlator $R_\xi^{\text{CubicS}}(y)$ at small y and large 'times', we would expect that $\frac{\widetilde{D}_\infty^{\text{SincG}}}{\widetilde{D}_\infty^{\text{Gauss}}} = \frac{D^{\text{SincG}}}{D^{\text{Gauss}}} \approx 0.80$ and $\frac{\tilde{\xi}_\infty^{\text{SincG}}}{\tilde{\xi}_\infty^{\text{Gauss}}} = \frac{\xi^{\text{SincG}}}{\xi^{\text{Gauss}}} \approx 3.6$ as discussed in Appendix I. Although $\left\{\tilde{\xi}_\infty, \widetilde{D}_\infty\right\}$ clearly exhibit a temperature dependence which will be discussed later on, these ratios are numerically found to be of the expected order of magnitude and reasonably constant for $t > t_{\text{sat}}$ at fixed T (cf. Tab. I). Actually the numerical ratios extracted from the measured $\bar{R}(t,y)$ *versus* the linearized $\bar{R}^{\text{lin}}(t,y)$ of Appendix E (for $R^{\text{CubicS}}(y)$) follow qualitatively the same trend in temperature, and are even quantitatively the same at high-T. This last point supports furthermore the idea that at high-T we recover the microscopic disorder correlator $\bar{R}(t,y) \approx \frac{cD}{T} \cdot \mathcal{R}_{\tilde{\xi}_\infty}^{\text{CubicS}}(y)$ but the average over $t > t_{\min}$ introduces an overall negative shift of the asymptote which eventually yields the
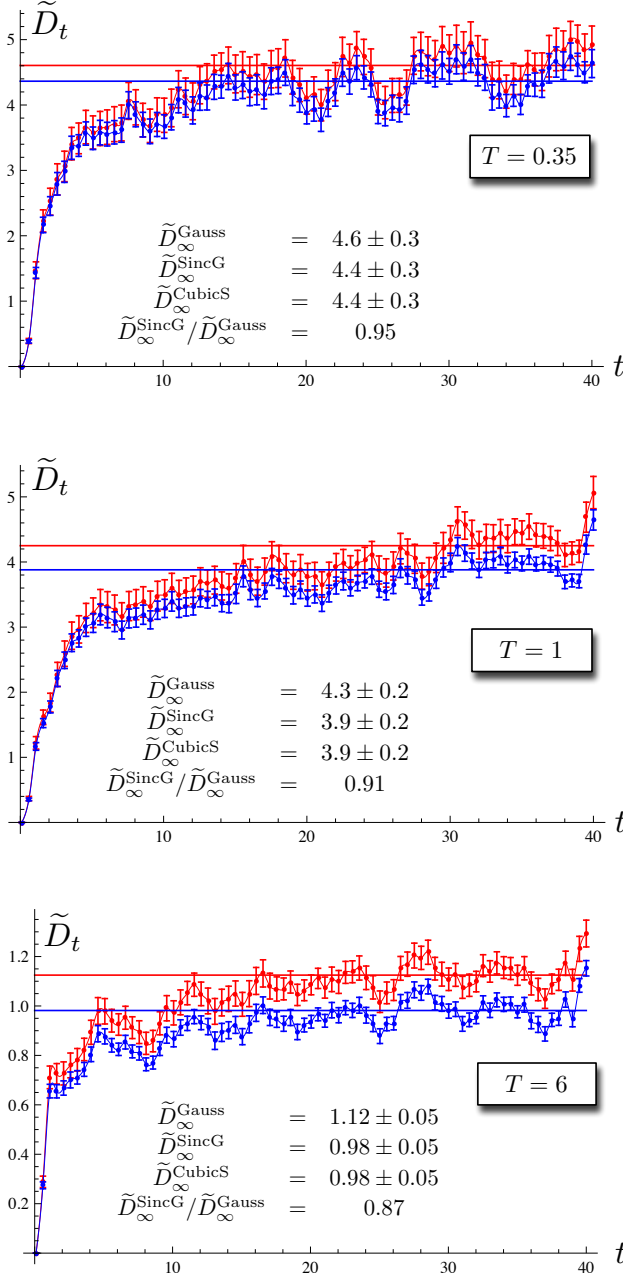
FIG. 6. (Color online) Fitting parameter $\widetilde{D}_t$ at fixed temperature $T \in \{0.35, 1, 6\}$ with respect to 'Gauss' (red) and 'SincG' (blue), 'CubicS' collapsing exactly on 'SincG'. The straight lines indicate the respective average value $\widetilde{D}_\infty$ for $t > t_{\min} = 25$, whose standard deviation is given explicitly for each fit.

FIG. 7. (Color online) Fitting parameter $\tilde{\xi}_t$ at fixed temperature $T \in \{0.35, 1, 6\}$, computed conjointly to $\widetilde{D}_t$ of Fig. 6 and following the same convention regarding the legend.

fixed ratios $\frac{\widetilde{D}_\infty^{\text{SincG}}}{\widetilde{D}_\infty^{\text{Gauss}}} \approx 0.89$ and $\frac{\tilde{\xi}_\infty^{\text{SincG}}}{\tilde{\xi}_\infty^{\text{Gauss}}} \approx 3.27$.

Beyond these asymptotic values of the fitting parameters, their short-'times' behavior can have either a deep physical meaning or be an artifact due to the inadequacy of the fitting function $\mathcal{R}(y)$ for the measured correlator $\bar{R}(t, y)$. The short-'times' increase of $\widetilde{D}_t$ will be dis-

cussed from an analytical point of view in Sec. V B, but for now we compare in Fig. 8 the evolution of the peak $\bar{R}(t, 0)$ deduced from the fits (combining $\mathcal{R}_{\tilde{\xi}=1}^{\text{fit}}(0)$, $\widetilde{D}_t^{\text{fit}}$ and $\tilde{\xi}_t^{\text{fit}}$) to the values measured numerically as a direct consistency check. In Fig. 8 (*top*) we see that at low-T the peak is correctly captured by 'Gauss', and increas-
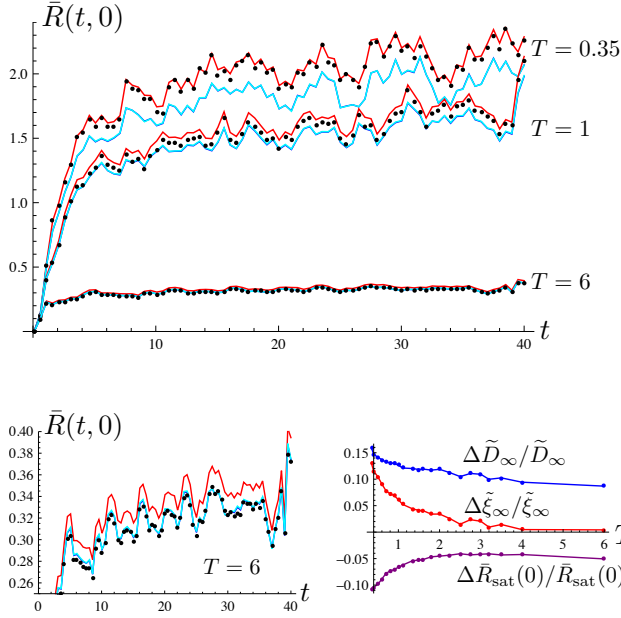
FIG. 8. (Color online) *Top*: 'Time'-evolution of the maximum of the correlator peak $\bar{R}(t,0)$ at fixed temperature $T \in \{0.35, 1, 6\}$, measured numerically (black dots) or predicted by the fitting functions via $\bar{R}^{\text{fit}}(t,0) = \mathcal{R}^{\text{fit}}_{\tilde{\xi}=1}(0) \cdot \widetilde{D}^{\text{fit}}_t / \tilde{\xi}^{\text{fit}}_t$ (red for 'Gauss' (88), blue for 'SincG' (89), cyan for 'CubicS' (I2)-(I3)). The curves for 'SincG' and 'CubicS' systematically coincide. *Bottom left*: Zoom on the high-T case, where the 'SincG' and 'CubicS' predict more accurately the peak at high-T, whereas at low-T 'Gauss' seems more suited. *Bottom right*: Decrease in the relative differences between the 'Gauss' and 'SincG' parameters with increasing temperature, averaged on the large-'time' window $t \in [25,40]$: $\frac{\Delta \widetilde{D}_\infty}{\widetilde{D}_\infty} = \frac{\widetilde{D}^{\text{SincG}}_\infty - \widetilde{D}^{\text{Gauss}}_\infty}{\widetilde{D}^{\text{SincG}}_\infty}$, $\frac{\Delta \tilde{\xi}_\infty}{\tilde{\xi}_\infty} = \frac{\tilde{\xi}^{\text{SincG}}_\infty - \tilde{\xi}^{\text{Gauss}}_\infty \xi^{\text{SincG}} / \xi^{\text{Gauss}}}{\tilde{\xi}^{\text{SincG}}_\infty}$ (cf. end of the Appendix. I) and $\frac{\Delta \bar{R}_{\text{sat}}(0)}{\bar{R}_{\text{sat}}} = \frac{\bar{R}^{\text{SincG}}_{\text{sat}}(0) - \bar{R}^{\text{Gauss}}_{\text{sat}}(0)}{\bar{R}^{\text{SincG}}_{\text{sat}}(0)}$.

ing the temperature the relative difference between the fits decreases anyway; however, zooming on the high-T (*bottom left*) we see that 'CubicS' and 'SincG' catches more precisely the peak. Comparing finally the relative differences between the fits as a function of T (*bottom right*), two temperature regimes can be postulated regarding the normalized function $\mathcal{R}(y)$: at high-T we have $\mathcal{R}(y) \approx \mathcal{R}^{\text{CubicS}}(y)$ with the relative behavior between the fits as expected from Appendix I (geometrical collapse of $\tilde{\xi}^{\text{SincG}}_\infty / \tilde{\xi}^{\text{Gauss}}_\infty \approx \xi^{\text{SincG}} / \xi^{\text{Gauss}}$, overestimation of the amplitude and thus of the peak by 'Gauss'); at low-T the modification of the function $\mathcal{R}(y)$ is essentially pushed into the increasing discrepancy $\Delta \tilde{\xi}_\infty / \tilde{\xi}_\infty$.

As a last consistency check before discussing the actual temperature-dependence of the parameters $\tilde{\xi}_\infty$ and $\widetilde{D}_\infty$, we have measured the evolution of the integral $2 \int_0^{y_m} dy \bar{R}(t,y)$ that should be exactly zero if $y_m \to \infty$. On our restricted numerical window however this integral

fluctuates indeed around zero but very noisily, and once normalized by $\widetilde{D}_\infty$ it remains bounded by 1 consistently with respect to the decomposition (42)-(43).

C. Temperature-dependence of the asymptotic effective disorder $\bar{R}_{\text{sat}}(y)$

In the previous section we have illustrated the 'time'-evolution of the correlator $\bar{R}(t,y)$ for three typical temperatures, and discussed its short-'times' *versus* saturation and low- *versus* high-T regimes regarding the shape $\mathcal{R}(y)$ of its central peak. Now we aim to characterize the temperature-dependence of the amplitude $\widetilde{D}_\infty$ and typical spread $\tilde{\xi}_\infty$ of the correlator, and point out the crossover between the two temperature regimes over the range $T \in [0.35, 6]$ – cf. Appendix H for the complete set of corresponding parameters.

In Fig. 9 we have juxtaposed all the temperature-dependent $\widetilde{D}_t$, $\tilde{\xi}_t$ and $\bar{R}_{\text{sat}}(y)$. We observe graphically that the amplitude $\widetilde{D}_t$ decreases strongly with T and the curves tend to accumulate at lower T, whereas for the typical spread $\tilde{\xi}_t$, it slightly increases (up to 30% nevertheless). These behaviors result in an overall damping of the effective disorder correlator $\bar{R}_{\text{sat}}(y)$ when the thermal fluctuations are developing.

The measured amplitude $\widetilde{D}_\infty$ as a function of T is reported in Fig. 10 for both 'Gauss' and 'SincG' (which collapses with 'CubicS') fits. Qualitatively it decreases in $1/T$ at high-T and saturates at low-T, accordingly to the scaling arguments and GVM predictions of the full model and the DP toymodel (cf. Sec. III B-III C). A parametrization of this temperature crossover has been defined in the relation $\widetilde{D}_\infty(T, \xi) = f(T, \xi) \frac{cD}{T}$ (45) with the interpolating parameter $f(T, \xi)$. Quantitatively its $\xi = 0$ limit requires at high-T that $f \lesssim 1$ without any additional numerical prefactor, but extracting the strength of disorder D from the $1/T$ behavior of $\widetilde{D}_\infty$ actually yields a systematic underestimation with respect to the microscopic disorder: $D^{\text{Gauss}} = 6.72 \pm 0.08$, $D^{\text{SincG}} = 5.92 \pm 0.05$ and $D^{\text{CubicS}} = 5.89 \pm 0.05$ (obtained on the three larger available temperatures), whereas $D = 8$ (86). We attribute again this discrepancy to the negative excursions of $\bar{R}(t,y)$ at large y which bias all the fits and preclude a quantitative test of $f(T, \xi)$.

The crossover temperature cannot be sharply determined from $\widetilde{D}_\infty(T, \xi)$, nevertheless the definition $T_c(\xi) = (\xi cD)^{1/3}$ obtained by GVM (46) and by scaling arguments (56) predicts with $\xi = 2$, $c = 1$ and $D = 8$ that $T_c \approx 2.5$. Without any corrective numerical constant this value is actually compatible with the crossover of the amplitude in Fig. 10 and also of the function $\mathcal{R}(y)$ in Fig. 8 (*bottom left*).

Finally the typical spread $\tilde{\xi}_\infty$ obtained in parallel to $\widetilde{D}_\infty$ is reported in Fig. 11. The collapse of the different fits for $\tilde{\xi}_\infty$ has already been discussed in the previous

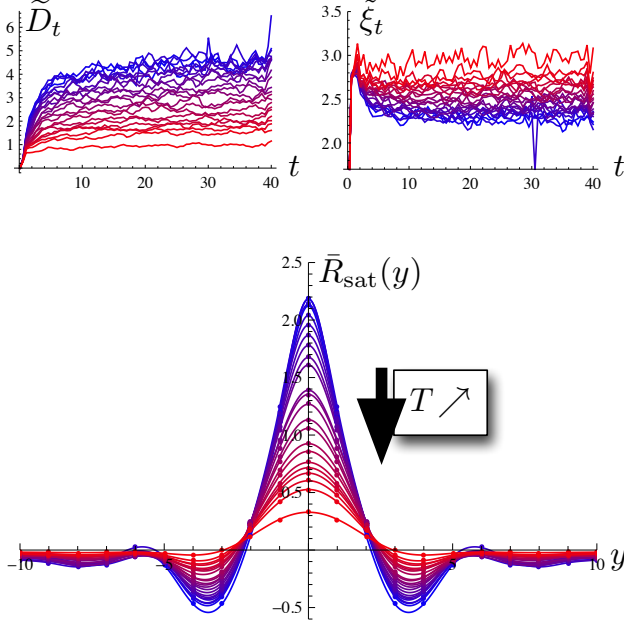FIG. 9. (Color online) Temperature-dependent $\widetilde{D}_t$ and $\tilde{\xi}_t$ for 'SincG' (*top*) and $\bar{R}_{\mathrm{sat}}(y)$ with $t_{\min} = 25$ (*bottom*), for $T \in [0.35, 6]$ as listed in Appendix H. For increasing temperatures (blue to red), $\widetilde{D}_t$ decreases whereas $\tilde{\xi}_t$ slightly increases ($\xi^{\mathrm{grid}} = 2$ for reference), resulting in an overall damping of the correlator $\bar{R}_{\mathrm{sat}}(y)$. The small negative excursion at low-T for $\tilde{\xi}_t$ is an example of the numerical sensitivity of the nonlinear fitting procedure.

subsection; it is compatible with the scenario of a high-T correlator $\mathcal{R}_{\mathrm{sat}}(y) \approx \mathcal{R}^{\mathrm{CubicS}}(y)$. However it displays a temperature-dependence that *a priori* corrects to first-order the minimal assumption that $\tilde{\xi}_\infty \approx \xi$ in our DP toymodel, since the thermal fluctuations seem to increase the effective $\tilde{\xi}_\infty$ compared to the microscopic disorder correlation length $\xi^{\mathrm{grid}} = 2$ (which consistently remains a lower bound in our measured $\tilde{\xi}_\infty^{\mathrm{CubicS}}$). We know from the linearized solution (40) that neglecting the KPZ nonlinearity we recover asymptotically $\frac{cD}{T} \mathcal{R}_\xi^{\mathrm{CubicS}}(y)$ for the correlator, so any modification of $\tilde{\xi}_\infty$ in this two-point correlator can only stem from the KPZ nonlinearity at high-T. A numerical artifact similar to the underestimation of $\widetilde{D}_\infty$ is not to be excluded, but no more conclusions can be drawn from our numerical results.

D. Fluctuations of $\overline{\overline{F_V(t, y)}}$

In its initial definition (12-13), the disorder free-energy $\bar{F}_V(t, y)$ is defined up to a constant $\mathrm{cte}_V(t)$ depending of the chosen path-integral normalization of $W_V(t, y)$ in (3). As far as statistical averages with quenched disorder are concerned, such as (6) and (22), this constant is irrelevant and thus usually completely skipped.
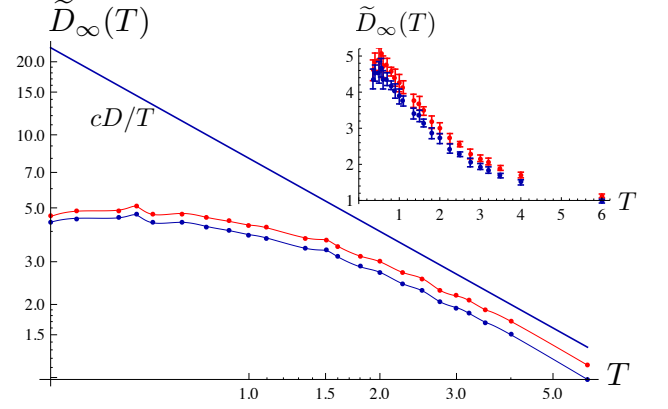
FIG. 10. (Color online) Temperature dependence of $\widetilde{D}_\infty$ with respect to 'Gauss' (red) and 'SincG' (blue). The straight line cD/T indicates the expected behavior in the high-T regime ($cD = 8$ for our data). *Inset*: Corresponding mean and standard deviation for the average of $\widetilde{D}_t$ over $t > t_{\min} = 25$.
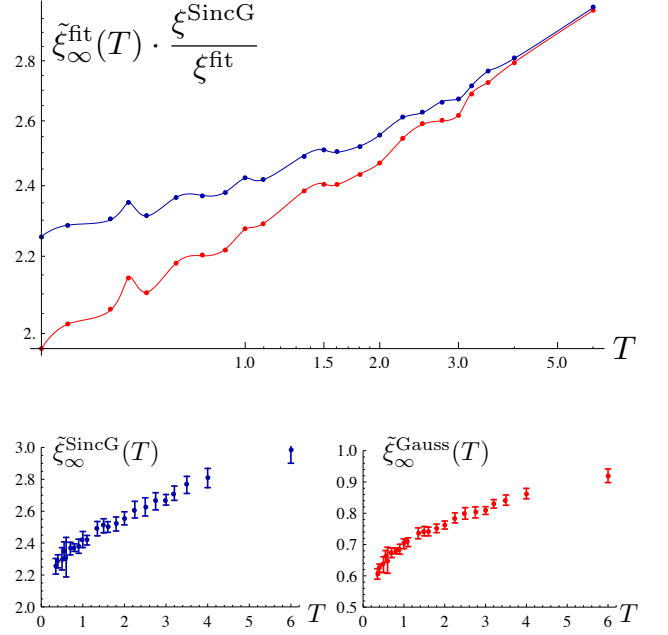
FIG. 11. (Color online) *Top*: Temperature dependence of $\tilde{\xi}_\infty$ with respect to 'Gauss' (red) and 'SincG' (blue), normalized for 'Gauss' with $\xi^{\mathrm{SincG}}/\xi^{\mathrm{Gauss}} \approx 3.6$ (cf. Appendix I). *Bottom*: Corresponding mean and standard deviation for the average of $\tilde{\xi}_t$ over $t > t_{\min} = 25$.

The Feynman-Kac equation (26) actually yields a univocal definition of $\bar{F}_V(t, y)$ which satisfies the STS (17), and as a consequence the evolution of its y-independent mean value is given by (33) starting from the initial condition $\bar{F}_V(0, y) \equiv 0$. In our numerical approach $\overline{\overline{F_V(t, y)}} = \mathrm{cte}(t)$ is in fact a tractable quantity which pro-
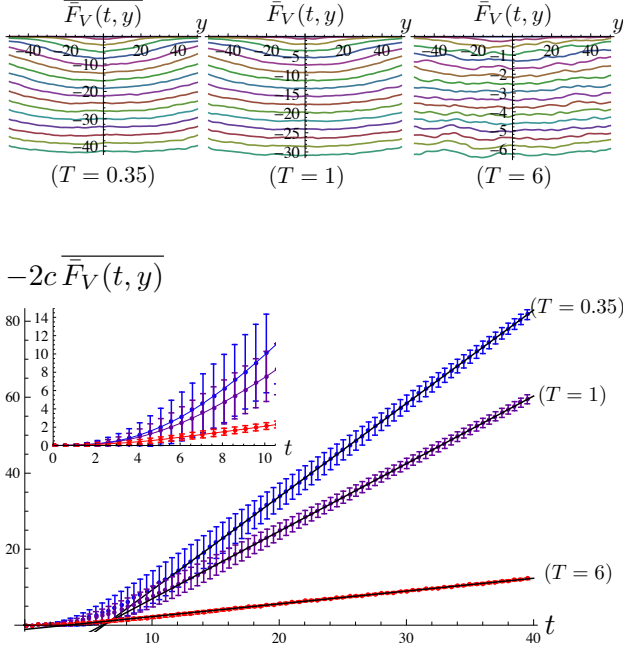
FIG. 12. (Color online) Disorder average of $\bar{F}_V(t,y)$ at fixed temperature $T \in \{0.35, 1, 6\}$. *Top:* $\overline{\bar{F}_V(t,y)}$ as a function of y, for increasing 'times' $t \in [0.1, 40]$ with 'time'-steps $\Delta t = 2.5$ (top to bottom). *Bottom:* $-2c\,\overline{\bar{F}_V(t,y)}$ averaged over y as a function 'time', the error-bars indicating the corresponding standard-deviation; the result of the linear fit for $t > t_{\min} = 25$ is indicated by the straight lines in black.

FIG. 13. (Color online) Temperature-dependent $-2c\,\overline{\bar{F}_V(t,y)}$ averaged over y as a function of 'time', for $T \in [0.35, 6]$ as listed in Appendix H. For increasing temperatures (*blue to red*) the slope decreases as expected by (33). *Inset*: Zoom on the short-'times' behavior in a logarithmic-scale, which shows qualitatively the existence of a saturation 'time' $t_{\rm sat} \approx 10$ marking the beginning of the linear regime at large 'times' (the dotted lines guide the eye for a quadratic behavior $\sim t^2$).

vides an independent way to measure $\bar{R}_{\rm sat}(y=0)$ from its large-'times' linear evolution. This is remarkable and a direct consequence of the KPZ nonlinearity, since linearizing (26) trivially predicts $\overline{\bar{F}_V^{\rm lin}(t,y)} = 0$.

In Fig. 12 we have plotted the disorder average of $\bar{F}_V(t,y)$ at our usual fixed temperature $T \in \{0.35, 1, 6\}$, keeping first the spatial resolution in (t,y) (*top*) and then averaging over the y-direction (*bottom*). $\overline{\bar{F}_V(t,y)}$ should be y-independent, but at short-'time' and low-T it displays a slight curvature that we attribute to the artificial thermal condition at $t_0 = 0.1$; the resulting standard-deviation is strongly reduced at higher T where this initial condition is more accurate with respect to thermal fluctuations.

At large 'times' $\overline{\bar{F}_V(t,y)}$ follows a robust linear behavior which extends down to $t_{\rm sat} \approx 10$, as emphasized in Fig. 12 and generalized to all the temperature spectrum in Fig. 13. Below $t_{\rm sat}$ no clear powerlaw could be identified though the logarithmic scale in Fig. 13 makes explicit a superlinear short-'time' behavior, *a priori* conditioned by the initial thermal condition but see Sec. V B.

We observe graphically in Fig. 14 that the slope is damped with increasing T, which corresponds to the decrease of the maximum $\bar{R}_{\rm sat}(y=0)$ and physically to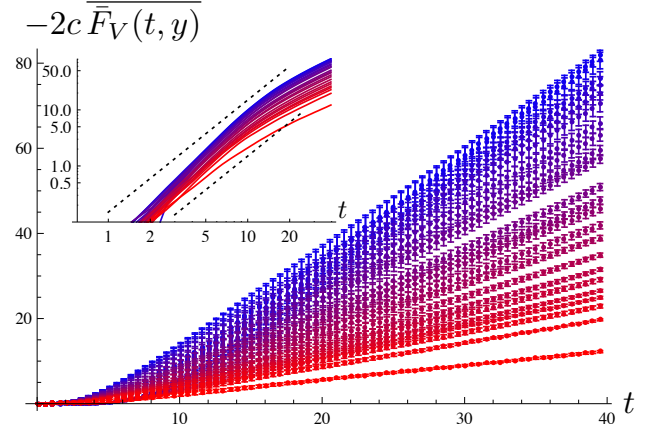 the damping of the effective disorder due to larger thermal fluctuations. A quantitative comparison of the different values of $\bar{R}_{\rm sat}(0)$ as a function of T is given in Fig.14, including a direct measurement on $\bar{R}_{\rm sat}(y)$, the predictions obtained by the fits, and the independent measurement via $\overline{\bar{F}_V(t,y)}$. We find an excellent agreement between these quantities, with a slight crossover of the direct measurement from the 'Gauss' to the 'SincG' fits, and a systematic overestimation of $-2c\,\partial_t\overline{\bar{F}_V(t,y)}$; this last point is an artifact of the short-'times' curvature in y of $\overline{\bar{F}_V(t,y)}$.

After this successful consistency check, one could wonder what would be the quantity which is the more relevant physically: the maximum $\bar{R}_{\rm sat}(y=0)$ or the amplitude $\widetilde{D}_\infty$? The first can be measured independently from $\overline{\partial_y\bar{F}_V(t,y)\partial_y\bar{F}_V(t,0)}$ and $\overline{\bar{F}_V(t,y)}$, whereas the second is obtained assuming a given fitting function $\mathcal{R}(y)$ and biased by the negative excursions at large y (the 'wings' of $\bar{C}(t,y)$). In the limit $\xi = 0$ on one hand $\bar{R}_{\rm sat}(0)$ diverges, whereas $\widetilde{D}_\infty$ remains finite, is given by $\frac{cD}{T}$ and its zero-temperature limit is thus ill-defined. At finite $\xi > 0$ on the other hand $\bar{R}_{\rm sat}(0)$ remains finite, tends to zero at high-T and saturates at low-T as does its amplitude $\widetilde{D}_\infty$. So we need a finite $\xi > 0$ in order to define $\bar{R}_{\rm sat}(0)$ and tackle properly its different limits in temperature; $\widetilde{D}_\infty$ is always regularized and captures the physical content of $\bar{R}_{\rm sat}(0)$, being thus better suited to characterize a potential universal behavior.
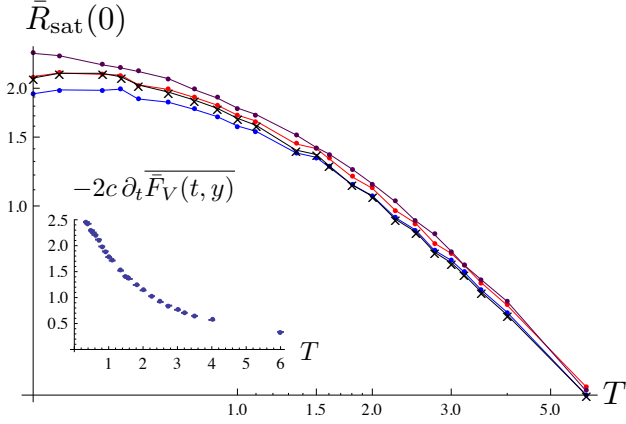
FIG. 14. (Color online) Temperature dependence of the maximum of $\bar{R}_{\text{sat}}(y)$ over 'times' $t \in [25, 40]$, measured by three different ways: first measured numerically directly $\bar{R}_{\text{sat}}(0)$ (black crosses), secondly deduced by the 'Gauss' and 'SincG' fits as in Fig. 8 (respectively red and blue dots), and thirdly measured indirectly from the linear slope of $-2c\,\overline{F_V(t,y)}$ in Fig. 12 (purple dots) and systematically slightly overestimated. *Inset*: The excellent linear behavior of $\overline{\overline{F_V(t,y)}}$ yields vanishing error bars for the slope on the range $t \in [25, 40]$.

E. Temperature-dependence of the roughness function $B(t,T)$ and its exponent $\zeta(t,T)$

Up to now we have analyzed in detail the disorder free-energy fluctuations, specifically the two-point correlator $\bar{R}(t,y) = \frac{1}{2}\partial_y^2 \bar{C}(t,y)$ and the mean $\overline{\overline{F_V(t,y)}}$. Keeping in mind the equivalence between the 'time' t for the DP endpoint and the lengthscale r on the 1D interface (cf. Fig. 1), we focus now on their consequences on the geometrical fluctuations, and specifically on their variance as a function of 'time', namely the roughness $B(t) = \overline{\langle y(t)^2 \rangle}$.

As recalled in Sec. II C after the definition (11), the roughness is expected to display at least two asymptotic powerlaw regimes, crossing from a pure thermal behavior $B(t) \gtrsim B_{\text{th}}(t) = \frac{Tt}{c}$ at short 'times' to the random-manifold $B_{\text{asympt}}(t) \sim \widetilde{D}_\infty^{2/3} t^{4/3}$ at large 'times' – as hinted by scaling arguments (66)-(67) and thus also predicted by GVM (50). Above T_c there is a single crossover Larkin 'time' $t_*(T) = \frac{T^5}{cD^2}$ (54) which diverges with T, and essentially prevents us from observing the completed crossover to the RM regime in our numerical approach in a reasonable computational time for $T > 2$. Below T_c however we expect from Ref. 34 the appearance of an intermediate 'Larkin-modified' roughness regime ending at the generalized Larkin 'time' $L_c(T,\xi)$ (49) which marks the beginning of the RM regime .

Though the GVM framework provides us a prediction $B_{\text{DP}}(t)$ for the full temperature-crossover of our DP toy-model (cf. Appendix A), a complete *quantitative* test of (A7-A10), (A16) and (A17) is hindered by the numeri-

cal constants that are *a priori* present in the determination of $\widetilde{D}$, $\tilde{\xi}$, T_c, L_c and the amplitude of the asymptotic roughness itself $A(c, D, T, \xi)$, due to previously discussed numerical artifacts and also to the GVM approximation. Nevertheless, we observe *qualitatively* these different roughness regimes, as plotted at fixed temperature $T \in \{0.35, 1, 1.8\}$ in Fig. 15, indicating both the total roughness $B(t) = \overline{\langle y(t)^2 \rangle}$ and its pure disorder component $B_{\text{dis}}(t) = B(t) - \frac{Tt}{c} = \overline{\langle y(t)^2 \rangle}^c$ as stated by the STS (B12)-(B13). In all three graphs we can follow the crossover from the thermal asymptote (red) to the RM asymptote (green) which stems from the increasing $B_{\text{dis}}(t)$ added to $B_{\text{th}}(t)$. Note that the RM asymptote has been constructed consistently with (50) with a numerical correction fixed once and for all from the dataset $T = 0.4$ averaged over $t \in [25, 40]$, assumed to be already in the RM regime:

$$\frac{B_{\text{asympt}}(t)}{t^{4/3}} \approx \text{corr}_{(T=0.4)} \cdot \frac{3}{2^{2/3}\pi^{1/3}} \left[\frac{\widetilde{D}_\infty^{\text{SincG}}(T,\xi)}{c^2} \right]^{2/3} \tag{90}$$

with $\text{corr}_{(T=0.4)} = 0.292 \pm 0.008$. This RM asymptote is graphically consistent with all the available datasets in the range $T \in [0.35, 1.8]$, which plays in favour of a numerical corrective factor common to all temperatures and absorbing the discrepancy in $B_{\text{asympt}}(t)$ stemming from $\widetilde{D}_\infty$ and the GVM. The low-T regime is illustrated by $T = 0.35$ where the intermediate 'Larkin-modified' regime is clearly present, whereas it has disappeared as such already at $T = 1$.

Larger 'times' have been explored at $T = 1.8$ which is believed to be close to T_c (cf. Sec.IV C), and is consistent with lower temperatures except for a sudden increase at $t > 400$ which can clearly be attributed to the finite size of the box $y \in [-y_m, y_m]$ – the condition $\sqrt{B(t)} < y_m$ translates into $B(t) < 160^2 = 2.5 \cdot 10^4$ for this dataset and yields an adequate upper bound in Fig. 15 (*bottom*). The corresponding upper bound for most of the datasets is $B(t) < 40^2 = 160$ thus the range of roughness displayed in all the other graphs.

Gathering in Fig. 16 the roughness $B(t)$ and $B_{\text{dis}}(t)$ over the range $T \in [0.35, 6]$, we observe as expected with increasing temperature that the disorder roughness $B_{\text{dis}}(t)$ is progressively damped by thermal fluctuations and thus that the intermediate 'Larkin-modified' regime shrinks with increasing temperature. The beginning of the RM regime is consequently pushed to larger 'times', as it could also be deduced by the condition that $B_{\text{dis}}(t)$ becomes comparable to $B_{\text{th}}(t)$ close to the Larkin 'time' $t = L_c$. From the point of view of the 1D interface, the temperature-dependence of $B_{\text{dis}}(t)$ can be physically understood with the following picture: at small lengthscales the thermal fluctuations make the interface rougher within the local valleys of the disordered free-energy landscape and $B(t) \gtrsim B_{\text{th}}(t)$ increases with T as expected; at large lengthscales on the contrary thermal fluctuations allow the interface to explore more
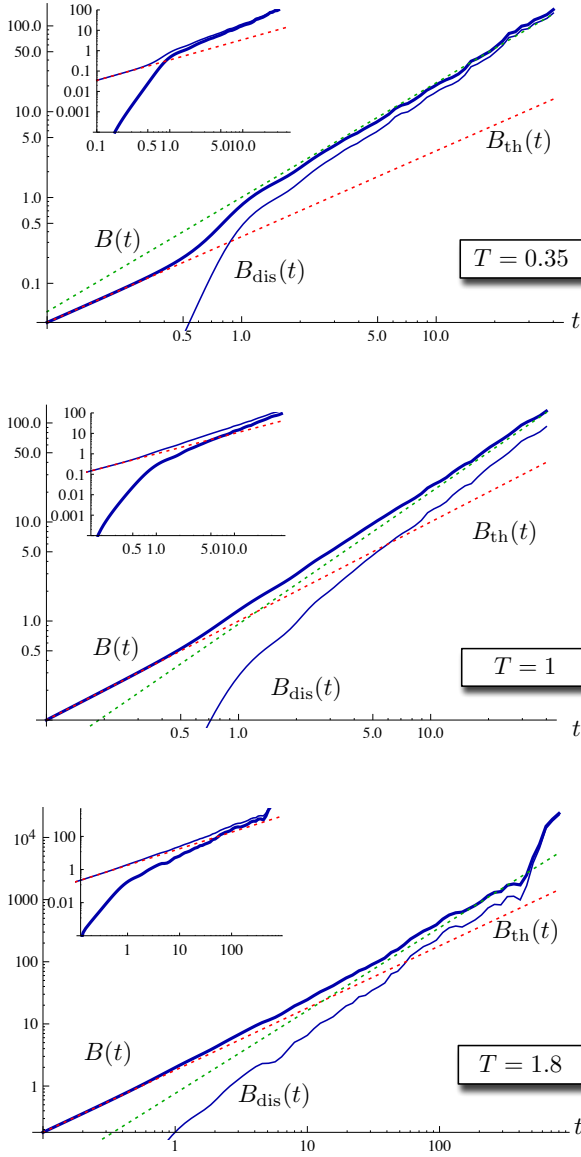
FIG. 15. (Color online) Roughness $B(t) = \overline{\langle y(t)^2 \rangle}$ and its disorder component $B_{\text{dis}}(t) = B(t) - \frac{Tt}{c} = \overline{\langle y(t)^2 \rangle}^c$ measured numerically at fixed temperature $T \in \{0.35, 1, 1.8\}$. *Main*: Focus on the crossover of $B(t)$ (thick) from the pure thermal behavior $B_{\text{th}}(t) = \frac{Tt}{c}$ (dotted red) at short 'times' to the asymptotic $B_{\text{asympt}}(t) \sim \widetilde{D}_\infty(T)^{2/3} t^{4/3}$ (dotted green) at asymptotically large 'times'; $B_{\text{dis}}(t)$ is the thinner lower curve. *Inset*: Focus on the short-'times' crossover of $B_{\text{dis}}(t)$ (thick), in parallel to $B(t)$ (thin).

effectively the free-energy landscape by overcoming some free-energy barriers in order to minimize its elastic energy and thus have $B_{\text{asympt}}(t)$ decreasing with T. From the point of view of the DP, these behaviors are encoded in the evolution of the translation-invariant distribution $\bar{\mathcal{P}}\left[\bar{F}, t\right]$ (17), the integration of the microscopic disorder $V(t', y')$ explored by the elastic DP over 'times' $[0, t]$
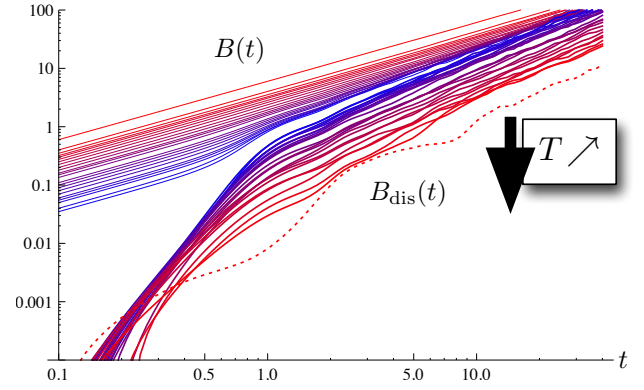

FIG. 16. (Color online) Temperature-dependent roughness $B(t) = \overline{\langle y(t)^2 \rangle}$ and its disorder component $B_{\text{dis}}(t)$ (in logarithmic scale, respectively top and bottom curves), for $T \in [0.35, 6]$ as listed in Appendix H (blue to red for increasing temperatures). $B_{\text{dis}}(t)$ for $T = 6$ is indicated in dotted red.

defining the effective disorder $\bar{F}_V(t, y)$ and consequently the DP-endpoint fluctuations (22). The saturation at low-T of the amplitude $\widetilde{D}_\infty$ in Fig. 10 and of the peak $\bar{R}(t, 0)$ in Fig. 14 naturally translates into a saturation of the asymptotic amplitude of the roughness (90).

In order to focus on the disorder contribution, we have computed numerically directly $\bar{F}_V(t, y)$, but regarding the roughness we had first to construct the total free-energy $F = F_{\text{th}} + \bar{F}$, then compute the total roughness $B(t)$ and eventually deduce its disorder component $B_{\text{dis}} = B - B_{\text{th}}$. This quantity is thus more subject to noise at higher T (see *i.e.* $T = 6$ in Fig. 16), but especially at low-T it clearly displays two regimes in 'time'. To address the question of a possible powerlaw at short-'times', the logarithmic slope $\zeta_{(\text{dis})}(t) = \frac{1}{2} \frac{\partial B_{(\text{dis})}(t)}{\partial \log t}$ is plotted in Fig. 17. While $\zeta(t)$ crosses over as expected from $\zeta_{\text{th}} = \frac{1}{2}$ to $\zeta_{\text{RM}} = \frac{2}{3}$ but excludes the definition of an intermediate-'times' powerlaw for $B(t)$, $\zeta_{\text{dis}}(t)$ on the contrary displays a plateau at low-T which disappears already at $T = 1$, a tendency confirmed at $T = 1.8$. Accordingly to the GVM prediction (A8) $B_{\text{dis}}(t)$ should start in $\sim \frac{\widetilde{D}}{c^2} t^2 / \tilde{\xi}$ in which case the value of the plateau would have 1 as a lower band and only a 'time'-dependence of $\widetilde{D}_t$ and/or $\tilde{\xi}_t$ could correct ζ_{dis} to match the GVM prediction, which is anyway not to be trusted *a priori* at 'times' shorter than L_c (cf. Sec. III B). The value of this plateau exhibits moreover a slight temperature-dependence, which cannot be accounted for by our DP toymodel but might also simply be an artifact of the thermal condition imposed at $t_0 = 0.1$. Note finally that all these effects on $B_{\text{dis}}(t)$ take place before $t_{\text{sat}} \approx 10$ as estimated on the saturation of the free-energy correlator $\bar{R}(t, y)$ in the previous sections.

As a last remark in this numerical study of the 1+1 DP fluctuations with a finite disorder correlation length, we
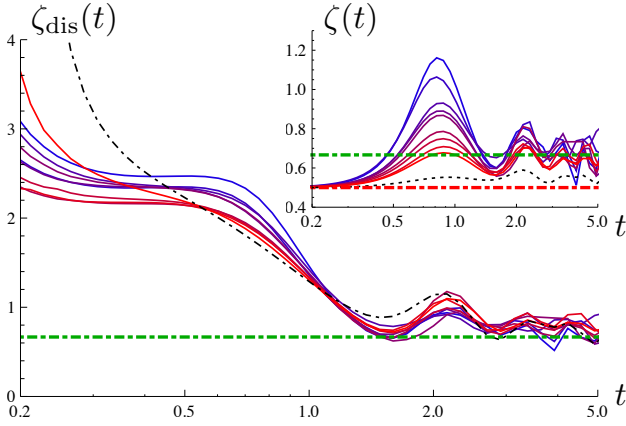
FIG. 17. (Color online) Logarithmic slope of the roughness, $\zeta(t)$ and $\zeta_{\rm dis}(t)$ obtained respectively from $B(t)$ and $B_{\rm dis}(t)$ of Fig. 16, for $T \in [0.35, 1]$ (blue to red for increasing temperatures) and $T = 1.8$ (in dashed dotted black). The thermal exponent $\zeta_{\rm th} = \frac{1}{2}$ and the RM exponent $\zeta_{\rm RM} = \frac{2}{3}$ are indicated by the dashed dotted lines, respectively red and green. At larger 'times' those logarithmic slopes are very noisy but still oscillate around the expected value $\zeta_{\rm RM} = \frac{2}{3}$.

check the assertion that the PDF $\mathcal{P}(t,y)$ of the DP endpoint is 'fairly Gaussian' (10), already checked at $\xi = 0$ in the RM asymptotic regime[40]. We have computed independently the higher moments $\overline{\langle |y(t)|^k \rangle}$ ($2 \leq k \leq 6$) of the PDF and renormalized them by the Gaussian 'time'-independent coefficients $\sqrt{2}\left[\Gamma\left(\frac{k+1}{2}\right)/\sqrt{\pi}\right]^{1/k}$ with Γ the Euler function. If $\mathcal{P}(t,y)$ is a pure Gaussian function, these renormalized moments should perfectly collapse on each other at all 'times', as it is the case in at short 'times' where $\mathcal{P} \approx \mathcal{P}_{\rm th}$ and remains reasonably so by naked-eye in the intermediate 'Larkin-modified' regime. At 'times' above the Larkin 'time' we observe only a very light fanning of the renormalized moments, showing the consistency of our observations at $\xi > 0$ with respect to the previous numerical studies at $\xi = 0$.

V. DISCUSSION

A. Synthetical outlook

We addressed throughout this paper the consequences of a *finite* correlation length $\xi > 0$ of the microscopic disorder $V(t,y)$ explored by a 1+1 DP, or alternatively of a 1D-interface finite width which is always present in experimental systems. On one hand, several analytical arguments yielding exact results at $\xi = 0$ break down as such, questioning their generalization to $\xi > 0$. On the other hand, despite a lack of exact analytical expressions the finiteness of this quantity allows to control the scalings and the low-temperature limit of the model (see Sec. III C-III D), avoiding the pathological and un-

physical divergences that appear at $\xi = 0$, in particular conjointly to the limit $T \to 0$.

In order to tackle the case at $\xi > 0$, the 1+1 DP formulation allows to follow effective quantities at fixed length-scale or growing 'time', in an approach thus conceptually similar to the FRG which focuses on the flow and fixed points of the disorder correlator (denoted Δ or R[32,33,64]). Considering the free-energy at fixed disorder (averaging over the thermal fluctuations but one step before the disorder average), it is thus possible to disconnect theoretically and numerically the two statistical averages, and even to focus on the pure disorder contributions thanks to the STS and the Feynman-Kac equations for $\bar{F}_V$ and its derivative η_V (see Sec. II D). Those two quantities are not directly accessible experimentally (except for liquid crystals, as discussed later in Sec. VI) and are *a priori* more complex to handle since they encode more information than direct observables such as the geometrical fluctuations and the roughness. However they actually display a simpler phenomenology by disconnecting the thermal and disorder effects and the different lengthscales, whereas the roughness $B(t)$ intricates all of them.

Although $\bar{\mathcal{P}}\left[\bar{F}\right]$ and $\bar{\mathcal{P}}\left[\eta\right]$ are not Gaussian at $\xi > 0$ not even in the infinite-'time' limit, their main features are encoded in the two-point correlators $\bar{C}(t,y)$ and $\bar{R}(t,y)$, *i.e.* the scalings of $\bar{C}$ and $\bar{R}$ dominate the higher moments of the PDFs, similarly to the case $\xi = 0$ (see Sec. III A). This supports consequently the construction of the toymodel of Sec. III B, which relies on the assumption that the PDFs can be approximated as Gaussian ones described by a given set of two-point correlators. The numerical results of Sec. IV are indeed qualitatively in agreement with the GVM predictions derived from this DP toymodel (see Appendix A), in the range of numerical parameters that we have considered (see Appendix H). The study of the two-point correlator $\bar{R}$ provides thus a vantage point on the DP properties, first at asymptotically large 'times' (keeping in mind that the infinite-'time' limit simplifies the analytical treatment of the RM regime, *i.e.* via a Fokker-Planck approach as in Appendix F) and secondly at finite 'time' with the connection to the short-'times' regime.

In order to characterize the asymptotic large-'times' behavior, which can potentially display universality, a central quantity is the saturation amplitude of the effective disorder *i.e.* $\widetilde{D}_\infty(T,\xi)$. At fixed $\xi > 0$ it is equivalent to the maximum of the saturation correlator $\bar{R}_{\rm sat}(y = 0)$ which is equal to $\widetilde{D}_\infty/\tilde{\xi}_\infty \cdot \mathcal{R}_{\tilde{\xi}=1}(y = 0)$. However for a δ-correlated microscopic disorder $R_{\xi=0}(y) = \delta(y)$, $\bar{R}_{\rm sat}(y = 0)$ diverges whereas the amplitude $\widetilde{D}_\infty/\tilde{\xi}_\infty$ remains well-defined. It is remarkable to notice that from the whole saturation correlator, the quantity $\widetilde{D}_\infty$ is the only feature that eventually plays a role in the asymptotic roughness in GVM or scaling arguments *e.g.* in (50), the specificity of the (normalized) RB disorder correlator $R_\xi(y)$ (1) and thus of the function $\mathcal{R}(y)$ being then gathered into a numerical constant. $\widetilde{D}_\infty(T,\xi)$ *appears to*

be the relevant quantity for a universal description of the crossover between low- and high-T asymptotic DP fluctuations, from an analytical point of view and in agreement with the numerical results in Sec. IV. Going one step further, the crossover from its $\xi = 0$ (or high-T) limit is better described by the interpolating parameter $f(T, \xi) = \widetilde{D}_\infty(T, \xi)/\left(\frac{cD}{T}\right)$ first introduced in (45) and expected to rescale also the characteristic scales such as $L_c(T, \xi)$ according to the relations (58)-(61) obtained by pure scaling arguments. The GVM framework yields the two predictions (46) and (70) for $f(T, \xi)$ derived from the value of the full-RSB cutoff (cf. Appendix A), and a third analytical prediction will be presented in the next subsection V B; all of them predict a monotonous crossover connecting the limits $T = 0$ and $\xi = 0$ (62)-(64) with a polynomial equation on $f(T, \xi)$, which is qualitatively consistent with the numerical results (see Fig. 10) but suffers quantitatively from the variational approximation and several corrective factors as discussed throughout Sec. IV. Nevertheless an important and successful test for all this discussion is the independent but consistent numerical determinations of $R_{\mathrm{sat}}(y = 0)$ in Fig. 14, also with respect to $\partial_t \overline{F_V(t, y)}$, and the adequacy of the deduced asymptotes $B_{\mathrm{asympt}}(t)$ in Fig. 15, having systematically tested and discussed the small and controlled discrepancies of the different fitting functions ('Gauss', 'SincG' and 'CubicS' defined in Sec. IV A).

Note that although the two communities of physicists and mathematicians work with two different conventions, respectively at fixed elastic constant c (the choice $c = 1$ essentially fixing the units of energy) versus at $c = T$ (as discussed in Appendix G), all the above discussion remains valid in both conventions, although the choice $c = T$ leads to other limits in temperature. The two opposite limits at high-T (or $\xi \approx 0$) $\widetilde{D}_\infty \approx \frac{cD}{T}$, and at low-$T$ (or $\xi > 0$ and below $T_c(\xi) = (\xi cD)^{1/3}$) $\widetilde{D}_\infty \approx \frac{cD}{T_c} = (c^2 D^2 \xi^{-1})^{1/3}$ translate with the convention $c = T$ into $\widetilde{D}_\infty \approx D$ and $\widetilde{D}_\infty \approx T^{2/3} D^{2/3} \xi^{-1/3}$ respectively above and below $T_c^{\mathrm{m}} = \sqrt{\xi D}$ (deduced self-consistently from $T_c^{\mathrm{m}} = (\xi cD)^{1/3} = (\xi T_c^{\mathrm{m}} D)^{1/3}$). In the course of the study of the rescaling of the correlator $\bar{C}(t, y)$ with respect to the roughness $B(t)$ in Ref. 46, it has been noticed that in the regime $|y| \lesssim \sqrt{B(t)}$ we have numerically as expected a linear behavior $\bar{C}(t, y) \propto |y|$ but with a by-product prefactor that corresponds precisely to our $\widetilde{D}_\infty$. Taking as a criterion the collapse of the curves $\bar{C}(t, y)$ at different temperatures on an arbitrary chosen curve, the temperature dependence of this prefactor is consistent with all our analysis on the origin and interpretation of $\widetilde{D}_\infty(T, \xi)$ (see the insets in Fig. 10 and Fig. 14 of Ref. 46, which illustrate respectively the conventions $c = T$ versus independently fixed $c = 1$ and T).

As for the finite-'time' behavior, especially at short-'times' it is sensitive to the specific microscopic disorder correlator, thus compromising a possible universality. The 'time'-evolution displays essentially two regimes on the fluctuations of the disorder free-energy, separated by t_{sat} (whose order of magnitude has been crudely estimated in our numerical study to $t_{\mathrm{sat}} \lesssim 10$): starting from the initial condition $\bar{R}(0, y) \equiv 0$, the central peak of the correlator $\bar{R}(t, y)$ develops itself keeping the integral $\int_{\mathbb{R}} dy\, \bar{R}(t, y) = 0$ constant, till it reaches the saturation shape $\widetilde{D}_\infty \mathcal{R}_{\tilde{\xi}}(y)$ compensated by negative bumps according to the generic decomposition (42)-(43) as illustrated in Fig. 3. Since $\partial_y^2 \bar{C}(t, y) = 2R(t, y)$, after the double integration (21) the correlator $\bar{C}(t, y)$ starts from the initial condition $\bar{C}(0, y) \equiv 0$ and at fixed 'time' above t_{sat} it is rounded at $|y| \lesssim \xi$, increases then linearly $\bar{C}(t, y) \approx \widetilde{D}_\infty |y|$ at $\xi \lesssim |y| \sqrt{B(t)}$ and is constant for any larger $|y|$ (see again Fig. 3). On one hand, the position ℓ_t of these 'wings' of $\bar{C}(t, y)$ or equivalently of the negative bumps of $\bar{R}(t, y)$ is discussed at length in Ref. 46 and identified to correspond physically to the typical position of the DP endpoint, $\ell_t \approx \sqrt{B(t)}$, in the different roughness regimes and even below the Larkin length L_c. On the other hand, what happens below t_{sat} cannot be understood without taking into account the whole microscopic disorder correlator $R_\xi(y)$, whose feedback via the KPZ nonlinearity at small $|y|$ modifies the amplitude $\widetilde{D}_\infty(T, \xi)$ and the shape $\mathcal{R}_{\tilde{\xi}}(y)$ above the saturation, especially in the low-T regime and in any case with $t_{\mathrm{sat}} \leq L_c$. Neglecting the KPZ nonlinearity yields the prediction (40)-(41) which mixes different limits: the $\xi = 0$ (high-T) amplitude $\widetilde{D}_\infty = \frac{cD}{T}$, the same correlator as the microscopic disorder $\mathcal{R}_{\tilde{\xi}}(y) = R_\xi(y)$, and the 'wings' rescaled with respect to the pure thermal roughness $B_{\mathrm{th}}(t)$ at all lengthscales (this diffusive behavior being for sure an artifact of the linearization). In the low-T regime, we believe that by generating relevant non-Gaussian correlations such as $\bar{R}_3$ and $\bar{C}_3$ below t_{sat}, the KPZ nonlinearity introduces an effective kernel for $\bar{R}$ that modifies simultaneously $\widetilde{D}_\infty$ and $\mathcal{R}_{\tilde{\xi}}(y)$, with in particular the saturation below T_c of the amplitude $\widetilde{D}_\infty \approx \frac{cD}{T_c}$ as predicted by scaling arguments in Sec. III C.

The phenomenology of the DP fluctuations is simpler from the point of view of the disorder free-energy $\bar{F}_V$, via its two-point correlators $\bar{R}$ and $\bar{C}$ which display two 'time'-regimes separated by t_{sat}. From the competition between the typical $\bar{F}_V$ and the thermal F_{th} the resulting roughness $B_{\mathrm{dis}}(t)$ also displays two regimes as observed numerically in Fig. 16 and 17. However, when recombined with the pure thermal effect the roughness $B(t)$ displays two or three 'time'-regimes respectively at high-T (thermal and RM regimes) and low-T (with an additional intermediate 'Larkin-modified' regime), with L_c at the beginning of the RM regime, as predicted by GVM and observed numerically. The disorder free-energy is an effective quantity which encodes the microscopic disorder explored by the polymer, there is consequently a feedback between the geometrical fluctuations $\mathcal{P}(t, y)$ and the free-energy correlations $\bar{C}(t, y)$: firstly the existence of 'wings' in $\bar{C}(t, y)$ are imposed physically by the finite variance of the PDF $\mathcal{P}(t, y)$ (the polymer does not explore often regions $|y| > \sqrt{B(t)}$ so these regions do not

contribute much to the correlator $\bar{C}(t,y)$); secondly the PDF $\mathcal{P}(t,y)$ is deduced from the competition between F_{th} and $\bar{F}_V \sim \bar{C}^{1/2}$, the maximum of the typical $\bar{F}_V$ being precisely fixed by the 'wings' of $\bar{C}$; thirdly the 'wings' of $\bar{C}$ or the bumps in $\bar{R}$ can be skipped for a GVM computation of the roughness, providing a self-consistent justification of our DP toymodel. Beyond the scaling in 'time' of those fluctuations, which we plainly understand physically now, their temperature dependence at all 'times' is finally determined by the integrated disorder up to $t_{\text{sat}} \leq L_c$, where the KPZ non-linearity plays a crucial role below $T_c(\xi)$.

B. Effective evolution in 'time' and temperature of the amplitude $\tilde{D}_t$

Having this global picture in mind, we can now gather all the physical intuition we have obtained and construct the following analytical argument in order to obtain an evolution equation for the amplitude $\tilde{D}_t$.

The evolution of the correlator $\bar{R}(t,y)$, given by the 'flow' equation (34), cannot be solved directly since it brings into play the three-point correlation function $\bar{R}_3(t,y)$, a hallmark of the KPZ non-linearity. To extract an exact information from this flow one should in principle solve the full hierarchy of equations connecting the whole set of n-point correlation functions, a task which seems however out of reach. As we will detail thereafter, the restriction of the flow to the vicinity of $y = 0$ leads in fact to an (approximate) closed equation on the height $\bar{R}(t,0)$ of the two-point correlator. It will allow to pinpoint the role of the non-linearity in the temperature-dependence of the asymptotic $\tilde{D}_\infty(T,\xi)$ and its interpolating parameter $f(\xi,T)$ defined by (45), and give more insight into the short-'time' behavior of $\tilde{D}_t$ and $\overline{\bar{F}_V(t,y)}$ (with respect to (33)).

1. Rescalings of R, $\bar{R}$, $\bar{R}_3$ and η_V

From (34), the flow of $\bar{R}(t,y)$ in $y = 0$ reads

$$\partial_t \bar{R}(t,0) = \frac{T}{c}\bar{R}''(t,0) - \frac{1}{c}\bar{R}'_3(t,0) - \frac{1}{t}\bar{R}(t,0) - DR''_\xi(0) \tag{91}$$

(throughout this section we denote for short the derivative with respect to y by a prime). Although this equation is exact, it cannot be solved directly since the three-point correlator $\bar{R}_3$ is not known. To go further and try to find out what relations between the physical parameters it might nevertheless imply, one has to surmise a (minimal) scaling form of the different correlators and their first derivatives.

Let's first consider the known scaling of the micro-

scopic disorder correlator $R_\xi(y)$:

$$DR_\xi(y) \overset{(y\to 0)}{\approx} D\Big[R_\xi(0) + R''_\xi(0)\frac{y^2}{2}\Big] = c_0\frac{D}{\xi}\Big[1 - c_1\frac{y^2}{2\xi^2}\Big] \tag{92}$$

where $c_0 = R_\xi(0)|_{\xi=1}$ and $c_1 = -\frac{R''_\xi(0)}{R_\xi(0)}\Big|_{\xi=1}$ are numerical constants, independent of ξ and reflecting the specific geometry of the correlator around the origin. For instance when the correlator is a Gaussian function $R_\xi(y) = \mathcal{R}^{\text{Gauss}}_\xi(y)$ defined by (88), one has $c_0 = \frac{1}{\sqrt{4\pi}}$ and $c_1 = \frac{1}{2}$.

By analogy with (92) and supported by the numerical test of our DP toymodel in Sec. IV B, we now assume that the correlator $\bar{R}(t,y)$ scales around $y \approx 0$ as

$$\bar{R}(t,y) \overset{(y\to 0)}{\approx} c_2\frac{\tilde{D}_t}{\xi}\Big(1 - c_3\frac{y^2}{2\xi^2}\Big) \tag{93}$$

Here, c_2 and c_3 are numerical constants independent of the parameters (c,D,T,ξ,t):

$$c_2 = \bar{R}(t,0)\Big|_{\substack{\xi=1 \\ \tilde{D}_t=1}}, \qquad c_2 c_3 = -\bar{R}''(t,0)\Big|_{\substack{\xi=1 \\ \tilde{D}_t=1}} \tag{94}$$

while $c_2\frac{\tilde{D}_t}{\xi}$ is the height of the central peak $\bar{R}(t,0)$ assumed to capture all the dependence in the parameters. c_2 is actually defined so that the $\xi \to 0$ limit (38) is recovered:

$$\tilde{D}_\infty(T,\xi) \equiv \lim_{t\to\infty}\tilde{D}_t = \int_\mathbb{R} dy \cdot \bar{R}(\infty,y) > 0 \tag{95}$$

$$\lim_{\xi\to 0}\tilde{D}_\infty(T,\xi) = \frac{cD}{T} \tag{96}$$

which is known to hold exactly, without any additional numerical constant. The constant c_2 depends on global properties of the infinite-'time' limit of the correlator, in the sense that it is constrained by (95)-(96). The main assumption in the scaling form (93) is actually that the curvature of the correlator $\bar{R}(t,y)$ at the top of its central peak happens on a scale $\xi/\sqrt{c_3}$ which corresponds to $\tilde{\xi}_\infty$ and is independent of 'time' and $\{c,D,T\}$. This assumption is not exact at all 'times', but we expect that it captures anyway the main features of the geometry of the correlator $\bar{R}(t,y)$ close to its central peak.

Finally the three-point correlation function is assumed to scale in $\tilde{D}_t$ and ξ in the same way as it naively does merely by counting the number of occurrences of η in the definition (D11) of $\bar{R}_3(t,y)$ (i.e. inferred from $\bar{R} \sim \overline{\eta\eta}$, $\bar{R}_3 \sim \overline{\eta\eta\eta}$ and rescaling also the derivative ∂_y):

$$\bar{R}'_3(t,0) = c_4\frac{\tilde{D}_t^{3/2}}{\xi^{5/2}} \quad \text{with} \quad c_4 = \bar{R}'_3(t,0)\Big|_{\substack{\xi=1 \\ \tilde{D}_t=1}} \tag{97}$$

Here c_4 is also assumed to be a numerical constant. If this form is again not expected to be exact at all 'times', it can still be thought as a reasonable approximation provided the three-point correlator $\bar{R}'_3(t,y)$ is analytic
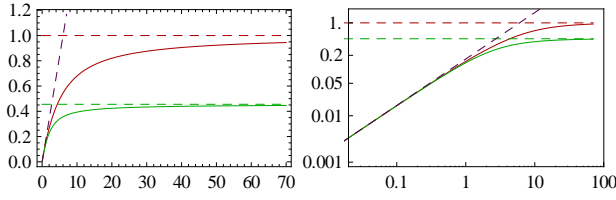
FIG. 18. (Color online) $\widetilde{D}_t$ as a function of t (*left*: linear scale, *right*: logarithmic scale). In green (bottom curve), the solution of the full differential equation (99); in red (top curve), the solution of the equation without the non-linear KPZ term; the dashed horizontal lines are the corresponding large-'time' asymptotics; in purple dashed, the short-'time' asymptotics (102). Chosen parameters: $c = D = T = \xi = 1$, $c_0 = c_2 = \frac{1}{\sqrt{4\pi}}$, $c_1 = c_3 = \frac{1}{2}$, $c_4 = \frac{1}{4}$.

around $y = 0$. This last assumption is justified for instance in view of the zero-temperature and infinite-'time' limit of the 'flow' equation (34) (under the stationarity condition $\partial_t \bar{R} = 0$), which yields that the three-point correlator $\lim_{t\to\infty} \bar{R}'_3(t, y)$ is merely proportional to $R''_\xi(y)$, which is analytic around $y = 0$.

Note finally that the scalings (92), (93), (97) are all compatible with the following rescaling in distribution (also inferred from $\overline{\eta\eta} \sim \bar{R}$)

$$\eta(t, y) \overset{(d)}{=} \left(\frac{\widetilde{D}_t}{a}\right)^{\frac{1}{2}} \eta(t, \tfrac{y}{a})\big|_{\xi/a} \qquad (98)$$

for all values of the rescaling parameter a. A way to reformulate the definitions (94) and (97) of the numerical constants $\{c_2, c_3, c_4\}$ is thus to identify those constants with the corresponding derivatives of the correlator $\bar{R}(t, y)$ taken at $a = \xi$ and $\widetilde{D}_t = 1$, which ensures their independence with respect to the other parameters.

2. Evolution of $\widetilde{D}_t$ and prediction for $\widetilde{D}_\infty$ and $f(T, \xi)$

Substituting the rescalings (92), (93), (97) into (91) transforms the equation for $\bar{R}(t, 0)$ into an effective closed evolution equation for the amplitude:

$$\partial_t \widetilde{D}_t + \frac{2}{t}\widetilde{D}_t = -c_3\frac{T}{c\xi^2}\widetilde{D}_t - \frac{c_4}{c_2}\frac{1}{c\xi^{3/2}}\widetilde{D}_t^{3/2} + \frac{c_0 c_1}{c_2}\frac{D}{\xi^2} \quad (99)$$

The non-linear KPZ term of the equation of evolution for $F(t, y)$ corresponds to the term $\propto \widetilde{D}_t^{3/2}$. The numerical solution of this equation is plotted in Fig. 18.

To tackle the infinite-'time' case, we have introduced in Sec. III B-III C the interpolating parameter f and identified it as the full-RSB cutoff in the GVM predictions (cf. Appendix A). By cancelling the right-hand side of (99) and introducing the interpolating parameter $f(c, D, T, \xi) = \widetilde{D}_\infty / \frac{cD}{T}$ as in (45), one obtains a new equation for f:

$$f^{3/2} = \frac{c_2 c_3}{c_4}\left[\frac{T}{T_c(\xi)}\right]^{3/2}\left(\frac{c_0 c_1}{c_2 c_3} - f\right) \qquad (100)$$

where $T_c(\xi) = (\xi c D)^{1/3}$ is the same characteristic temperature as the one obtained in Sec. III C by scaling.

Noting that c_2 is defined in (94) precisely so that it absorbs all the quantitative contribution of the geometry of $\bar{R}$, the condition (96) guarantees that $\lim_{\xi\to 0} f = 1$. The $\xi \to 0$ solution of (100) is then $f = \frac{c_0 c_1}{c_2 c_3}$ so one obtains eventually that $\frac{c_0 c_1}{c_2 c_3} = 1$. This is valid for all values of the parameters if the $\{c_i\}$ are indeed parameter-independent. However those numerical constants are constrained only by the geometry of $\bar{R}(t, y)$, and we know from the numerical study in Sec. IV C that at large 'times' the correlator saturates to a $\bar{R}_{\text{sat}}(y) \approx \widetilde{D}_\infty \mathcal{R}(y)$ with only a slight T-dependence of the function $\mathcal{R}$.

Disregarding this possible but small modification of the numerical constant depending on T, the equation for the interpolating parameter finally reads

$$f^\gamma = \frac{c_0 c_1}{c_4}\left(\frac{T}{T_c}\right)^\gamma (1 - f) \quad \text{with} \quad \gamma = \frac{3}{2} \qquad (101)$$

Strikingly, it takes a form very similar to the equations (46) and (70) obtained in Sec. III from the GVM approach, with an exponent $\gamma = 6$ instead of $\gamma = \frac{3}{2}$. In fact the value of this exponent only influences the specific monotonous crossover from the high-T regime, where the KPZ term has little influence ($f \lesssim 1$) to the low-T asymptotics where f is linear in T as $f \overset{(T\to 0)}{\sim} \left(\frac{c_0 c_1}{c_4}\right)^{\frac{1}{\gamma}}\frac{T}{T_c}$.

The value of γ modifies the numerical constants in this last regime but does not influence the power-law dependence in the physical parameters, gathered in $T_c(\xi)$. The equation (101) is a consistency check with respect to the two GVM predictions (46) and (70), and the strictly monotonous behavior of $\bar{R}(t, 0)$ and $\widetilde{D}_\infty$ observed numerically in Sec. IV C.

3. Short-'time' evolution of $\widetilde{D}_t$ and saturation at t_{sat}

Leaving the infinite-'time' case, we consider now the opposite regime of short 'times' where the evolution (99) of $\widetilde{D}_t$ can be solved first in the absence of the non-linear KPZ term, predicting that $\widetilde{D}_t$ is linear in t at short 'times':

$$\widetilde{D}_t \overset{(t\to 0)}{\simeq} \frac{c_0 c_1}{3c_2}\frac{D}{\xi^2}t \qquad (102)$$

This behavior can also be checked by naked eye directly on (99) searching for a solution $\widetilde{D}_t \propto t$. Note the factor 3 in the denominator, due to the two terms in the left-hand side of (99). Assuming that the solution $\widetilde{D}_t$ is also linear at short 'times' while keeping the KPZ term actually yields the same result (since then $\widetilde{D}_t^{3/2} \ll \widetilde{D}_t \ll t^0$).

One checks that this self-consistent hypothesis is correct by solving (99) numerically (cf. Fig. 18). The independence on T in the short-'time' regime (102) is also compatible with the direct simulation of the continuum DP (in a logarithmic scale of Fig. 9). The behavior (102)

thus holds in generality, and allows to define a saturation scale t_{sat} at which $\widetilde{D}_t$ reaches its asymptotic value

$$\widetilde{D}_\infty = \frac{c_0 c_1}{3 c_2} \frac{D}{\xi^2} t_{sat} \quad i.e. \quad t_{sat} = \frac{3 c_2}{c_0 c_1} \frac{c \xi^2}{T} f \qquad (103)$$

Accordingly to this equation, the saturation occurs earlier at higher temperatures, the thermal fluctuations actually smoothing the evolution of the disorder correlator.

Another consequence of the short-'time' behavior (102) deals with the short-'time' dynamics of the mean-value $-2c \overline{\overline{F_V(t,y)}}$ discussed in Sec. IV D and depicted in Fig. 13. Inserting the short-'time' $\widetilde{D}_t$ of (102) into the assumed scaling $\bar{R}(t,0) = c_2 \frac{\widetilde{D}_t}{\xi}$ of (93) and into the exact relation (33), one obtains from the initial condition $\bar{F}_V(t,y) \equiv 0$ that $-2c\, \partial_t \overline{\overline{F_V(t,y)}} \overset{(t \to 0)}{=} \frac{c_0 c_1}{3} \frac{D}{\xi^3} t$ hence the prediction

$$- 2c \overline{\overline{F_V(t,y)}} \overset{(t \to 0)}{=} \frac{2 c_0 c_1}{3} \frac{D}{\xi^3} t^2 \qquad (104)$$

This quadratic behaviour in t is compatible with the superlinear short-'time' regime observed in logarithmic scale in the inset of Fig. 13. However our numerical data do not clearly display such a t^2 behavior (delineated with dashed lines) on the whole range of temperatures, an effect that we attribute to the thermal initial condition taken at $t_0 = 0.1$ which alters the short-'time' power-law behavior that should be observed with the ideal initial condition $\bar{F}_V(0,y) \equiv 0$ at $t_0 = 0$.

This saturation 'time' is different from the characteristic 'time' $t^* = \frac{t^5}{cD^2}$ recently discussed in Ref. 65 for the evolution of the free-energy fluctuations in the high-temperature regime and which corresponds to the Larkin length appearing by scaling at high-T or $\xi = 0$ as discussed in (54). This scale t^* allows to draw apart a short-'time' diffusive and the large-'time' KPZ regime in the evolution of the fluctuations of $F(t,y)$ (see also Ref. 46 for a related study), while the scale t_{sat} we examine in this section, singular in the limit $\xi \to 0$, captures the short-'time' effects inherently due to the finiteness of ξ via the KPZ non-linearity.

To summarize, at finite ξ the non-linear KPZ term does not modify the short-'time' regime but induces a saturation of $\widetilde{D}_t$ at shorter 'times' with increasing T and to an asymptotic value $\widetilde{D}_\infty < \frac{cD}{T}$. The high- and low-temperature asymptotic regimes $\widetilde{D}_\infty \overset{(T \gg T_c)}{=} \frac{cD}{T}$ and $\widetilde{D}_\infty \overset{(T \ll T_c)}{=} \frac{cD}{T_c}$ are both independently well-controlled, and the evolution equation (99) we presented thus allows to tackle the crossover from one regime to the other, but only in an effective way. An interesting open question is to provide a proper analytical derivation of the full temperature crossover and to fix the value of its exponent γ.

VI. LINK TO EXPERIMENTS

We discuss in this last section the consequences of the finite $\xi > 0$ and its associated low-T regime for two specific experiments.

On one hand domain walls in ultrathin magnetic films[1–3] are well described by the DES model of a 1D interface defined in Sec. II A, and both their static geometrical properties and their quasistatic dynamical properties (in the so-called 'creep' regime) are thus captured by the DP endpoint $y(t)$ fluctuations.

On the other hand, a second instance of experiments encompassed by the KPZ theory is provided by interfaces in liquid crystals[66–68], whose geometrical fluctuations are directly described by the DP free-energy $F(t,y)$ properly recentered.

A. Temperature-dependence of the asymptotic roughness

As emphasized in Sec. III C and IV E, a prominent feature of the DP in a correlated disorder is that the amplitude of the roughness $B(t)$ is modified by the microscopic length ξ even at very large lengthscales (in the RM regime), provided that the temperature is lower than the characteristic temperature $T_c = (\xi cD)^{1/3}$. Interfaces in ferromagnetic thin films are a prototype system[11] for the experimental study of 1D interfaces, and in particular their roughness exponent has been measured[1,3] to be $\zeta_{RM} \approx 0.66$ in agreement with the KPZ exponent $\zeta_{RM} = \frac{2}{3}$. As estimated in Ref. 34 (Sec. VII B), the order of magnitude of T_c could be of room-temperature for these systems, which makes it even more relevant to determine whether they lie in the low-T or in the high-T regime.

One could in principle distinguish between those two temperature regimes through the prefactor A_{RM} of the asymptotic roughness at large lengthscales:

$$A_{RM} \overset{(T \gg T_c)}{\sim} \left(\frac{D}{cT} \right)^{\frac{2}{3}} \qquad A_{RM} \overset{(T \ll T_c)}{\sim} \left(\frac{D^2}{c^4 \xi} \right)^{\frac{2}{9}} \qquad (105)$$

as given by scaling arguments (66)-(67), predicted by GVM in (A15)-(A17), and consistent with the numerical study of the roughness in Sec. IV E.

The main problem regarding such a study is that the elastic constant c and possibly the disorder strength D may depend themselves on temperature, making it difficult to characterize the low-T regime by a temperature-independent A_{RM}, or to interpret a measure of the scaling in temperature $A_{RM} \sim T^{2\text{þ}}$ with þ the *thorn* exponent. In any case, a change of regime in the temperature-dependence of A_{RM} would provide a strong evidence for a low-T to high-T crossover. Promising experiments have actually been performed regarding the temperature dependence in ultrathin Pt/Co/Pt films, as analyzed in Ref. 69 where a fine study is devoted to the thermal rounding at the depinning transition.

In case of an elastic constant depending linearly on the temperature $c = \kappa T$, we would expect a roughness amplitude similar to $A_{\mathrm{RM}}^{\mathrm{m}}$ obtained under the usual mathematicians convention $c = T$, as exposed in Appendix G and with an additional dependence in κ.

B. Quasistatic creep regime

The creep motion of 1D interfaces, describing the quasistatic but non-linear response of the interface to an external driving field, could also be an interesting benchmark for the $\xi > 0$ DP model predictions.

Even though its description[32,33] is not directly covered by the equilibrium statistical properties of the interface we have presented here, it happens that the characteristic lengthscales governing its scaling are actually believed to be the static ones. As detailed in Ref. 34 (Sec. VII B), those lengthscales are modified in the low-T regime, implying that the characteristic free-energy barriers scale differently with the temperature above or below T_c. This behavior could provide an experimental criterion to distinguish between the low-T and high-T regime, especially since the exponent of the creep law has been successfully tested on domain walls in ultrathin magnetic films on several order of magnitude in the velocity[1-3].

A challenging situation would be that of an interface moving in a gradient of temperature, as studied numerically in Ref. 70, with a gradient spanning T_c itself and with an elastic constant c (or the disorder strength D) which could again depend or not on the temperature.

C. High-velocity regime in liquid crystals

Another experimental system where our approach might prove instructive is that of growing interfaces in liquid crystal turbulence[66-68]. The corresponding setup consists in a thin layer of liquid crystal subjected to a constant voltage U and to an alternating electric field which can generate two distinct turbulent modes (called 'dynamical scattering modes') DSM1 and DSM2, the later being more stable than the former. Starting from a dot (respectively a line) of DSM2 in a DSM1 background, one thus observes the growth of circular (respectively flat) interface. We refer the reader to Ref. 68 for a complete account of the phenomena at hand.

The fluctuations of this interface are actually remarkably well described by the KPZ theory, providing a benchmark for its predictions not only about scaling exponents but also about scaling functions. Contrarily to the case of magnetic interfaces, the fluctuations of the interface *position* are described by the random variable $\bar{F}(t,y)$ that plays the role of the disorder free-energy in the context of the DP, as defined by (12)-(13). Besides, for the liquid crystal interface, t is the physical time and y the longitudinal direction of the interface.

For the circular interface, it has been shown that the experimentally measured $\bar{C}(t,y)$ defined by (19), once properly rescaled, matches very well the prediction of the KPZ theory at $\xi = 0$: $\bar{C}(t,y)$ can be fitted by the corresponding Airy$_2$ correlator[59]. Although the lengthscale ξ of the disorder correlations is below the optical resolution of the experiment – no rounding of the cusp of $\bar{C}(t,y)$ is observed – it is still finite and should be relevant by inducing a crossover between two 'temperature' regimes to identify. The (non-centered) displacement $h(t,y)$ of the interface evolves according to

$$\partial_t h(t,y) = v_\infty + \nu \partial_y^2 h(t,y) + \frac{\lambda}{2} \left[\partial_y h(t,y) \right]^2 + V(t,y) \tag{106}$$

where v_∞ represents the mean displacement velocity. Comparing this equation to the flow of $F_V(t,y)$ (25), one thus reads the correspondence $\lambda = \frac{1}{c}$, $\nu = \frac{T}{2c}$, or equivalently $c = \frac{1}{\lambda}$, $T = \frac{2\nu}{\lambda}$. It can be argued[67,68] that in the experimental configuration of the growing dot, the parameter λ is directly given by the mean velocity $\lambda = v_\infty$. This velocity itself is well described by a growing affine function of the applied constant voltage U, in the probed voltage range $26\,\mathrm{V} < U < 30\,\mathrm{V}$ (see Fig. 20 in Ref. 68). One may surmise that the parameter ν, which describes the diffusive fluctuations of the interface, is independent of the constant voltage U (although this point is not discussed in Ref. 68), and similarly for the amplitude D of the disorder fluctuations.

If those assumptions are true, one can deduce from the correspondence $c = \frac{1}{\lambda}$, $T = \frac{2\nu}{\lambda}$ that the *low-temperature* regime of our description (where ξ matters in the scaling of the fluctuations amplitude) corresponds to a *high-velocity* $\lambda = v_\infty$ regime for the liquid crystal interface – and inversely for the low-velocity range being described by our high-temperature regime. A natural question is thus to determine whether the experiments are done in the high- or low-velocity regime. A test observable is provided by the amplitude of the fluctuations of $h(t,y)$, denoted Γ in Ref. 68, and defined in the large-time regime from the scaling

$$h(t,y) \overset{(d)}{=} v_\infty t + (\Gamma t)^{\frac{1}{3}} \chi_2(y) \tag{107}$$

where χ_2 is the Airy$_2$ process. In our notations, one has

$$\Gamma = \frac{\widetilde{D}^2}{c} \tag{108}$$

This is read for instance from the factor $a^{\frac{1}{2}} \widetilde{D}^{\frac{1}{2}}$ which rescales the disorder free-energy in (73) with the choice $a = (\widetilde{D}/c^2)^{\frac{1}{3}} t^{\frac{2}{3}}$ of (77). Equivalently, one has $(\Gamma t)^{\frac{1}{3}} = \widetilde{E}$ where $\widetilde{E}$ is the factor in (77) which rescales the free-energy in (78). From our intuition based on scaling arguments, the relation (108) should thus remain valid on the whole temperature range. The high-T and low-T re-

sults $\widetilde{D} \overset{(T \gg T_c)}{=} \frac{cD}{T}$ and $\widetilde{D} \overset{(T \ll T_c)}{=} \frac{cD}{T_c}$ thus imply for Γ

$$\begin{cases} \lambda \ll \lambda_c : & \Gamma^{\text{low } \lambda} = \dfrac{D^2 \lambda}{\nu^2} \\ \lambda \gg \lambda_c : & \Gamma^{\text{high } \lambda} = \dfrac{D^{\frac{4}{3}}}{\lambda^{\frac{1}{3}} \xi^{\frac{2}{3}}} \end{cases} \text{ with } \lambda_c = \left(\frac{\nu^3}{\xi D} \right)^{\frac{1}{2}} \quad (109)$$

The crossover between those two regimes occurs at a characteristic λ_c which is similar to the inverse of the characteristic temperature $T_c^{\mathfrak{m}} = \sqrt{\xi D}$ in the conventions of mathematicians (see Appendix G), as expected since $T \propto \frac{1}{\lambda}$ and $c = \frac{1}{\lambda}$. Strikingly, the crossover occurs between a low-λ regime (our high-T) where Γ is an increasing function of λ and a high-λ regime (our low-T) where Γ is a decreasing function of λ. Note that the limit $\lambda \to 0$ in (106) is exactly the 'linearized' KPZ problem whose evolution has been solved at all 'times' in (40)-(41) and should thus be described exactly the microscopic disorder correlator $R_\xi(y)$ at asymptotically large 'times' (39).

In Ref. 68, the authors have measured Γ as a function of the voltage U and found a decreasing dependence, attributing it to a dependence in U of the parameters D or ν in the expression $\Gamma^{\text{low } \lambda} = \frac{D^2 \lambda}{\nu^2}$ (tackled with $\xi = 0$ in our language, when $\xi \gtrsim 0$ can be neglected). In that spirit, (109) was first announced at the very conclusion of Ref. 46 but with respect to the parameter ν and with the two regimes being separated by the characteristic value $\nu_c = (\xi \lambda^2 D)^{1/3}$. We propose here another scenario where D and ν are independent of U, and Γ follows its high-λ expression $\Gamma^{\text{high } \lambda} = \frac{D^{\frac{4}{3}}}{\lambda^{\frac{1}{3}} \xi^{\frac{2}{3}}}$. If confirmed (e.g. by an independent measure of the parameter ν), this would provide a clear evidence that the system lies deep in the high-λ regime, and would to our knowledge constitute the first example of a phenomenon depicted by the 'low-temperature' KPZ regime.

VII. CONCLUSION

We have studied in this paper both analytically and numerically the consequences of a finite disorder correlation length ξ on the static properties of a 1D interface depending on the lengthscale – or equivalently a growing 1+1 directed polymer at a fixed 'time' – in a random-bond quenched disorder accounting for a weak collective pinning. The two-point correlator $\bar{R}(t, y)$ of the *derivative* of the disorder free-energy (the 'random phase' $\eta_V(t, y)$) at fixed 'time' t emerged as a central quantity in the determination of the dependence on the temperature T and the other parameters of the model (the disorder correlation length ξ, the elastic constant c and the disorder strength D), as summarized in Sec. V A.

The characteristic temperature $T_c = (\xi c D)^{1/3}$ separates two temperature-regimes in the 'time'-evolution of $\bar{R}(t, y)$, which is characterized by its amplitude $\widetilde{D}_t$ and the shape of its central peak $\mathcal{R}(y)$, from the point of view

of our DP toymodel which focuses on the small transverse displacements $|y|$ (which are the most probable to be visited by the polymer and thus the more relevant ones). Although *a priori* the full shape of the correlator $\bar{R}(t, y)$ should matter, we showed that the asymptotic height of its central peak, parametrized by $\widetilde{D}_\infty(T, \xi)/\tilde{\xi}$ with $\tilde{\xi} \approx \xi$, captures the main features of the crossover between low-T and high-T in the large-'time' random-manifold regime; the amplitude of the geometrical fluctuations in this asymptotic regime are actually not affected by ξ at high-T, whereas on the contrary at low-T it plays a crucial role and keeps this amplitude bounded. We showed that, surprisingly, the ratio $f(T, \xi)$ between the actual value of $\widetilde{D}_\infty(T, \xi)$ at finite ξ and its value $\frac{cD}{T}$ at $\xi = 0$ is directly related to a replica-symmetry-breaking cutoff parameter u_c appearing in the GVM replica approach, endowing this cutoff with an unsuspected physical meaning (see Sec. III B). Moreover, $\widetilde{D}_t$ evolves at finite t according to two 'time' regimes, an initial regime and a saturation regime separated by a single 'time'-scale t_{sat} which allows to understand how, depending on the temperature, the geometrical fluctuations depicted by the roughness $B(t)$ display in turn two (at high T) or three (at low T) 'time' regimes. Finally the function $\mathcal{R}(y)$ for 'times' above t_{sat} is strongly reminiscent of the microscopic disorder correlator $R_\xi(y)$ at high-T, but still needs to be characterized at low-T with some additional kernel to be determined analytically.

We supported this picture through extensive numerical simulations of the $\xi > 0$ KPZ equation, which permitted in particular to evaluate $\widetilde{D}_\infty(T)$ numerically at a fixed value of ξ. In agreement with an effective equation that we put forward for $\widetilde{D}_\infty(T)$, it appears that this quantity presents a crossover from low- to high-T, and not a phase transition that would be characterized by a non-analytic dependence of $\widetilde{D}_\infty$ in T. We cannot strictly exclude nonetheless the scenario of a phase transition because of inherent numerical imperfections in the simulations and because the analytical equation on $\widetilde{D}_\infty(T)$ is either effective (101) or obtained in the GVM approximation (46) and (70). A rigorous procedure is needed to elucidate this alternative. Possible approaches encompass from an extension to the $\xi > 0$ case of recent results[18,54,56,57] in the $\xi = 0$ KPZ class, to an adaptation of FRG arguments[31–33] to the study of the correlator $\bar{R}(t, y)$.

More broadly, it would be interesting to identify possible connections between the 'time' equation of evolution (34) of the correlator $\bar{R}(t, y)$, and the FRG flow equation of evolution with respect to scale ℓ of the renormalized disorder correlator in a FRG approach. Although the FRG framework holds perturbatively in $\epsilon = 4 - d$ (hence $\epsilon = 3$ in our settings) the two varieties of flow equations bear striking resemblance. In particular, the high-temperature regime has been studied in Ref. 31 by neglecting the non-linear contributions to the FRG flow, allowing to recover the same scalings as ours for

$T \gg T_c$. On the other hand, neglecting the non-linearity of the flow in our settings (Appendix E) indeed yields the correct high-temperature scaling $\widetilde{D}_\infty = \frac{cD}{T}$ but does not provide for instance the correct roughness exponent $\zeta_{\mathrm{RM}} = \frac{2}{3}$ (when we consider the scaling of the negative bumps at large y, as in (41)). One would thus need a controlled expansion in order to draw a meaningful unified picture. Another related question deals with the $T = 0$ singularity of the FRG renormalized correlator which appears at a finite scale ℓ_c and plays an important role in the physical description of metastability in random manifolds. Our result should help to understand in which order the limits $T \to 0$ and $\xi \to 0$ are to be taken. Last, a FRG approach, through the possible existence of a zero and a finite temperature fixed point, may allow to distinguish between the crossover and the phase-transition scenari.

The richness of the KPZ universality class also allows to translate the occurrence of low- *vs* high-temperature regimes into different languages. We have illustrated this fact in the analysis of a liquid crystal experiment[66–68] (Sec. VI) where the low-temperature regime corresponds to a high-velocity regime – yet to be ascertained experimentally. On the mathematical side, keeping ξ finite amounts to generalize the Airy$_2$ process in a non-trivial way (see also Ref. 46). In the language of replicæ[28], it corresponds to solving the problems of bosons with attractive but non-δ interactions in one dimension, for which the $\xi = 0$ Bethe Ansatz solution is not known to generalize. The same search for an extension also applies to the Airy$_1$ process, which describes a point-to-line DP problem (with 'flat' initial conditions), which finds an experimental incarnation for instance in flat interfaces in liquid crystals.

One may finally wonder how the existence of a low-temperature regime extends to phenomena which do not fall *a priori* into the KPZ universality class. A basic assumption made at the very start is that the disorder is Dirac δ-correlated along the longitudinal 'time' direction. The disorder is nevertheless always correlated in both directions in physical systems; one generalization of our results would be to take this property into account. Such correlations may also account for overhangs present in interfaces, once smoothed out by a change of scale. The generalization is non-trivial in the sense that the equations of evolution become non-local in 'time'. More broadly, the cases of non-RB disorder and/or higher dimensions, where a mapping to a directed-path problem is not always possible, are still open.

Appendix A: Reminder of previous GVM roughness predictions

For completeness, here we recall and adapt the roughness predictions for the static 1D interface obtained in Ref. 34, first assuming that the disorder correlator $R_\xi(x)$ in (1) was a normalized Gaussian function of variance $2\xi^2$, then using the replica trick in order to average over disorder and finally performing a Gaussian Variational Method (GVM) with a full replica-symmetry-breaking (RSB) variational Ansatz as introduced by Mézard and Parisi in Ref. 45 and 71, further investigated also by Goldschmidt and Blum in Ref. 43. We emphasize in particular the role of the interpolating parameter $f(T,\xi)$ between the high- and low-temperature regimes.

For the full DES model of the 1D interface, we had obtained for the variance of the relative displacements $B(r) \equiv \overline{\langle \Delta u(r)^2 \rangle}$ at the lengthscale r:

$$B(r) = \frac{Tr_0}{c} \left(\frac{r}{r_0} + \bar{B}_{\mathrm{dis}} \left(\frac{r}{r_0} \right) \right) \quad \text{(A1)}$$

$$\bar{B}_{\mathrm{dis}}(\bar{r}) = \frac{1}{v_c} \sum_{k=2}^{\infty} \frac{(-\bar{r})^k}{k!} \left[\frac{1}{5k-6} + (1-v_c) \right] \quad \text{(A2)}$$

$$r_0 = \frac{5^5 \pi}{3^7} \frac{1}{cD^2} \left(\frac{T}{v_c} \right)^5 \quad \text{(A3)}$$

$$v_c^6 = \widetilde{A}_1(5/6 - v_c) \,, \ \widetilde{A}_1 = \frac{5^5 \pi}{2 \times 3^7} \left(\frac{T}{T_c} \right)^6 \quad \text{(A4)}$$

$$T_c \equiv (\xi cD)^{1/3} \quad \text{(A5)}$$

where the four DES parameters $\{c, D, T, \xi\}$ are respectively the elastic constant c (elastic energy per unit of length along the interface), the disorder strength D (the typical amplitude of the random potential), the temperature T and the disorder correlation length ξ (or width of the interface). r_0 is the Larkin length introduced in (58) and marking the beginning of the asymptotic 'random-manifold' regime, $v_c(T,\xi)$ the full-RSB cutoff and T_c the characteristic temperature separating the low- and high-temperature regimes.

As for our DP 'rounded' toymodel, assuming that the effective disorder correlator of $\eta_V(t,y)$ (20) is of the form $\bar{R}(t,y) = \widetilde{D} \cdot \mathcal{R}_{\tilde{\xi}}(y)$ we have performed a GVM procedure on the following statistical average obtained from (22) using replicæ to average over disorder:

$$\overline{\langle y(t)^k \rangle} = \lim_{n \to 0} \int dy_1 (\cdots) dy_n \cdot y_1^k \cdot e^{-\sum_{a=1}^{n} F_{\mathrm{th}}(t,y_a)/T}$$

$$\cdot \exp \left[-\frac{\widetilde{D}}{2} \sum_{a,b=1}^{n} \mathcal{R}_{\tilde{\xi}}(y_a - y_b)/T^2 \right] \quad \text{(A6)}$$

With the function $\mathcal{R}_{\tilde{\xi}}(y)$ the same normalized Gaussian

function of variance $2\tilde{\xi}^2$, we have obtained for the variance of the DP's endpoint fluctuations $B_{\mathrm{DP}}(t) \equiv \overline{\langle y(t)^2 \rangle}$ after a growing 'time' t:

$$B_{\mathrm{DP}}(t \geq t_c) = \frac{3}{2} \left(\frac{2\widetilde{D}^2}{\pi c^4} \right)^{1/3} t^{4/3} - \tilde{\xi}^2 \quad \text{(A7)}$$

$$B_{\mathrm{DP}}(t \leq t_c) = \frac{Tt}{c} + \frac{\widetilde{D}}{c^2\sqrt{\pi}} \cdot t^2 \left(\tilde{\xi}^2 + \frac{Tt}{c} \right)^{-1/2} \quad \text{(A8)}$$

$$t_c = \frac{3^3\pi}{2^4} \frac{c}{\widetilde{D}^2} \left(\frac{T}{u_c} \right)^3 \quad \text{(A9)}$$

$$u_c^4 = \widetilde{A}_2(3/4 - u_c), \; \widetilde{A}_2 = \frac{3^3\pi}{2^4} \frac{T^4}{(\tilde{\xi}\widetilde{D})^2} \text{(A10)}$$

where, as before, the four parameters $\left\{ c, T, \widetilde{D}, \tilde{\xi} \right\}$ are respectively the elastic constant c, the temperature T, the effective strength of disorder $\widetilde{D}$, the effective interface width $\tilde{\xi}$ and $u_c(T,\xi)$ the full-RSB cutoff.

However, the second GVM computation was performed *at a fixed 'time' t*, so the effective parameters $\widetilde{D}_t$ and $\tilde{\xi}_t$ have *a priori* also a 'time' dependence. Assuming that they both saturate quite quickly, we can safely compare the two sets of predictions (A1)-(A5) and (A7)-(A10) with the translation of 'time' t into the lengthscale r, the approximation $\tilde{\xi} \approx \xi$, and the identification of t_c with r_0 for the Larkin length. As for the full-RSB cutoffs, the definitions $f^{1D}(T,\xi) \equiv \frac{6}{5} v_c(T,\xi)$ and $f^{\mathrm{toy}}(T,\xi) \equiv \frac{4}{3} u_c(T,\xi)$ yield then two similar equations for the interpolating parameter $f(T,\xi)$, respectively (70) and (46), if we impose by hand $\widetilde{D} = \frac{cD}{T} f^{\mathrm{toy}}(T,\xi)$ in order to match the Larkin lengths t_c and r_0. Their numerical discrepancy can be safely attributed to the GVM approximation. The structure $f^6 \propto (T/T_c)^6 (1-f)$ stems in both cases from the comparison of $\xi_{\mathrm{th}}(T)^2 = (\frac{T^3}{cD})^2$ and $\xi^2 = \xi_{\mathrm{th}}(T_c)^2$, the equation (A4) being initially of the form:

$$\xi^2 + \frac{16\pi}{9} \xi_{\mathrm{th}}(T)^2 \left(\frac{6}{5} v_c \right)^{-6} \left(\frac{6}{5} v_c - 1 \right) = 0 \quad \text{(A11)}$$

As discussed in Ref. 11, the Larkin length is a physical benchmark for the roughness, firstly as the beginning of its asymptotic 'random-manifold' regime, secondly with its relation to the maximum value of the GVM self-energy $[\sigma](v_c)$ and thus to the full-RSB cutoff itself $v_c(T,\xi)$, and thirdly consistent with its original definition by Larkin[44] as the lengthscale at which the typical relative displacement of the 1D interface corresponds to its effective width $B(L_c(T,\xi)) \approx \xi_{\mathrm{eff}}(T,\xi)^2$ which fixes the amplitude of the RM roughness $B(r > L_c) \approx A(c,D,T,\xi)r^{4/3}$:

$$A_{(c,D,T,\xi)}^{\mathrm{GVM}} \leftrightarrow L_c^{\mathrm{GVM}}(T,\xi) \leftrightarrow [\sigma](v_c)^{\mathrm{GVM}} \leftrightarrow v_c \quad \text{(A12)}$$

Using (A4), (A3) and (66), we give the GVM predictions

for the quantities

$$L_c^{\mathrm{GVM}}(T,\xi) \overset{(\mathrm{A1})}{=} \frac{32\pi}{9} \left(\frac{6}{5} v_c \right)^{-5} r_*(T), \; r_*(T) \equiv \frac{T^5}{cD^2} \text{(A13)}$$

$$\begin{aligned} A_{(c,D,T,\xi)}^{\mathrm{GVM}} &= \left[D^{3/10} c^{-3/5} L_c^{\mathrm{GVM}}(T,\xi)^{-1/10} \right]^{4/3} \quad \text{(A14)} \\ &= \left[\left(\frac{D}{cT} \right)^{1/3} \cdot \left(\frac{9}{32\pi} \right)^{1/15} \cdot \left(\frac{6}{5} v_c \right)^{1/3} \right]^2 \end{aligned}$$

at low- *versus* high-temperatures:

$$v_c \overset{(\xi \to 0)}{\approx} \frac{5}{6}, \; v_c \overset{(T \to 0)}{\approx} \frac{5}{6} \left(\frac{16\pi}{9} \right)^{1/6} \frac{T}{T_c} \approx 1.11 \frac{T}{T_c} \quad \text{(A15)}$$

$$L_c^{\mathrm{GVM}}(T,0) \approx \frac{32\pi}{9} \frac{T^5}{cD^2} \approx 11.17 \cdot r_*(T) \quad \text{(A16)}$$

$$L_c^{\mathrm{GVM}}(0,\xi) \approx \frac{32\pi}{9} \left(\frac{16\pi}{9} \right)^{-5/6} \frac{T_c^5}{cD^2} \approx 2.66 \cdot r_*(T_c)$$

$$A_{(c,D,T,0)}^{\mathrm{GVM}} \approx \left(\frac{9}{32\pi} \right)^{2/15} \left(\frac{D}{cT} \right)^{2/3} \approx 0.72 \left(\frac{D}{cT} \right)^{2/3} \quad \text{(A17)}$$

$$A_{(c,D,0,\xi)}^{\mathrm{GVM}} \approx \left(\frac{9}{32\pi} \right)^{2/15} \left(\frac{16\pi}{9} \right)^{1/9} \left(\frac{D}{cT_c} \right)^{2/3} \approx 0.88 \left(\frac{D}{cT_c} \right)^{2/3}$$

Appendix B: Statistical Tilt Symmetry (STS)

We justify in this appendix the decomposition of the free-energy $F_V(t,y)$ defined by (12) into the sum of a disorder-independent term $F_{V\equiv0}(t,y)$ and a translationally invariant term $\bar{F}_V(t,y)$ (13-16), from the complementary viewpoints of path-integrals and of stochastic differential equations. This symmetry arises from three ingredients: the precise form of the elastic energy density $\frac{c}{2}(\partial_t y)^2$, the invariance in distribution of the disorder $V(t,y)$ by translation along y and the continuum nature of the transverse direction y. We refer the reader to Ref.[18,72–74] for previous discussions of the STS.

The weight of trajectories $\{y(t)\}$ starting in $(0,0)$ and arriving in (t_1, y_1) can be compared to the weight of those arriving in $(t_1, 0)$ from the change of coordinates:

$$\bar{y}(t) \equiv y(t) - \frac{y_1}{t_1} t \quad \text{(B1)}$$

with now the initial and final conditions $\bar{y}(0) = \bar{y}(t_1) = 0$. Introducing the tilted disorder

$$\mathcal{T}_{y_1}^{t_1} V(t,y) \equiv V \left(t, y + \frac{y_1}{t_1} t \right) \quad \text{(B2)}$$

and performing the change (B1) in the path-integral of the unnormalized weight (3) one obtains:

$$W_V(t_1, y_1) = e^{-y_1^2/(2B_{\mathrm{th}}(t_1))} W_{\mathcal{T}_{y_1}^{t_1} V}(0, t_1) \quad \text{(B3)}$$

thanks to the form $\frac{c}{2}(\partial_t y)^2$ of the elastic energy density which allows to identify a translated path integral

over $\{\bar{y}(t)\}$ and to single out the thermal contribution with $B_{\text{th}}(t) = \frac{Tt}{c}$. The measure of the path-integral remains unchanged ($\mathcal{D}y(t) = \mathcal{D}\bar{y}(t)$) since the change of variable (B1) is a translation. Using the definitions (13), this equality writes for the disorder free-energy

$$\bar{F}_V(t_1, y_1) = \bar{F}_{\mathcal{T}_{y_1}^{t_1} V}(t_1, 0) \tag{B4}$$

This means that the whole dependence in the arrival point y_1 of the disorder free-energy can be absorbed into a tilt $\mathcal{T}_{y_1}^{t_1}$ of the disorder potential. Using that at fixed final time t_1 the disorder is translation-invariant in y i.e. $\bar{\mathcal{P}}[V] = \bar{\mathcal{P}}[\mathcal{T}_{y_1}^{t_1} V]$ one obtains the symmetry $\bar{\mathcal{P}}[\bar{F}_V(t, y+Y)] = \bar{\mathcal{P}}[\bar{F}_V(t, y)]$ as announced in (17). This translation invariance in the y-direction is valid for any functional of $\bar{F}_V(t, x)$, and yields in particular for the k-point correlators:

$$\overline{\bar{F}_V(t_1, y_1 + Y) \dots \bar{F}_V(t_1, y_k + Y)}$$
$$= \overline{\bar{F}_V(t_1, y_1) \dots \bar{F}_V(t_1, y_k)} \tag{B5}$$

The same result (17) can also be deduced from the strict point of view of stochastic differential equations. Note first that the initial condition $\frac{W_V(0,y)}{W_{V\equiv 0}(0)} = \delta(y)$ translates for $\bar{F}_V$ as $\bar{F}_V(0, y) \equiv 0$ which is trivially translation-invariant along the y-direction. Showing the STS (17) thus amounts to checking that this property is preserved in time through the evolution equation evolution (26) for $\bar{F}_V$. Consider for this purpose a 'Galilean transformation' of $\bar{F}_V(t, y)$, which consists in defining $\bar{F}_V^v(t, y)$ through

$$\bar{F}_V(t, y) \equiv \bar{F}_V^v(t, y - vt) \tag{B6}$$

where v represents the 'velocity' of the tilt $y \mapsto y + vt$. One sees directly from (26) that the terms in v in the equation of evolution for $\bar{F}_V^v(t, y)$ compensate between left and right hand side: $\bar{F}_V^v(t, y)$ verifies the *same* equation of evolution as $\bar{F}_V(t, y)$, but in a tilted disorder $V^v(t, y) = V(t, y + vt)$. Since the initial condition is also the same, one obtains:

$$\bar{F}_V^v(t_1, y_1) = \bar{F}_{V^v}(t_1, y_1) \tag{B7}$$

Choosing $v = y_1/t_1$ in (B6) and (B7) yields again (B4).

Another but less general incarnation of the STS arises when considering the geometrical fluctuations instead of the free-energy. Defining the 'generating function' of the moments of $y(t_1)$

$$W_V^\lambda(t_1) = \int_{y(0)=0} \mathcal{D}y(t)\, e^{-\frac{1}{T}\mathcal{H}[y,V;t_1] + \lambda y(t_1)} \tag{B8}$$

where the final-time condition is free (or equivalently, $y(t_1)$ is integrated over), the disorder average of the variance of the endpoint $y(t_1)$ is given by:

$$\overline{\langle y(t_1)^2\rangle_c} \equiv \overline{\langle y(t_1)^2\rangle - \langle y(t_1)\rangle^2} = \partial_\lambda^2\big|_{\lambda=0} \overline{\log W_V^\lambda(t_1)} \tag{B9}$$

We note that performing an appropriate tilt encoding the thermal roughness, namely $y(t) = \bar{y}(t) + \lambda B_{\text{th}}(t)$ one obtains for the generic function:

$$W_V^\lambda(t_1) = e^{B_{\text{th}}(t_1)\lambda^2/2}\, W_{\tilde{V}}^{\lambda=0}(t_1) \tag{B10}$$

where $\tilde{V}(t,y) \equiv V(t, y + \frac{\lambda T}{2c}t)$ is a tilted disorder. Taking the logarithm and averaging over disorder, one obtains for (B9):

$$\overline{\langle y(t_1)^2\rangle_c} = \frac{Tt_1}{c} = B_{\text{th}}(t_1) \tag{B11}$$

and $\overline{\langle y(t_1)^k\rangle_c} = \partial_\lambda^k\big|_{\lambda=0} \overline{\log W_V^\lambda(t_1)} = 0$ for $k > 2$. It would be tempting to conclude from these averaged cumulants that the average of the whole distribution $\overline{P_V(t_1, y_1)}$ is a normal law $\mathcal{N}(0, B_{\text{th}}(t_1))$; this is only true in the trivial case without disorder where $P_{V\equiv 0}(t, y) = P_{\text{th}}(t, y) = \mathcal{N}(0, B_{\text{th}}(t_1))$. Indeed the normalization at fixed disorder $\bar{W}_V(t_1)$ of definition (5) prevents a direct disorder average on (B3). As for the roughness $B(t)$, the property (B11) can be reformulated in an intrinsic way comparing the cumulants with respect to the thermal, disorder and the joint disorder-thermal distributions:

$$B(t) \equiv \overline{\langle y(t)^2\rangle} = \overline{\langle y(t)^2\rangle_c} + \overline{\langle y(t)\rangle^2}^c \tag{B12}$$

$$B_{\text{dis}}(t) \equiv B(t) - B_{\text{th}}(t) = \overline{\langle y(t)\rangle^2}^c \tag{B13}$$

Physically this decomposition allows to focus on the pure disorder contribution of the roughness $B_{\text{dis}}(t)$, which is equivalent to the full roughness at large 'times'. Such a simple relation is possible for the second cumulant thanks to the following generic identity valid in presence of two probability laws p_1 and p_2 (respectively thermal and disorder distribution in our case):

$$\text{Var}_{p_2 \circ p_1} = \mathbb{E}_{p_2} \circ \text{Var}_{p_1} + \text{Var}_{p_2} \circ \mathbb{E}_{p_1} \tag{B14}$$

Appendix C: Derivation of the Feynman-Kac 'time'-evolution equations

We rederive in this appendix the 'time'-evolution equation (23) of the weight $Z_V(t, y) = \frac{W_V(t,y)}{\bar{W}_{V\equiv 0}(t)}$, defined with respect to the pseudo free-energy $F_V(t, y)$ in (12). Given in Ref. 29, this evolution equation is the starting point of the Feynman-Kac equations of Sec. II D which define univocally the pseudo free-energy quantities $F_V(t, y)$, $\bar{F}_V(t, y)$ and its random phase $\eta_V(t, y)$ with their *ad hoc* initial conditions. However, the normalization of the weight $Z_V(t, y)$ is not conserved in presence of disorder, so it requires a careful treatment in order to yield its continuous formulation (23).

Using infinitesimal 'propagators' in a path-integral formulation of the weight Z_V[49], we derive thereafter the evolution equation first using its propagation equation in continuous time and secondly constructing explicitly

the weight with the propagators in discretized time. We rederive this result for completeness, to pinpoint the required hypotheses and the possible issues in a generalization regarding the form of the elasticity.

1. Propagation equation in continuous time

We first define the following propagator (with $\beta \equiv \frac{1}{T}$):

$$Z_V(t_1, y_1|t_0, y_0) = \int_{y(t_0)=y_0}^{y(t_1)=y_1} \widetilde{\mathcal{D}}y(t)\, e^{-\beta\mathcal{H}[y,V;t_0,t_1]} \quad (C1)$$

$$\mathcal{H}[y, V; t_0, t_1] = \int_{t_0}^{t_1} dt\left[\frac{c}{2}(\partial_t y)^2 + V(t, y(t))\right] \quad (C2)$$

which represents the weight of trajectories starting in y_0 at time t_0 and ending in y_1 at time $t_1 > t_0$. Note that by definition $Z_V(t, y) = Z_V(t, y|0, 0)$. Paths $y(t)$ are weighted by a measure $\widetilde{\mathcal{D}}y(t)$ ensuring that for purely thermal paths the weight is normalized. Explicitly, with the normalization $\bar{W}_V(t)$ defined by (4), the measure

$$\widetilde{\mathcal{D}}y(t) = \frac{\mathcal{D}y(t)}{\bar{W}_{V\equiv 0}(t_1 - t_0)} \quad (C3)$$

in (C1) ensures that

$$\int dy_1\, Z_{V\equiv 0}(t_1, y_1|t_0, y_0) = 1 \quad (C4)$$

a property which is not true anymore for any V. Here, $\int dy$ denotes $\int_{-\infty}^{+\infty} dy$ as in the rest of this appendix. The advantage of using this choice of normalization is that $Z_V(t, y)$ obeys the so-called *stochastic heat equation* (23), which can be shown using the Feynman-Kac formula.

From its definition, we see that the propagator (C1) presents several useful properties. For $t_1 \to t_0$ it goes to a Dirac delta:

$$\lim_{t_1 \to t_0} Z_V(t_1, y_1|t_0, y_0) = \delta(y_1 - y_0) \quad (C5)$$

since the trajectory endpoint y_1 remains very close to its departure point at small times; to be more precise, we read from (C1) the expression of the infinitesimal propagator δZ_V, valid for t_1 close to t_0:

$$\delta Z_V(t_1, y_1|t_0, y_0) \overset{(t_1 \approx t_0)}{=}$$
$$\frac{1}{\sqrt{2\pi}}\sqrt{\frac{\beta c}{t_1 - t_0}}e^{-\frac{\beta c}{2}\frac{(y_1 - y_0)^2}{t_1 - t_0} - \beta(t_1 - t_0)V(t_1, y_1)} \quad (C6)$$

The prefactor ensures the normalization condition (C4) and also yields (C5) in the limit $t_1 \to t_0$. It is rather important not to overlook this prefactor since it ensures that the infinitesimal propagator (C6) evolves in time according to the forward and backward equations (already close to the final one on Z_V):

$$\partial_{t_1}\delta Z_V = +\left[\frac{1}{2\beta c}\partial_{y_1}^2 - \beta V(t_1, y_0)\right]\delta Z_V \quad (C7)$$

$$\partial_{t_0}\delta Z_V = -\left[\frac{1}{2\beta c}\partial_{y_0}^2 - \beta V(t_1, y_1)\right]\delta Z_V \quad (C8)$$

Last, the non-infinitesimal time evolution is described by the propagation equation

$$Z_V(t_1, y_1|t_0, y_0) = \int dy\, Z_V(t_1, y_1|t, y)Z_V(t, y|t_0, y_0) \quad (C9)$$

which expresses that the path integral (C1) can be cut at any time $t_0 < t < t_1$ provided the intermediate values y of the path at time t are integrated upon. Using (C5), the limit $t \to t_1$ of the equation of propagation (C9) yields a trivial identity. To go further, we can differentiate (C9) with respect to time t and then use that for t close to t_1 the infinitesimal propagator verifies the backwards evolution (C8) in order to write

$$\int dy\left[\frac{1}{2\beta c}\partial_y^2 - \beta V(t_1, y_1)\right]\delta Z_V(t_1, y_1|t, y)\, Z_V(t, y|t_0, y_0)$$
$$= \int dy\, \delta Z_V(t_1, y_1|t, y)\partial_t Z_V(t, y|t_0, y_0)\} \quad (C10)$$

Integrating by parts and taking the limit $t \to t_1$ thanks to (C5) finally yields the expected stochastic heat equation

$$\partial_t Z_V(t, y|t_0, y_0) = \left[\frac{1}{2\beta c}\partial_y^2 - \beta V(t, y)\right]Z_V(t, y|t_0, y_0) \quad (C11)$$

Note that a propagator obeying such an equation of evolution cannot keep its normalization constant since in general

$$\partial_t \int dy\, Z_V(t, y|t_0, y_0) = -\beta\int dy\, V(t, y)Z_V(t, y|t_0, y_0) \quad (C12)$$

is non-zero. We also remark that considering an elastic energy including higher powers of $\partial_t y$ than $(\partial_t y)^2$ in (C2) would be problematic for finding the equation of evolution: the infinitesimal propagator (C6) would contain terms of the form $\frac{(y_1 - y_0)^p}{(t_1 - t_0)^{p-1}}$, making it not obvious to determine the equivalent of (C7-C8) and deriving the evolution corresponding to (C11).

2. Explicit propagator in discretized time

A second approach to explicit the normalization properties of the path integral is to work in discretized time. A path is going from y_i to y_f between time t_i and t_f in N time steps $\delta t \equiv \frac{t_f - t_i}{N}$, so at times $t_k = t_i + k\frac{t_f - t_i}{N}$. We define the weight (or probability density) of a free path as

$$\mathcal{P}[y_0 \dots y_N] = \left[\frac{\beta c}{2\pi\delta t}\right]^{\frac{N}{2}}\exp\left[-\beta\sum_{0 \le k < N}\delta t\frac{c}{2}\left(\frac{y_{k+1} - y_k}{\delta t}\right)^2\right]$$

$$= \prod_{0 \le k < N} g(\delta t, y_{k+1} - y_k) \quad (C13)$$

where we have denoted the microscopic propagator by

$$g(t, y) = \sqrt{\frac{\beta c}{2\pi t}}e^{-\beta c\frac{y^2}{2t}} \quad (C14)$$

One defines the discrete equivalent in Itō's discretization to the continuous propagator (C1) as

$$\mathcal{Z}_V^N(t_{\mathrm{f}}, y_{\mathrm{f}}|t_{\mathrm{i}}, y_{\mathrm{i}}) = \int dy_0 \ldots dy_N \; \mathcal{P}[y_0 \ldots y_N]$$
$$\times \, \delta(y_0 - y_{\mathrm{i}})\delta(y_N - y_{\mathrm{f}}) \qquad \text{(C15)}$$
$$\times \exp\left[-\beta \sum_{0 \le k < N} \delta t \, V(t_k, y_k)\right]$$

with the expectation that this result does not depend on N in the large N limit. The following decomposition makes the link with the continuum formulation (C1-C3):

$$dy_0 \ldots dy_N \; \mathcal{P}[y_0 \ldots y_N] \exp\left[-\beta \sum_{0 \le k < N} \delta t \frac{c}{2}\left(\frac{y_{k+1} - y_k}{\delta t}\right)^2\right]$$
$$= \underbrace{\frac{dy_0 \ldots dy_N}{\left[\frac{\beta c}{2\pi\delta t}\right]^{-\frac{N}{2}}}}_{\equiv \widetilde{\mathcal{D}}y(t)} \underbrace{\exp\left\{-\beta\delta t \sum_{0 \le k < N}\left[\frac{c}{2}\left(\frac{y_{k+1} - y_k}{\delta t}\right)^2 + V(t_k, y_k)\right]\right\}}_{\equiv e^{-\beta\mathcal{H}[y,V;t_0,t_1]}}$$
$$\text{(C16)}$$

At $V \equiv 0$ the normalization corresponding to (C4) still holds: the writing (C13) is a product of normalized probability densities. The propagation equation (C9) is readily verified: for all intermediate times $t = t_\ell$ one has

$$\int dy \, \mathcal{Z}_V^N(t_{\mathrm{f}}, y_{\mathrm{f}}; t, y)\mathcal{Z}_V^N(t, y; t_{\mathrm{i}}, y_{\mathrm{i}})$$
$$= \int dy \int dy_0 \ldots dy_\ell dy'_\ell \ldots dy_N \, \delta(y_0 - y_{\mathrm{i}})\delta(y_\ell - y)\delta(y'_\ell - y)$$
$$\times \, \delta(y_N - y_{\mathrm{f}})P[y_0 \ldots y_N] \exp\left[-\beta \sum_{0 \le k < N} \delta t \, V(t_k, y_k)\right]$$
$$= \int dy_0 \ldots dy_\ell \ldots dy_N \, \delta(y_0 - y_{\mathrm{i}})\delta(y_N - y_{\mathrm{f}})$$
$$\times \, P[y_0 \ldots y_N] \exp\left[-\beta \sum_{0 \le k < N} \delta t \, V(t_k, y_k)\right]$$
$$= \mathcal{Z}_V^N(t_{\mathrm{f}}, y_{\mathrm{f}}|t_{\mathrm{i}}, y_{\mathrm{i}}) \qquad \text{(C17)}$$

The derivation of the stochastic heat equation can then be made explicit: fixing now y_{i} and t_{i} (and skipping them in the all following weights $Z_V(\ldots|t_{\mathrm{i}}, y_{\mathrm{i}})$), one compares two histories $(t_0, y_0; \ldots; t_N, y_N)$ and $(t_0, y_0; \ldots; t_N, y_N; t_{N+1}, y_{N+1})$

$$\mathcal{Z}_V^{N+1}(t_{N+1}, y_{\mathrm{f}}) = \int dy_{N+1} \ldots dy_0 \delta(y_0 - y_{\mathrm{i}})\delta(y_{N+1} - y_{\mathrm{f}})$$
$$\times \, g(\delta t, y_{N+1} - y_N)e^{-\beta\delta t V(t_{N+1}, y_{N+1})}$$
$$\times \, \mathcal{P}[y_0 \ldots y_N]e^{-\beta\delta t \sum_{0 \le k < N} V(t_k, y_k)}$$
$$\text{(C18)}$$

where we have isolated the contribution of the last time step. Expanding the exponential $e^{-\beta\delta t V(t_{N+1}, y_{N+1})}$

(which is valid at minimal order in δt), yields at order δt:

$$\mathcal{Z}_V^{N+1}(t_{N+1}, y_{\mathrm{f}}) - \mathcal{Z}_V^N(t_N, y_{\mathrm{f}}) \simeq -\delta t \beta V \mathcal{Z}_V^N(t_N, y_{\mathrm{f}})$$
$$+ \int dy_{N+1} \ldots dy_0 \delta(y_0 - y_{\mathrm{i}})\delta(y_{N+1} - y_{\mathrm{f}})$$
$$\times \, \big[g(\delta t, y_{\mathrm{f}} - y_N) - \delta(y_{\mathrm{f}} - y_N)\big]$$
$$\times \, \mathcal{P}[y_0 \ldots y_N]e^{-\beta\delta t \sum_{0 \le k < N} V(t_k, y_k)} \qquad \text{(C19)}$$

where the third line reads

$$g(y_{\mathrm{f}} - y_N, \delta t) - \delta(y_{\mathrm{f}} - y_N)$$
$$= g(\delta t, y_{\mathrm{f}} - y_N) - g(0, y_{\mathrm{f}} - y_N) \qquad \text{(C20)}$$
$$\approx \delta t \, \partial_t g(\delta t, y_{\mathrm{f}} - y_N) \qquad \text{(C21)}$$

Using now $\partial_t g(\delta t, y_{\mathrm{f}} - y_N) = \frac{1}{2\beta c}\partial_{y_{\mathrm{f}}}^2 g(\delta t, y_{\mathrm{f}} - y_N)$ and, in the integral, $\partial_{y_{\mathrm{f}}}^2 = \partial_{y_{N+1}}^2$ and integrating by parts we get finally

$$\frac{\mathcal{Z}_V^{N+1}(t_{N+1}, y_{\mathrm{f}}) - \mathcal{Z}_V^N(t_N, y_{\mathrm{f}})}{\delta t} \approx$$
$$\left[\frac{1}{2\beta c}\partial_{y_{\mathrm{f}}}^2 - \beta V(t_{\mathrm{f}}, y_{\mathrm{f}})\right]\mathcal{Z}_V^N(t_N, y_{\mathrm{f}})$$
$$\text{(C22)}$$

which corresponds to the continuum equation (C11) in the limit $\delta t \to 0$. Note moreover that from (C18) the following exact recurrence equation for the propagator can be read:

$$\mathcal{Z}_V^{N+1}(t_{\mathrm{f}} + \delta t, y_{\mathrm{f}}) =$$
$$\int dy \, g(\delta t, y_{\mathrm{f}} - y)e^{-\beta\delta t V(t_N, y)}\mathcal{Z}_V^N(t_{\mathrm{f}}, y) \qquad \text{(C23)}$$

and is the continuous analogue of the transfer matrix equation for a directed polymer constrained on a discretized lattice.

Note that similarly to the continuous case, the specific form of the short-range elasticity implies the Gaussian form of the microscopic propagator (C14), which thus satisfies the diffusion equation leading to the discrete stochastic heat equation (C22). However a different elasticity will in general not be Gaussian and consequently radically change its evolution equation.

Appendix D: 'Time'-evolution equations of averages using the functional Itō formula

Aiming at the derivation the evolution equations for $\partial_t\bar{C}(t, y)$ and $\partial_t\bar{R}(t, y)$ given in Sec. II E, we first present in this appendix the functional Itō formula[75] applied to a field $X(t, y)$ obeying a generic Langevin equation, then we particularize it to the case of multi-point correlators, obtaining finally the flow equations (34)-(35).

The Feynman-Kac evolution equations (25), (26) and (27) of F_V, $\bar{F}_V$ and η_V take the form of a generic Langevin equation for a field $X(t, y)$:

$$\partial_t X(t, y) = \mathcal{G}[X(t, y); t, y] + \mathcal{V}(t, y) \qquad \text{(D1)}$$

where $\mathcal{V}(t, y)$ is a centered Gaussian noise with correlations

$$\overline{\mathcal{V}(t, y)\mathcal{V}(t', y')} = D\delta(t' - t)\mathcal{R}(y' - y) \qquad \text{(D2)}$$

For $X(t, y)$ being $F_V(t, y)$, $\bar{F}_V(t, y)$ and $\eta_V(t, y)$ one reads $\mathcal{G}$ respectively as $\mathcal{G}[F]$ from (F2), $\bar{\mathcal{G}}[\bar{F}; t, y]$ from (F4), and $\mathcal{G}_\eta[\eta; t, y]$ from (F6). For F and $\bar{F}$ one has $\mathcal{R}(y) = R_\xi(y)$ while $\mathcal{R}(y) = -R_\xi''(y)$ for $X = \eta$ (note that this particular notation is specific only to this appendix). In what follows one denotes $\mathcal{G}[X; t, y]$ for short instead of $\mathcal{G}[X(t, y); t, y]$. Our aim is to deduce, from the Langevin equation (D1), evolution equations for the statistical average of functions of $\{X(t, y_i)\}$ at different points $\{y_i\}$, such as the two-point correlation function $\overline{X(t, y_1)X(t, y_2)}$.

This is fairly straightforward to obtain the time-derivative of $\overline{X(t, y)}$ by directly averaging (D1) which yields $\partial_t \overline{X(t, y)} = \overline{\mathcal{G}[X; t, y]}$ (e.g. (32) and (33)). The same cannot be applied to $\overline{X(t, y)^2}$ since, when writing

$$\partial_t \overline{X(t, y)^2} = 2\overline{X(t, y)\partial_t X(t, y)} \qquad \text{(D3)}$$
$$= 2\overline{X(t, y)\mathcal{G}[X; t, y]} + 2\overline{X(t, y)\mathcal{V}(t, y)} \quad \text{(D4)}$$

one cannot easily eliminate $\mathcal{V}$ from the last term. To tackle such correlation functions, one may use the functional Itō formula which reads as follows, for the Langevin equation (D1) with continuous argument y and non Dirac delta correlated random potential $\mathcal{V}$:

$$\partial_t \overline{g[X]} = \int dy \, \overline{\mathcal{G}[X; t, y] \frac{\delta g[X]}{\delta X(y)}}$$
$$+ \frac{D}{2} \int dy dy' \, \mathcal{R}(y' - y) \overline{\frac{\delta^2 g[X]}{\delta X(y)\delta X(y')}} \quad \text{(D5)}$$

where $g[X]$ is a functional of X. For $g[X] = \mathcal{O}(X(y_1))$ where y_1 is fixed (e.g. an observable depending on the sole DP endpoint), one thus finds

$$\partial_t \overline{\mathcal{O}(X(t, y_1))} = \overline{\mathcal{G}[X; t, y_1]\partial_X \mathcal{O}(X(t, y_1))}$$
$$+ \frac{D}{2}\mathcal{R}(0)\overline{\partial_X^2 \mathcal{O}(X(t, y_1))} \quad \text{(D6)}$$

For $\mathcal{O}(X) = X^2$ one finds

$$\partial_t \overline{X(t, y_1)^2} = 2\overline{\mathcal{G}[X; t, y_1]X(t, y_1)} + D\mathcal{R}(0) \qquad \text{(D7)}$$

which is the correct form of (D4). Note that the result is singular for $\xi \to 0$ in our cases of interest $\mathcal{R} = R_\xi$ and $\mathcal{R} = -R_\xi''$.

Another example is provided by the computation of the time evolution of the average of multiple-point correlators, for which (D5) yields:

$$\partial_t \overline{X(t, y_1)X(t, y_2)} = \overline{\mathcal{G}[X; t, y_1]X(t, y_2)} \qquad \text{(D8)}$$
$$+ \overline{\mathcal{G}[X; t, y_2]X(t, y_1)} + D\mathcal{R}(y_2 - y_1)$$

which yields back (D7) for $y_1 = y_2$. More generally, one has, noting $\partial_1 \mathcal{O}$ (respectively $\partial_2 \mathcal{O}$) the derivative of $\mathcal{O}$ with respect to its first (respectively second) argument:

$$\partial_t \overline{\mathcal{O}(X(t, y_1), X(t, y_2))}$$
$$= \overline{\mathcal{G}[X; t, y_1]\partial_1 \mathcal{O}(\ldots)} + \overline{\mathcal{G}[X; t, y_2]\partial_2 \mathcal{O}(\ldots)}$$
$$+ \frac{D}{2}\Big[\mathcal{R}(0)\partial_{11} + 2\mathcal{R}(y_2 - y_1)\partial_{12} + \mathcal{R}(0)\partial_{22}\Big]\overline{\mathcal{O}(\ldots)}$$
$$\text{(D9)}$$

We now derive the evolution equation for the correlator $\bar{R}(t, y)$ of $\eta_V(t, y)$. We first explicit some useful parity symmetry. The equation for $\eta_V(t, y)$ is the same as for $-\eta_{V^R}(t, -y)$ with a reflected disorder $V^R(t, y) = V(t, -y)$. This proves that

$$\eta_V(t, y) = -\eta_{V^R}(t, -y) \qquad \text{(D10)}$$

at all times. Since the distributions of V and V^R are the same, one can replace in averages every $\eta(t, -y)$ by $-\eta(t, y)$ without changing the result (so from on we skip the index V). In other words, $\eta(t, y)$ is an odd function of y in distribution. We now define a three-point correlation function

$$\bar{R}_3(t, y) = \overline{\eta(t, y)^2 \eta(t, 0)} \qquad \text{(D11)}$$

To simplify the notations, and since one only considers one-time observables at time t, we now drop the dependence in t and denote the derivation with respect to y by a prime. Using the noted parity (which also extend to the derivatives; e.g.: $\eta'(y)$ is an even function of y in distribution[76]) together with the statistical invariance by translation, one finds for instance, by translating all arguments by $-y$

$$\bar{R}''(y) = \overline{\eta''(y)\eta(0)} \overset{\text{(tr.)}}{=} \overline{\eta''(0)\eta(-y)} \overset{\text{(par.)}}{=} \overline{\eta''(0)\eta(y)} \quad \text{(D12)}$$
$$\frac{1}{2}\bar{R}_3'(y) = \overline{\eta'(y)\eta(y)\eta(0)} \overset{\text{(tr.)}}{=} \overline{\eta'(0)\eta(0)\eta(-y)}$$
$$\overset{\text{(par.)}}{=} \overline{\eta'(0)\eta(0)\eta(y)} \qquad \text{(D13)}$$

We are now ready to determine the time-evolution of $\bar{R}(t, y)$ combining (D8) and (F6):

$$\partial_t \bar{R}(t, y) = \partial_t \overline{\eta(0)\eta(y)} \qquad \text{(D14)}$$
$$\overset{\text{(D8)}}{=} \frac{T}{2c}\Big[\overline{\eta''(0)\eta(y)} + \overline{\eta''(y)\eta(0)}\Big]$$
$$- \frac{1}{c}\Big[\overline{\eta'(0)\eta(0)\eta(y)} + \overline{\eta'(y)\eta(y)\eta(0)}\Big]$$
$$- \frac{1}{t}\Big[2\overline{\eta(0)\eta(y)} + y\,\overline{\eta'(y)\eta(0)}\Big] - D R_\xi''(y)$$

We eventually recognize thanks to (D12) and (D13) that

$$\partial_t \bar{R}(t, y) = \frac{T}{c}\partial_y^2 \bar{R}(t, y) - \frac{1}{c}\partial_y \bar{R}_3(t, y)$$
$$- \frac{1}{t}\Big[\bar{R}(t, y) + \partial_y(y\,\bar{R}(t, y))\Big] - D R_\xi''(y)$$
$$\text{(D15)}$$

This equation is valid at all times and would in principle allow to studying of the 'flow' of $\bar{R}(t,y)$ starting from its initial condition $\bar{R}(0,y) \equiv 0$. Due to the non-linear KPZ term, it is however non-closed on the two-point correlation function $\bar{R}(t,y)$ and brings into the game a three-point correlation function $\bar{R}_3(t,y)$, making it necessary to solve the full hierarchy of equations for the n-point functions to determine $\bar{R}(t,y)$. Yet, using a scaling Ansatz in $y = 0$, the equation (D15) still enables to determine the time evolution of the height of the $\bar{R}(t,y)$ in $y = 0$ (see Sec. V).

Similarly, defining the three-point correlation function for $\bar{F}$

$$\bar{C}_3(t,y) \equiv -2\overline{\left[\bar{F}(t,y) - \bar{F}(t,0)\right]\left[\bar{F}'(t,0)\right]^2} \quad \text{(D16)}$$

one obtains the flow of $\bar{C}(t,y)$ using (F4) in (D9) with $\mathcal{O}(X_1, X_2) = (X_1 - X_2)^2$, $X_1 = \bar{F}(t,y)$ and $X_2 = \bar{F}(t,0)$:

$$\partial_t \bar{C}(t,y) = \frac{T}{c}\left[\bar{C}''(t,y) - \bar{C}''(t,0)\right] - \frac{y}{t}\bar{C}'(t,y) - \frac{1}{c}\bar{C}_3(t,y) - 2D\left[R_\xi(y) - R_\xi(0)\right] \quad \text{(D17)}$$

Appendix E: Solution of the linearized dynamics of $\bar{F}$ for a generic disorder correlator $R_\xi(y)$

In this appendix, we determine the explicit form of the correlator $\bar{C}(t,y)$ (resp. $\bar{R}(t,y)$) of the disorder free-energy $\bar{F}$ (resp. of the random phase $\bar{\eta}$), in the approximation where the 'time'-evolution equation of those quantities is linearized. The crossover from finite to infinite 'time' regime is discussed.

The evolution equations (35) for $\bar{C}(t,y)$ and (34) for $\bar{R}(t,y)$ are not closed because of the three-point correlation functions $\bar{C}_3(t,y)$ and $\bar{R}_3(t,y)$. It is yet instructive to solve those equations in the approximation where those three-point functions are set to zero. An equivalent alternative approach is to solve directly the equation (26) for $\bar{F}$ or (27) for η by neglecting again the non-linear terms in those equations (see also Appendix C 'Short-time dynamics (diffusive scaling)' of Ref. 46, for the explicit case of Gaussian function for the microscopic disorder correlator $R_\xi(y)$). We denote by $\bar{C}^{\text{lin}}(t,y)$ and $\bar{R}^{\text{lin}}(t,y) = \frac{1}{2}\partial_y^2 \bar{C}^{\text{lin}}(t,y)$ their solutions, which are expected to be valid either at small 'times' for all y (because the initial condition ensures those functions vanish uniformly at 'time' 0) or at all 'times' but small y in the high-temperature regime (see Sec. V B for a discussion).

The equations at hand are linear and are thus solved e.g. using Green functions, and the solution takes the form

$$\bar{C}^{\text{lin}}(t,y) = D \int dw\, K_t(y,w) R_\xi(w) \quad \text{(E1)}$$

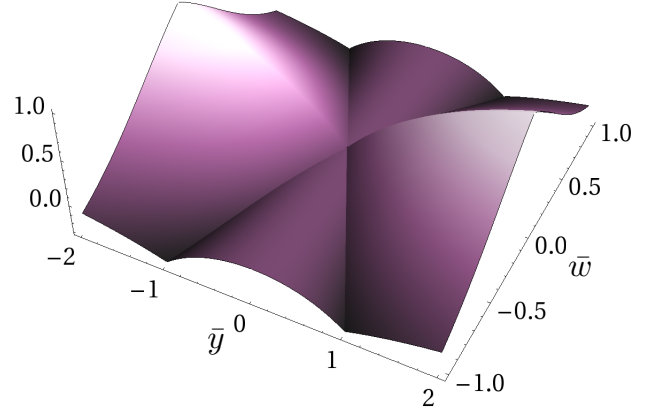FIG. 19. Kernel $\hat{K}(\bar{y},\bar{w})$ defined in (E5) linking the linearized free-energy correlator $\bar{C}^{\text{lin}}(t,y)$ and the disorder correlator $R_\xi(y)$ with the combination of (E3)-(E4).

where the kernel reads $K_t(y,w) = \int_0^t ds\, K_s(y,w;t)$ with

$$K_s(y,w;t) = \frac{\beta ct}{2\sqrt{\pi}}\frac{1}{\sqrt{\beta cst(t-s)}} \quad \text{(E2)}$$
$$\times\left[2e^{-\frac{\beta ct}{4}\frac{w^2}{s(t-s)}} - e^{-\frac{\beta c}{4}\frac{(tw-sy)^2}{ts(t-s)}} - e^{-\frac{\beta c}{4}\frac{(tw+sy)^2}{ts(t-s)}}\right]$$

The scaling analysis of this expression may be obtained by setting $s = t\tau$. To this end, we assume the natural rescaling $R_\xi(a\bar{y}) = a^{-1}R_{\xi/a}(\bar{y})$ of the disorder correlator. One obtains that the free-energy correlator rescales *purely diffusively* as

$$\bar{C}^{\text{lin}}(t,y) = \frac{cD}{T}\sqrt{B_{\text{th}}(t)}\,\hat{C}_{\frac{\xi}{\sqrt{B_{\text{th}}(t)}}}\left(\frac{y}{\sqrt{B_{\text{th}}(t)}}\right) \quad \text{(E3)}$$

with as usual $B_{\text{th}}(t) = \frac{Tt}{c}$ and with the scaling function

$$\hat{C}_{\bar{\xi}}(\bar{y}) = \int d\bar{w}\,\hat{K}(\bar{y},\bar{w})R_{\bar{\xi}}(\bar{w}) \quad \text{(E4)}$$

$$\hat{K}(\bar{y},\bar{w}) = \int_0^1 \frac{d\tau}{2\sqrt{\pi}}\frac{1}{\sqrt{\tau(1-\tau)}} \quad \text{(E5)}$$
$$\times\left[2e^{-\frac{\bar{w}^2}{4\tau(1-\tau)}} - e^{-\frac{(\bar{w}-\tau\bar{y})^2}{4\tau(1-\tau)}} - e^{-\frac{(\bar{w}+\tau\bar{y})^2}{4\tau(1-\tau)}}\right]$$

Under this scaling, the whole $\{c, D, T\}$-dependence is absorbed in the prefactor $\frac{cD}{T}$. The scaling kernel $\hat{K}(\bar{y},\bar{w})$, illustrated on Fig. 19 is continuous but non-analytical on the lines $|\bar{y}| = |\bar{w}|$, as can be seen from the direct computation of (E5), which, using the symmetry by even parity is expressed for $\bar{y} \geq 0$ as:

$$\hat{C}_{\bar{\xi}}(\bar{y}) \stackrel{(\bar{y}\gtreqless 0)}{=} \int_0^{\bar{y}} d\bar{w}\,\hat{K}^<(\bar{y},\bar{w})R_{\bar{\xi}}(\bar{w}) \quad \text{(E6)}$$
$$+ \int_{\bar{y}}^\infty d\bar{w}\,\hat{K}^>(\bar{y},\bar{w})R_{\bar{\xi}}(\bar{w})$$

$$\frac{\hat{K}^<(\bar{y},\bar{w})}{2\sqrt{\pi}} = 1 - \text{Erf}\,\bar{w} - \frac{e^{\frac{\bar{y}^2}{4}}}{2}\left(2 - \text{Erf}\frac{\bar{y}}{2} - \text{Erf}\frac{\bar{y}+2\bar{w}}{2}\right)$$

$$\frac{\hat{K}^>(\bar{y},\bar{w})}{2\sqrt{\pi}} = 1 - \text{Erf}\,\bar{w} - \frac{e^{\frac{\bar{y}^2}{4}}}{2}\left(2 + \text{Erf}\frac{\bar{y}-2\bar{w}}{2} - \text{Erf}\frac{\bar{y}+2\bar{w}}{2}\right)$$
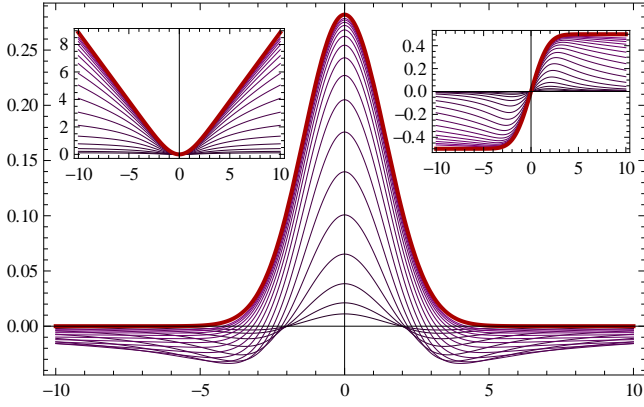
FIG. 20. (Color online) The finite-'time' correlator $\bar{R}^{\mathrm{lin}}(t,y)$ (thin purple lines) for the 'Gauss' disorder correlator $R_\xi(y) = R_\xi^{\mathrm{Gauss}}(y)$, plotted as a function of y for different 'times', compared to its infinite-time limit $R_\xi(y)$ (thick red line), with $\xi = 1$, $c = 1$, $D = 1$, and $T = 1$. Larger 'times' correspond to lighter colors. *Left inset*: same behavior for $\bar{C}^{\mathrm{lin}}(t,y)$. *Right inset*: same behavior for $\frac{1}{2}\partial_y\bar{C}^{\mathrm{lin}}(t,y) = \int_0^y dy'\,\bar{R}^{\mathrm{lin}}(t,y')$.

Those expressions describe through (E3) the complete transition from the initial regime where the correlator is close to zero to the infinite-time asymptotic regime, where one should recover $\lim_{t\to\infty}\bar{R}^{\mathrm{lin}}(t,y) = \frac{cD}{T}R_\xi(y)$ (see Sec. F 3).

As we now detail, this infinite-'time' limit is however not obvious to extract from (E6) and is in fact directly related to the non-analyticity of $\hat{K}(\bar{y},\bar{w})$. Carefully integrating by part and differentiating with respect to $\bar{y}$ leads to the following expression, valid provided that $R_\xi(y)$ is bounded at infinity

$$\frac{1}{2}\hat{C}'(\bar{y}) \overset{(\bar{y}\geq 0)}{=} R_{\bar{\xi}}^{(-1)}(\bar{y}) + \int_0^\infty d\bar{w}\,\bar{w}e^{-\bar{w}(\bar{w}+\bar{y})}R_{\bar{\xi}}^{(-1)}(\bar{w})$$
$$- \int_{\bar{y}}^\infty d\bar{w}\,\bar{w}e^{-\bar{w}(\bar{w}-\bar{y})}R_{\bar{\xi}}^{(-1)}(\bar{w}) \qquad \text{(E7)}$$

Here $R_{\bar{\xi}}^{(-1)}(\bar{y})$ is the primitive of $R_{\bar{\xi}}(\bar{y})$ which vanishes in 0. It verifies the scaling relation $R_\xi^{(-1)}(a\bar{y}) = R_{\xi/a}^{(-1)}(\bar{y})$ and its small $\bar{\xi}$ limit is half of the Heaviside step function $\lim_{\bar{\xi}\to 0} R_{\bar{\xi}}^{(-1)}(\bar{y}) = \frac{1}{2}\Theta(\bar{y})$, provided now that $R_{\bar{\xi}}(\bar{y})$ describes a RB disorder. Its occurrence as the first term of (E7) arises from the jump of the slope of $\hat{K}(\bar{y},\bar{w})$ in $\bar{y} = \bar{w}$, depicted in Fig. 19. Using those properties one obtains

$$\lim_{t\to\infty}\frac{1}{2}\hat{C}'_{\frac{\xi}{\sqrt{B_{\mathrm{th}}(t)}}}\left(\frac{y}{\sqrt{B_{\mathrm{th}}(t)}}\right) \overset{\longrightarrow \frac{1}{2}\int_0^\infty d\bar{w}\,\bar{w}e^{-\bar{w}^2}\Theta(\bar{w})}{}$$
$$= R_\xi^{(-1)}(y) + \lim_{t\to\infty}\left\{\overbrace{\int_0^\infty d\bar{w}\,\bar{w}e^{-\bar{w}(\bar{w}+y^t)}R_{\xi^t}^{(-1)}(\bar{w})}\right.$$
$$\left.- \underbrace{\int_{y^t}^\infty d\bar{w}\,\bar{w}e^{-\bar{w}(\bar{w}-y^t)}R_{\xi^t}^{(-1)}(\bar{w})}_{\longrightarrow \frac{1}{2}\int_0^\infty d\bar{w}\,\bar{w}e^{-\bar{w}^2}\Theta(\bar{w})}\right\}$$
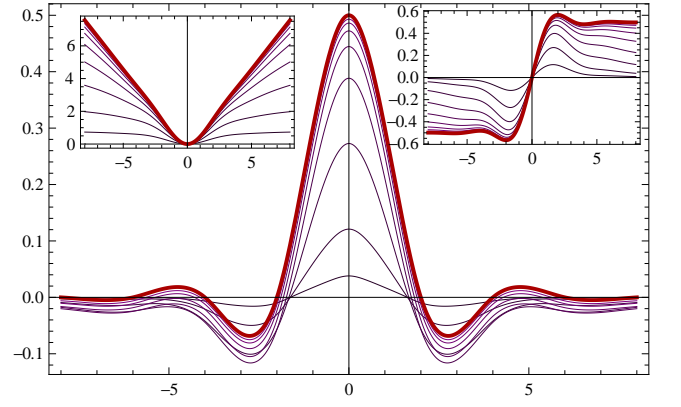$$= R_\xi^{(-1)}(y) \qquad \text{(E8)}$$

FIG. 21. Same correlators as in Fig. 20, now corresponding to the 'CubicS' disorder correlator $R_\xi(y) = R_\xi^{\mathrm{CubicS}}(y)$, defined in (I2)-(I3). Parameters are $\xi = 2$, $c = 1$, $D = 1$, and $T = 1$.

where we have denoted for short $y^t = y/\sqrt{B_{\mathrm{th}}(t)}$ and $\xi^t = \xi/\sqrt{B_{\mathrm{th}}(t)}$. Differentiating with respect to y, one obtains the expected result $\lim_{t\to\infty}\bar{R}^{\mathrm{lin}}(t,y) = \frac{cD}{T}R_\xi(y)$, while keeping t finite yields the decomposition (40-41) of $\bar{R}(t,y)$ announced in Sec. III A. The short to large-'time' behavior of the correlators is illustrated in Fig. 20 for the Gaussian disorder correlator $R_\xi(y) = \mathcal{R}_\xi^{\mathrm{Gauss}}(y)$ defined in (88).

As depicted in Fig. 21, one may also measure numerically the correlator $\bar{R}^{\mathrm{lin}}(t,y)$ for the disorder correlator $R_\xi(y) = R_\xi^{\mathrm{CubicS}}(y)$ defined in (I2)-(I3). As in Sec. IV B we fitted the average of this correlator over large 'times' at $\xi = 2$, $c = 1$, $D = 1$ and $T = 1$, using the 'Gauss' and the 'SincG' fitting functions. Parameters are found to be

$$\widetilde{D}_{\mathrm{sat}}^{\mathrm{SincG}}/\widetilde{D}_{\mathrm{sat}}^{\mathrm{Gauss}} \simeq 0.89 \qquad \tilde{\xi}_{\mathrm{sat}}^{\mathrm{SincG}}/\tilde{\xi}_{\mathrm{sat}}^{\mathrm{Gauss}} \simeq 3.27 \quad \text{(E9)}$$

which correspond to the *same* results as in the high-temperature regime of Sec. IV B (see Table I). We checked that this numerical results depend only slightly on the value of the temperature, decreasing with T.

Appendix F: Fokker-Planck equations for the pseudo free-energy

Starting from the path integral formulation of the pseudo free-energy, the average over thermal fluctuations yields the so-called 'Feynman-Kac' equations for $\partial_t W_V(t,y)$, $\partial_t\bar{F}_\eta(t,y)$, $\partial_t\eta_V(t,y)$. In this section, we re-examine the possible steady-state solutions of the Fokker-Planck equations, obtained after the disorder average over the random potential, and try to generalize them from the uncorrelated disorder ($\xi = 0$) to the case of a random-bond correlated disorder ($\xi > 0$ and short-range correlator).

1. FP equations for F_V, $\bar{F}_V$ and η_V

The pseudo free-energy $F_V(t,y)$ follows the KPZ equation (25):

$$\partial_t F_V(t,y) = \mathcal{G}\left[F_V(t,y)\right] + V(t,y) \qquad (\text{F1})$$

$$\mathcal{G}\left[F\right] \equiv \frac{T}{2c}\partial_y^2 F(y) - \frac{1}{2c}\left[\partial_y F(y)\right]^2 \qquad (\text{F2})$$

and similarly the disorder free-energy $\bar{F}_V(t,y)$ follows the *tilted* KPZ equation (26) depending explicitly on (t,y):

$$\partial_t \bar{F}_V(t,y) = \bar{\mathcal{G}}\left[\bar{F}_V(t,y); t,y\right] + V(t,y) \qquad (\text{F3})$$

$$\bar{\mathcal{G}}\left[\bar{F}; t,y\right] \equiv \mathcal{G}\left[\bar{F}\right] - \frac{y}{t}\partial_y \bar{F}(y) \qquad (\text{F4})$$

as its corresponding random phase $\eta_V(t,y) = \partial_y \bar{F}_V(t,y)$:

$$\partial_t \eta_V(t,y) = \mathcal{G}_\eta\left[\bar{\eta}_V(t,y); t,y\right] + \partial_y V(t,y) \qquad (\text{F5})$$

$$\mathcal{G}_\eta\left[\eta; t,y\right] \equiv \frac{T}{2c}\partial_y^2 \eta(y) - \frac{\partial_y\left[\eta(y)^2\right]}{2c} - \partial_y\left[\frac{y}{t}\eta(y)\right] \quad (\text{F6})$$

Combining the Feynman-Kac equations (25)-(27) and the random-potential disorder correlator:

$$\overline{V(t,y)V(t',y')} = D \cdot \delta(t-t') \cdot R_\xi(y-y') \qquad (\text{F7})$$

the 'time'-evolution of the free-energy distribution $\bar{\mathcal{P}}\left[F,t\right]$ is then given by the functional FP equation (obtained *e.g.* from Itō's lemma):

$$\partial_t \bar{\mathcal{P}}\left[F,t\right] = \int dy \frac{\delta}{\delta F(y)}\left\{-\mathcal{G}\left[F\right]\bar{\mathcal{P}}\left[F,t\right]\right\}$$
$$+ \frac{D}{2}\int dy\, dy' \cdot R_\xi(y-y')\frac{\delta^2 \bar{\mathcal{P}}\left[F,t\right]}{\delta F(y)\delta F(y')} \qquad (\text{F8})$$

with those two terms stemming respectively from the deterministic operator $\mathcal{G}$ and the remaining stochastic term in the Feynman-Kac equation. The distribution $\bar{\mathcal{P}}\left[\bar{F}_V,t\right]$ follows the same functional FP equation, with the tilt of the deterministic operator $\mathcal{G}\left[F\right] \mapsto \bar{\mathcal{G}}\left[\bar{F}; t,y\right]$, whereas the random-phase counterpart satisfies:

$$\partial_t \bar{\mathcal{P}}\left[\eta,t\right] = \int dy \frac{\delta}{\delta \eta(y)}\left\{-\mathcal{G}_\eta\left[\eta; t,y\right]\bar{\mathcal{P}}\left[\eta,t\right]\right\}$$
$$- \frac{D}{2}\int dy\, dy' \cdot R_\xi''(y-y')\frac{\delta^2 \bar{\mathcal{P}}\left[\eta,t\right]}{\delta \eta(y)\delta \eta(y')} \qquad (\text{F9})$$

The detailed notations $F_V(t,y)$, $\bar{F}_V(t,y)$ and $\eta_V(t,y)$ have been simplified to the random functions $F(y)$, $\bar{F}(y)$ ad $\eta(y)$ of respective distributions $\bar{\mathcal{P}}\left[F,t\right]$, $\bar{\mathcal{P}}\left[\bar{F},t\right]$ and $\bar{\mathcal{P}}\left[\eta,t\right]$ at a fixed 'time' t, though their random nature is initially stemming from the microscopic random potential V.

2. Steady-state solution at $\xi = 0$

For an uncorrelated disorder, the disorder correlator reduces to a normalized Dirac δ-function $R_{\xi=0}(y) = \delta(y)$

and the Gaussian distribution

$$\bar{\mathcal{P}}_{\text{st}}\left[F\right] \propto \exp\left\{-\frac{\lambda}{2}\int dy\left[\partial_y F(y)\right]^2\right\} \qquad (\text{F10})$$

is a steady-state solution of (F8), *i.e.* $\partial_t \bar{\mathcal{P}}_{\text{st}}\left[F\right] = 0$, provided that $\lambda^{-1} = \frac{cD}{T}$ (see Ref. 29). This condition comes solely from the counterbalance of the diffusive term $\frac{T}{2c}\partial_y^2 F(y)$ and the stochastic term $\frac{D}{2}\frac{\delta \bar{\mathcal{P}}[F]}{\delta F(y)}$. As for the contribution of the non-linear KPZ term $-\frac{1}{2c}\left[\partial_y F(y)\right]^2$, it disappears[13] under the boundary condition $F'(y)|_{y\pm\infty} = 0$.

There is no 'time' dependence in the FP equation (F1), but the Gaussian PDF (F10) is a steady-state solution only at $t = \infty$ for our physical definition of the pseudo free-energy (12) which satisfies

$$\partial_y F_V(t,y) = \partial_y F_{\text{th}}(t,y) + \partial_y \bar{F}_V(t,y) = c\frac{y}{t} + \eta_V(t,y) \qquad (\text{F11})$$

and it then becomes equivalent to the two normalized Gaussian PDF:

$$\bar{\mathcal{P}}_{\text{G}}^0\left[\bar{F}\right] = \frac{1}{C_1(\lambda)}\exp\left\{-\frac{\lambda}{2}\int dy\left[\partial_y \bar{F}(y)\right]^2\right\} \quad (\text{F12})$$

$$\bar{\mathcal{P}}_{\text{G}}^0\left[\eta\right] = \frac{1}{C_2(\lambda)}\exp\left\{-\frac{\lambda}{2}\int dy\left[\eta(y)\right]^2\right\} \qquad (\text{F13})$$

with $C_2(\lambda)$ defined by $\int \mathcal{D}\eta(y) \cdot \bar{\mathcal{P}}_{\text{G}}^0\left[\eta\right] = 1$ and similarly for $C_1(\lambda)$. Choosing $\lambda^{-1} = \frac{cD}{T}$ and the boundary condition $\bar{F}'(y)|_{y\pm\infty} = \eta(y)|_{y\pm\infty} = 0$, the FP equation eventually yields for the Gaussian distributions:

$$\partial_t \bar{\mathcal{P}}_{\text{G}}^0\left[\bar{F}\right] = \frac{1}{t}\bar{\mathcal{P}}_{\text{G}}^0\left[\bar{F}\right] \cdot \log\left\{C_1(\lambda)\bar{\mathcal{P}}_{\text{G}}^0\left[\bar{F}\right]\right\} \qquad (\text{F14})$$

$$\partial_t \bar{\mathcal{P}}_{\text{G}}^0\left[\eta\right] = \frac{1}{t}\bar{\mathcal{P}}_{\text{G}}^0\left[\eta\right] \cdot \left\{\int dy\,\delta(0) + \log\left\{C_1(\lambda)\bar{\mathcal{P}}_{\text{G}}^0\left[\eta\right]\right\}\right\}$$

the equivalent equation for $\partial_t \bar{\mathcal{P}}_{\text{G}}^0\left[\eta\right]$ being apparently ill-defined in the functional derivative framework, due to an additive divergent constant $\delta(0)$. So the Gaussian distributions (F12) and (F13) (with $\xi = 0$) become a steady-state solution only at infinite 'time' in order to cancel the whole contribution (F14), since the value of λ has been fixed as a 'time'-independent constant.

Actually the chosen boundary condition is the only one physically possible at all 'times':

$$\partial_y \bar{F}_V(t,y)|_{y\pm\infty} = \eta_V(t,y)|_{y\pm\infty} = 0 \qquad (\text{F15})$$

since by construction $\bar{\mathcal{P}}_{\text{G}}^0\left[\bar{F}\right]$ and $\bar{\mathcal{P}}_{\text{G}}^0\left[\eta\right]$ penalize the functions $\bar{F}(y)$ and $\eta(y)$ whose fluctuations extend too much in the y-direction. The boundary condition at $y = \pm\infty$ is thus free from that point of view but should also be compatible with $\overline{\eta_V(t,y)} = 0$ (32).

3. Steady-state solution of the linearized FP equation at $\xi > 0$

The Gaussian PDF (F12)-(F13) can be generalized with the introduction of the correlator $\bar{R}^{-1}(t,y)$ whose

functional inverse is defined by (20):

$$\bar{\mathcal{P}}_{\mathrm{G}}\left[\bar{F}, t\right] \propto e^{-\frac{1}{2}\int dy\, dy'\, \bar{F}'(y)\bar{R}^{-1}(t,|y-y'|)\bar{F}'(y')} \qquad \text{(F16)}$$

$$\bar{\mathcal{P}}_{\mathrm{G}}\left[\eta, t\right] \propto e^{-\frac{1}{2}\int dy\, dy'\, \eta(y)\bar{R}^{-1}(t,|y-y'|)\eta(y')} \qquad \text{(F17)}$$

with the proper 'time'-dependent normalization of PDF such that $\int \mathcal{D}\bar{F}(y) \cdot \bar{\mathcal{P}}_{\mathrm{G}}\left[\bar{F}, t\right] = \int \mathcal{D}\eta(y) \cdot \bar{\mathcal{P}}_{\mathrm{G}}\left[\eta, t\right] = 1$.

These expressions actually describe correctly the distributions corresponding to the *linearized* problem, namely to the equations (F1-F6) where the KPZ quadratic contributions to the functionals $\mathcal{G}$ are set to 0. Indeed, the solution in the fields F_V, $\bar{F}_V$ and η_V of those equations is linear in the disorder potential $V(t, y)$, whose distribution is Gaussian, implying that the distributions of the fields are themselves Gaussian. We refer the reader to Appendix E for motivations to study the linearized problem and for a solution leading to the two-point correlator $\bar{R}^{\mathrm{lin}}(t, y)$ given in (40-41), and actually providing the full 'time'-dependent distributions through (F16-F17) with $\bar{R} = \bar{R}^{\mathrm{lin}}$.

At $\xi = 0$ the solution of the full problems (F1-F6) is not Gaussian at finite 'time', as known from the exact solutions[18,54,56,57] but becomes Gaussian at infinite 'time', as detailed in the previous subsection. At $\xi > 0$ this last property does however not hold anymore. Indeed, anticipating slightly on Sec. V B, if the steady distribution of η were Gaussian then the three-point function $\bar{R}_3(t, 0)$ would be zero by parity in the field η, and from (91) the infinite-'time' limit of the height $\bar{R}(t, 0)$ of the correlator would be the same in the linearized and in the original problem, which is not true.

Another way to illustrate this fact is to try to solve the FP equation (F8) inserting the Gaussian Ansatz (F16). Using the fast decay of $R(y)$ and $R'(y)$ at large y for the vanishing of boundary terms, we obtain from the right hand side of (F8)

$$\frac{\partial_t \bar{\mathcal{P}}_{\mathrm{G}}\left[\bar{F}, t\right]}{\bar{\mathcal{P}}_{\mathrm{G}}\left[\bar{F}, t\right]} = \frac{1}{2}\int dy\, d\tilde{y}\, \bar{F}''(\tilde{y})\bar{R}^{-1}(t,|\tilde{y}-y|)$$
$$\times \left\{ D\int dy'\, \mathcal{F}(t,|y-y'|)\bar{F}''(y') - 2\bar{\mathcal{G}}\left[\bar{F}; t, y\right] \right\} \qquad \text{(F18)}$$
$$- \frac{T}{2c}\int dy\, dy' \cdot \delta(y-y')\delta''(y-y')$$

with the definition:

$$\mathcal{F}(t, y_1 - y_2) \equiv \int dy_3\, R(|y_1-y_3|)\bar{R}^{-1}(t,|y_2-y_3|) \qquad \text{(F19)}$$

On the other hand, the left hand side of (F8) yields, differentiating with respect to 'time':

$$\frac{\partial_t \bar{\mathcal{P}}_{\mathrm{G}}\left[\bar{F}, t\right]}{\bar{\mathcal{P}}_{\mathrm{G}}\left[\bar{F}, t\right]} = -\frac{1}{2}\int dy\, dy'\, \bar{F}'(y)\partial_t \bar{R}^{-1}(t,|y-y'|)\bar{F}'(y')$$
$$\text{(F20)}$$

Considering first the linearized case, the identification of (F18) and (F20) yields, upon appropriate integrations by part, an equation of the form

$$\int dy\, dy'\, \bar{F}'(y')M(t; y', y)\bar{F}'(y) = 0 \qquad \text{(F21)}$$

where $M(t; y', y) = M(t; y' - y)$ is a translation-invariant symmetric functional operator which combines $\bar{R}$ and R. Since (F21) is valid for any function $\bar{F}'$ decaying fast enough at infinity, solving this equation amounts to canceling the operator $M(t; y', y)$. After some manipulations aiming at casting the functional equation $M(t; y', y) = 0$ into a diagonal form, the linearized form of the 'flow' equation (34) on $\bar{R}(t, y)$ is precisely recovered, namely

$$\partial_t \bar{R}(t, y) = \frac{T}{c}\partial_y^2 \bar{R}(t, y) - \frac{1}{t}\left\{ \bar{R}(t, y) + \partial_y\left[y\bar{R}(t, y)\right] \right\}$$
$$- DR_\xi''(y) \qquad \text{(F22)}$$

In the process, the divergent part on the last line of (F18) was discarded. This flow equation was obtained in Appendix D using Itō's lemma, including the non-linearized case, and without having singular terms to discard (which we attribute to an artifact of functional calculus in the computation above). The infinite-'time' steady-state solution thus verifies: $\frac{T}{c}\partial_y^2\bar{R}(\infty, y) - DR_\xi''(y) = 0$ which implies directly the expected result $\bar{R}(\infty, y) = \frac{cD}{T}R_\xi(y)$. It ensures that $\mathcal{F}(t, y) \to (\frac{cD}{T})^{-1}\delta(y)$ in (F19) as t goes to infinity, which actually prevents the divergent term to appear in (F18). The finite-'time' solution is studied in Appendix E.

Taking however the corresponding steady-state distribution (F16) with $\bar{R}(t, y) = \frac{cD}{T}R_\xi(y)$ as trial steady solution for the full equation (F8) yields a remaining term, arising from the non-linearity, cubic in $\bar{F}$ (*i.e.* not of the form (F21)), which vanishes only at $\xi = 0$.

Appendix G: Scaling laws in the convention of mathematicians

The DES model defined in Sec. II A depends on the four independent parameters $\{c, D, T, \xi\}$, with the elastic constant c being fixed independently from the temperature in the usual convention considered by physicists. However, an alternative convention used by mathematicians is $c = T$, whose consequences on the scaling arguments of Sec. III C and the saddle-point arguments of Sec. III D are discussed in this appendix.

One is interested in the generic scaling of the prefactor of the roughness $B(t; c, D, T, \xi)$ in the random-manifold regime (of roughness exponent $\zeta_{\mathrm{RM}} = \frac{2}{3}$):

$$B(t; c, D, T, \xi) \overset{t\to\infty}{\sim} A_{\mathrm{RM}}(c, D, T, \xi)t^{2\zeta_{\mathrm{RM}}} \qquad \text{(G1)}$$

The scaling in temperature of the prefactor is described by the *thorn* exponent þ defined by $A(c, D, T, \xi) \sim T^{2þ}$. We have derived in section III C from a scaling analysis that, depending on the temperature regime with respect to $T_c = (\xi cD)^{1/3}$, the expressions of the prefactor $A_{\mathrm{RM}}(c, D, T, \xi)$ are

$$A_{\mathrm{RM}} \overset{(T\gg T_c)}{=} \left(\frac{D}{cT}\right)^{\frac{2}{3}} \qquad A_{\mathrm{RM}} \overset{(T\ll T_c)}{=} \left(\frac{D^2}{c^4\xi}\right)^{\frac{2}{9}} \qquad \text{(G2)}$$

While $\beta_{\mathrm{RM}}^{T \gg T_c} = -\frac{1}{3}$ at high temperatures, the existence of the *microscopic* length $\xi > 0$ alters the value of the thorn exponent to $\beta_{\mathrm{RM}}^{T \ll T_c} = 0$ at low temperatures, even though this exponent describes *large-scale* properties of the polymer.

In this appendix, we determine how those exponents change when taking the particular convention $c = T$, often chosen in the mathematics community – prompting us to denote by a subscript '$\mathfrak{m}$' the observables defined with this convention *e.g.*

$$B^{\mathfrak{m}}(t; D, T, \xi) \overset{t \to \infty}{\sim} A_{\mathrm{RM}}^{\mathfrak{m}}(D, T, \xi) t^{2\zeta_{\mathrm{RM}}} \quad (\mathrm{G3})$$

Physically, the choice $c = T$ amounts to render the elastic weight temperature-independent, (3) becoming

$$W_V^{\mathfrak{m}}(t_1, y_1) = \int_{y(0)=0}^{y(t_1)=y_1} \mathcal{D}y \, e^{-\int_0^{t_1} dt \left[\frac{(\partial_t y)^2}{2} + \frac{1}{T} V(t, y(t)) \right]} \quad (\mathrm{G4})$$

Here $\frac{1}{T}$ only tunes the relative importance of disorder with respect to elasticity. The parametrization $c = T$ also arises in the continuum limit of the discrete simple SOS directed polymer model[31,46] and is thus of interest to analyze numerical results of this system.

Before handling the different limits with respect to T of (G4) in a functional integral saddle-point approach similar to that of section III D, we first recall some results on the asymptotics of integrals with one variable. The aim is to determine a (logarithmic) equivalent at large p of integrals of the form $I(p) = \int dy \, f(y) e^{-pg(y)}$. The following result holds: if $g(y)$ has a unique, finite, minimum value reached in $y^\star$, then

$$I(p) \overset{p \to \infty}{\sim} f(y^\star) e^{-pg(y^\star)} \quad (\mathrm{G5})$$

Here $y^\star$ is the point (or one point) where the minimum of $g(y)$ is reached, and is thus by definition independent of p. Powerlaw corrections in p may arise from the integration of fluctuations around $y^\star$, but they disappear *e.g.* in ratios of the following form (see (72) and (78) for the DP):

$$\frac{\int dy \, f(y) e^{-pg(y)}}{\int dy \, e^{-pg(y)}} \overset{p \to \infty}{\sim} \frac{f(y^\star) e^{-pg(y^\star)}}{e^{-pg(y^\star)}} = f(y^\star) \quad (\mathrm{G6})$$

The existence of the finite minimum is crucial, as illustrated from the derivation of Stirling's formula for the equivalent of the factorial. Starting from

$$p! = \int_{\mathbb{R}^+} dy \, e^{-y} y^p = \int_{\mathbb{R}^+} dy \, e^{-y} e^{p \log y} \quad (\mathrm{G7})$$

one may be tempted to apply (G5) with

$$f(y) = e^{-y} \qquad g(y) = -\log y \quad (\mathrm{G8})$$

which, assuming blindly that $g(y)$ reaches a *finite* minimum in $y^\star$ would yield the wrong result $p! \overset{p \to \infty}{\sim} e^{-y^\star} e^{p \log y^\star}$. The loophole here is that

$g(y) = -\log y$ reaches no finite minimum on $\mathbb{R}^+$. On this simple example, the clue is to rescale y by a factor p ($y = p\bar{y}$) and write instead of (G7)

$$p! = p^{p+1} \int_{\mathbb{R}^+} d\bar{y} \, e^{-p\bar{y}} \bar{y}^p = p^{p+1} \int_{\mathbb{R}^+} d\bar{y} \, e^{-p(\bar{y} - \log \bar{y})} \quad (\mathrm{G9})$$

now with $f(\bar{y}) = 1$ and $g(\bar{y}) = \bar{y} - \log \bar{y}$ which is minimal in $\bar{y}^\star = 1$ one obtains correctly[77] $p! \overset{p \to \infty}{\sim} p^{p+1} e^{-p}$. Note that, coming back to the initial variable y, we see that the optimum $y^\star$ of $g(y)$ in (G8) was not finite but diverging to infinity as $y^\star = p\bar{y}^\star = p$ for $p \to \infty$. In other words, the rescaling $y = p\bar{y}$ in (G9) allows to find the optimal y at the correct scale in the large parameter p.

Consider first the well-controlled high-temperature regime. Since the rescaling of section III C is at $c = T = 1$, it is compatible with the mathematician's convention and one can export directly (54)-(55) imposing $c = T$

$$B^{\mathfrak{m}}(t; D, T, \xi) = \xi_{\mathrm{th}}^{\mathfrak{m}}(T)^2 B\left(\frac{t}{t_*^{\mathfrak{m}}(T)}; 1, 1, \frac{\xi}{\xi_{\mathrm{th}}^{\mathfrak{m}}(T)}\right) (\mathrm{G10})$$

$$t_*^{\mathfrak{m}}(T) = \frac{T^4}{D^2}, \, \xi_{\mathrm{th}}^{\mathfrak{m}}(T) = \frac{T^2}{D} \quad (\mathrm{G11})$$

The regime $\xi \ll \xi_{\mathrm{th}}^{\mathfrak{m}}(T)$, or equivalently $T \gg T_c^{\mathfrak{m}}$, with $T_c^{\mathfrak{m}} = \sqrt{\xi D}$ describes the high-temperature limit and consists in replacing $\frac{\xi}{\xi_{\mathrm{th}}^{\mathfrak{m}}(T)}$ by 0 in (G10). In the large-time limit ($t \gg t_*^{\mathfrak{m}}(T)$), this yields $A_{\mathrm{RM}}^{\mathfrak{m}}(D, T, \xi)|_{(T \gg T_c^{\mathfrak{m}})} = (DT^{-2})^{\frac{2}{3}}$ and the high-temperature thorn exponent is thus $\beta_{\mathrm{RM}}^{\mathfrak{m}} \overset{(T \gg T_c)}{=} -\frac{2}{3}$.

The low-temperature regime is however less direct to handle, since the rescaling (56-57) of section III C is not at $c = T$ and thus cannot be directly exported to the mathematician's convention. Anyway as first choice the rescaling $a = \xi, b = \xi^2$ allows to rescale at $\xi = 1$ and to respect the mathematician's convention: the elastic term is unchanged ($c = T$) in the weight

$$W_V^{\mathfrak{m}}(t_1, y_1) \overset{(d)}{=} \int_{\bar{y}(0)=0}^{\bar{y}(t_1)=y_1/\xi} \mathcal{D}\bar{y} \, e^{-\int_0^{t_1/\xi^2} dt \left[\frac{(\partial_t \bar{y})^2}{2} + \frac{T_c^{\mathfrak{m}}}{T} V_1(t, \bar{y}(t)) \right]} \quad (\mathrm{G12})$$

where $V_1(t, y(t)) \equiv V(t, y(t))|_{D=1, \xi=1}$, from which one reads

$$B^{\mathfrak{m}}(t; D, T, \xi) = \xi^2 B^{\mathfrak{m}}\left(\frac{t}{\xi^2}; 1, \frac{T}{T_c^{\mathfrak{m}}}, 1\right) \quad (\mathrm{G13})$$

However, the limit $T \to 0$ cannot be taken by candidly replacing $\frac{T}{T_c^{\mathfrak{m}}}$ by 0 in (G13). This would lead to $A_{\mathrm{RM}}^{\mathfrak{m}}|_{(T \ll T_c^{\mathfrak{m}})} = \xi^{-2/3}$ and yield a corresponding zero thorn exponent, but this appears incorrect as we now discuss. Indeed, the term $\frac{T_c^{\mathfrak{m}}}{T}$ in the Hamiltonian in (G12) appears only in front of the disorder term, and not in front of both

contributions as in (72). In terms of path integrals

$$B^{\mathfrak{m}}(t_1; D, T, \xi) =$$

$$\xi^2 \frac{\displaystyle\int_{y(0)=0} \mathcal{D}y \; y(\tfrac{t_1}{\xi})^2 \, e^{-\int_0^{\frac{t_1}{\xi}} dt \, \frac{1}{2}(\partial_t y)^2} \, e^{-\frac{T_c}{T}\int_0^{\frac{t_1}{\xi}} dt \, V_1(t, y(t))}}{\displaystyle\int_{y(0)=0} \mathcal{D}y \; e^{-\int_0^{\frac{t_1}{\xi}} dt \, \frac{1}{2}(\partial_t y)^2} \, e^{-\frac{T_c}{T}\int_0^{\frac{t_1}{\xi}} dt \, V_1(t, y(t))}}$$

$$(G14)$$

the large prefactor $\frac{T_c}{T}$ actually selects the path which minimizes the disorder contribution along the polymer trajectory, and not the full Hamiltonian as in (72), and this path is 'too anomalous' (no elastic constraint enforces it to stay in a bounded region as $T \to 0$). To contend with this singular limit, instead of starting with (G13), one may better work in the physicists convention starting from the scaling construction (56)-(57), where the low T behavior is controlled. One checks that the only possible rescaling of (G13) into a physicists roughness $B(t; c, D, T, \xi)$ satisfying $c = D = \xi = 1$ is:

$$a = \xi \, , \; \widetilde{E} = (\xi T D)^{1/3} \, , \; b = t_{**}^{\mathfrak{m}}(T) = \left(\frac{\xi^5 T^2}{D}\right)^{1/3}$$

$$(G15)$$

$$B^{\mathfrak{m}}(t; D, T, \xi) \equiv B(t; T, D, T, \xi)$$

$$= \xi^2 B\left(\frac{t}{t_{**}^{\mathfrak{m}}(T)}; 1, 1, \frac{T}{(\xi T D)^{1/3}}, 1\right) \quad (G16)$$

This rescaling is similar in spirit to the rescaling $y = p\bar{y}$ in (G9) for the saddle-point asymptotics study of $p!$: it allows to find the optimal path $y(t)$ at the correct scale in the large parameter $\frac{T_c^{\mathfrak{m}}}{T}$ encountered in (G13). The limit $T \to 0$ in the mathematician's $B^{\mathfrak{m}}(t; D, T, \xi)$ coincides with the limit $T \to 0$ in the physicist's roughness of (G16) since $\frac{T}{(\xi T D)^{\frac{1}{3}}} \xrightarrow{T \to 0} 0$. One reads from (G16) at asymptotically large time, according to the known results $\zeta_{\mathrm{RM}} = 2/3$:

$$B^{\mathfrak{m}}(t; D, T, \xi) \overset{t \to \infty}{\sim} \xi^2 A_{\mathrm{RM}}\left(1, 1, \frac{T}{(\xi T D)^{1/3}}, 1\right) \left[\frac{t}{t_{**}^{\mathfrak{m}}(T)}\right]^{2\zeta_{\mathrm{RM}}}$$

$$(G17)$$

In the low-temperature regime ($T \ll T_c^{\mathfrak{m}}$) the physicist's $A_{\mathrm{RM}}\left(1, 1, \frac{T}{(\xi T D)^{1/3}}, 1\right)$ remains finite and goes to a T-independent finite constant in the limit $T \to 0$, as discussed previously in Sec. III D. This finally yields

$$A_{\mathrm{RM}}^{\mathfrak{m}}(D, T, \xi) \overset{(T \ll T_c^{\mathfrak{m}})}{=} \left(\frac{D^2}{T^4 \xi}\right)^{\frac{2}{9}}$$

$$(G18)$$

At low temperature, the mathematician's thorn exponent þ is thus *non-zero*: $\text{þ}_{\mathrm{RM}}^{\mathfrak{m}}|_{(T \ll T_c^{\mathfrak{m}})} = -\frac{4}{9}$.

Appendix H: Set of parameters for the numerical simulations

We have listed thereafter the parameters of the numerical study presented throughout Sec. IV, and initially defined in Sec. IV A.

The discretization grids for the generation of the random potential and for the recording of the data are fixed once and for all to the following values for all the computations (the last three parameters are respectively the number of points for the linear grid in t, the logarithmic grid in t and the linear grid in y as defined in Fig. 4):

D^{grid}	ξ_t^{grid}	ξ_y^{grid}	nbptlint	nbptlogt	nbptliny
4	1	2	80	80	100

The following sets of data have been generated, with the elastic constant being fixed at $c = 1$ and at different temperatures T. The number of configurations 'NconfV' per data set have fluctuated as a compromise between the convergence of the disorder average and a reasonable computation time, as already mentioned in Sec. IV A. The first column gathers the sets used for the study of $\bar{R}(t, y)$, $\widetilde{D}_t$ and $\widetilde{\xi}_t$, whereas the second column corresponds to the additional sets which explore larger 'times' $t < t_m$ and have thus been used for the study of the roughness $B(t)$:

no	T	t_m	y_m	NconfV	t_m	y_m	NconfV
1	0.35	40	50	572			
2	0.4	40	50	1092			
3	0.5	40	50	728			
4	0.55	40	50	540			
5	0.6	40	50	654			
6	0.7	40	50	1281			
7	0.8	40	50	2665			
8	0.9	40	50	900			
9	1	40	50	1350			
10	1.1	40	50	1040	100	70	518
11	1.35	40	50	1050	300	60	390
12	1.5	40	50	1435	200	80	1600
13	1.6	40	50	1600			
14	1.8	40	50	1000	800	160	159
15	2	40	50	1750			
16	2.25	40	50	1300			
17	2.5	40	50	1900			
18	2.75	40	50	1000			
19	3	40	50	2300			
20	3.2	40	50	1000			
21	3.5	40	50	1825			
22	4	40	50	1100			
23	6	40	50	900	80	50	280

Appendix I: Effective correlator of a 2D cubic-splined microscopic disorder

As described in Sec. IV, a given configuration of the microscopic disorder $V(t,y)$ is generated first by picking up a set of random numbers $\{V_j\}$ on a grid of spacing $\left\{\xi_t^{\rm grid}, \xi_y^{\rm grid}\right\}$ with a normal distribution of variance $D^{\rm grid}$, and then by interpolating between the grid points with a 2D cubic spline (cf. Fig. 22 *top*).

In the reduced case of a 1D cubic spline between a set of points at a fixed position t on the grid, it is possible to determine analytically the effective correlator of the 1D cubic-splined random potential with a normalized function $R_{\xi_y}^{\rm CubicS}(y)$ (cf. (1)). For the 2D spline we then assume that the effective two-point disorder correlator is given by the translational-invariant:

$$\overline{V(t,y)V(0,0)} = D \cdot R_{\xi_t}^{\rm CubicS}(t) \cdot R_{\xi_y}^{\rm CubicS}(y) \qquad (\mathrm{I1})$$

with $\xi_t = \xi_t^{\rm grid}$ and $\xi_y = \xi_y^{\rm grid}$ by construction, and because of the passage from the discretized y_j to the continuous variable y an amplitude $D = D^{\rm grid}\xi_t^{\rm grid}\xi_y^{\rm grid}$.

In practice, for $2n+1$ points indexed by $j = -n,\ldots,n$ on a grid of spacing ξ, a random value V_j is attached on each site $y_j = j\xi$ of the grid following the statistical distribution $\overline{V_j} = 0$ and $\overline{V_j V_{j'}} = \delta_{jj'}$. A cubic spline of $\{V_j\}_{-n\leq j\leq n}$ is a function $V(y)$ which is a cubic polynomial on each lattice segment $y \in [y_j, y_{j+1}]$, continuous on each lattice site y_j and with its first and second derivatives also continuous at $y = y_j$. Combining the equations of the cubic-splined parameters for a given set $\{V_j\}$ and the disorder average over those possible sets, we obtain the following *symmetric* effective correlator in the limit of $n \to \infty$:

$$R_\xi^{\rm CubicS}(0 \leq y \leq \xi)$$
$$= -\frac{1}{\xi^4}(y-\xi)\left[(4-3\sqrt{3})y^2 + \xi y + \xi^2\right] \qquad (\mathrm{I2})$$
$$R_\xi^{\rm CubicS}(y_j \leq y \leq y_{j+1})$$
$$= -\frac{3}{\xi^4}(y-y_j)(y-y_{j+1})\left(\sqrt{3}-2\right)^j \qquad (\mathrm{I3})$$
$$\times \left[y - y_{j-1} - \sqrt{3}(y-y_j)\right]$$

where there is a distinction between the central segment $0 \leq y \leq \xi$ which contains the auto-correlation

$$R_\xi^{\rm CubicS}(y = y_{j=0}) = \overline{V_0^2} = \overline{V_j^2} = 1$$

and the other segments $y_j \leq y \leq y_{j+1}$ $(j = 1\ldots n)$ with oscillations constrained by the cancellation at $y = y_{j\neq j}$

$$R_\xi^{\rm CubicS}(y = y_{j\neq 0}) = \overline{V_0 V_{j\neq 0}} = 0$$

Note that this correlator has been obtained exactly by averaging over disorder the cubic splines, whose coefficients depend linearly in the random potential and thus allow an analytical computation of this average.
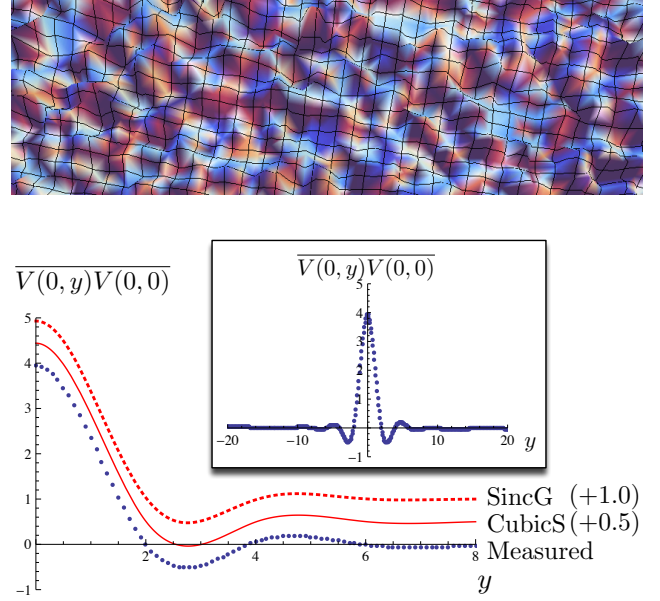

FIG. 22. (Color online) *Top:* Visualization of a single disorder configuration $V(t,y)$; the mesh accounts for the grid $\{y_j\}$, and fluctuates smoothly. *Bottom:* Graph of the numerically-measured effective-1D cubic-splined disorder correlator (blue), with the 'SincG' and 'CubicS' (red, respectively dashed and continuous) superimposed with a slight translation for more visibility. *Inset:* Full effective disorder correlator at fixed $t = 0$, computed over $10'000$ disorder configurations with $D^{\rm grid} = 4$, $\xi_y^{\rm grid} = 2$ and $\xi_t^{\rm grid} = 1$.

For the microscopic disorder correlator (I1) the function R_ξ is thus exactly known, but it is not the case for the effective disorder $\overline{\eta(t,y)\eta(0,0)} = \widetilde{D} \cdot R_{\tilde{\xi}}(y)$. As explained in Sec. IV we try nevertheless to extract the effective parameters at fixed time $\left\{\widetilde{D}, \tilde{\xi}\right\}$ with three different fitting functions normalized to 1: a Gaussian (88) ('Gauss'), a sinus cardinal with a Gaussian envelope (89) ('SincG') and the exact cubic-spline correlator (I2)-(I3) ('CubicS'). The comparison between those three options accounts for a consistency check for the determination of the effective parameters via the stability of the function. Having first tested this procedure on $\overline{V(t,y)V(0,0)}$ (I1), by fitting it separately at fixed time $t = 0$ *versus* at fixed position $y = 0$:

$$\overline{V(t,0)V(0,0)} = \left[D \cdot R_{\xi_y}(0)\right] \cdot R_{\xi_t}(t) \propto R_{\xi_t}(t)$$
$$\overline{V(0,y)V(0,0)} = \left[D \cdot R_{\xi_t}(0)\right] \cdot R_{\xi_y}(y) \propto R_{\xi_y}(y) \qquad (\mathrm{I4})$$

we summarize thereafter the values obtained for the amplitude D and the correlation lengths $\xi_{t,y}$ with respect to the grid parameters (those are kept at fixed value throughout all our computations). The errors are provided by the nonlinear-regression procedure on a correlator obtained over $10'000$ disorder configurations:

	D	ξ_y	ξ_t	$R_1(0)$
Grid	4	2	1	-
Gauss	10.08 ± 0.08	0.625 ± 0.005	0.312 ± 0.003	$\frac{1}{\sqrt{4\pi}}$
SincG	8.04 ± 0.02	2.020 ± 0.004	1.012 ± 0.002	$\frac{1}{\mathrm{Erf}(\pi)}$
CubicS	7.95 ± 0.02	2.006 ± 0.004	1.005 ± 0.002	1

As we can check both in this table and visually in Fig. 22 (*bottom*), the sinus cardinal R^{SincG} catches the main phenomenological features of the exact R^{CubicS}, *i.e.* the amplitude of the central peak and the position of the first oscillation, and keeps satisfied the relations $\xi_{t,y} = \xi_{t,y}^{\mathrm{grid}}$ and $D = D^{\mathrm{grid}}\xi_t^{\mathrm{grid}}\xi_y^{\mathrm{grid}}$.

As for the Gaussian fit, it overestimates the amplitude of the peak and underestimates its typical variance. For the latter it is simply due to the geometrical definitions of the parameter ξ proper to each of these functions, and which can be merged up to a numerical constant ($\xi^{\mathrm{CubicS}}/\xi^{\mathrm{Gauss}} \approx 3.6$). For the first, it stems from the fact that a normalized Gaussian function is used to fit a normalized function which has negative contributions: the integral of the central peak has thus an unnormalized integral larger than 1, and fitting it by a Gaussian naturally yields a larger corresponding amplitude ($D^{\mathrm{CubicS}}/D^{\mathrm{Gauss}} \approx 0.80$). This discrepancy will actually be present in all the similar fitting procedure in Sec. IV.

* Elisabeth.Agoritsas@unige.ch
[1] S. Lemerle, J. Ferré, C. Chappert, V. Mathet, T. Giamarchi, and P. Le Doussal, Phys. Rev. Lett. **80**, 849 (1998).
[2] V. Repain, M. Bauer, J.-P. Jamet, J. Ferré, A. Mougin, C. Chappert, and H. Bernas, Europhysics Letters **68**, 460 (2004).
[3] P. J. Metaxas, J. P. Jamet, A. Mougin, M. Cormier, J. Ferré, V. Baltz, B. Rodmacq, B. Dieny, and R. L. Stamps, Phys. Rev. Lett. **99**, 217208 (2007).
[4] T. Tybell, P. Paruch, T. Giamarchi, and J.-M. Triscone, Phys. Rev. Lett. **89**, 097601 (2002).
[5] P. Paruch, T. Giamarchi, and J.-M. Triscone, Phys. Rev. Lett. **94**, 197601 (2005).
[6] N. A. Pertsev, D. A. Kiselev, I. K. Bdikin, M. Kosec, and A. L. Kholkin, Journal of Applied Physics **110**, 052001 (2011).
[7] S. Santucci, K. J. Måløy, A. Delaplace, J. Mathiesen, A. Hansen, J. O. Haavig Bakke, J. Schmittbuhl, L. Vanel, and P. Ray, Phys. Rev. E **75**, 016104 (2007).
[8] M. Alava and K. Niskanen, Rep. Prog. Phys. **69**, 669 (2006).
[9] M. Alava, M. Dubé, and M. Rost, Advances in Physics **53**, 83 (2004).
[10] S. Santucci, R. Planet, K. J. Måløy, and J. Ortín, Europhysics Letters **94**, 46005 (2011).
[11] E. Agoritsas, V. Lecomte, and T. Giamarchi, Physica B: Condensed Matter **407**, 1725 (2012).
[12] M. Kardar, G. Parisi, and Y.-C. Zhang, Phys. Rev. Lett. **56**, 889 (1986).
[13] J. Krug, Advances in Physics **46**, 139 (1997).
[14] I. Corwin, Random Matrices: Theory and Applications **1**, 1130001 (2012).
[15] H. Spohn, Physica A **369**, 71 (2006).
[16] T. Kriecherbauer and J. Krug, Journal of Physics A: Mathematical and Theoertical **43**, 403001 (2010).
[17] T. Sasamoto and H. Spohn, Journal of Statistical Mechanics: Theory and Experiment **2010**, P11013 (2010).
[18] G. Amir, I. Corwin, and J. Quastel, Communications on Pure and Applied Mathematics **64**, 466 (2011).
[19] A. Borodin, I. Corwin, and P. Ferrari, "Free energy fluctuations for directed polymers in random media in 1+1 dimension," arXiv:1204.1024v1 [math.PR] (2012).
[20] K. Johansson, Communications in Mathematical Physics **209**, 437 (2000).
[21] M. Prähofer and H. Spohn, Phys. Rev. Lett. **84**, 4882 (2000).
[22] D. Forster, D. R. Nelson, and M. J. Stephen, Phys. Rev. A **16**, 732 (1977).
[23] T. Halpin-Healy and Y.-C. Zhang, Physics Reports **254**, 215 (1995).
[24] J. Krug and H. Spohn, "Solids far from equilibrium," (Cambridge University Press, 1991) Chap. Kinetic roughening of growing surfaces, p. 479.
[25] M. Kulkarni and A. Lamacraft, "From GPE to KPZ: finite temperature dynamical structure factor of the 1D Bose gas," arXiv:1201.6363v1 [cond-mat.quant-gas] (2012).
[26] J. Rambeau and G. Schehr, Europhysics Letters **91**, 60006 (2010).
[27] P. J. Forrester, S. N. Majumdar, and G. Schehr, Nuclear Physics B **844**, 500 (2011).
[28] M. Kardar, Nuclear Physics B **290**, 582 (1987).
[29] D. A. Huse, C. L. Henley, and D. S. Fisher, Phys. Rev. Lett. **55**, 2924 (1985).
[30] M. Balázs, J. Quastel, and T. Seppäläinen, J. Amer. Math. Soc. **24**, 683 (2011).
[31] S. Bustingorry, P. Le Doussal, and A. Rosso, Phys. Rev. B **82**, 140201 (2010).
[32] L. Balents and D. S. Fisher, Phys. Rev. B **48**, 5949 (1993).
[33] P. Chauve, T. Giamarchi, and P. Le Doussal, Phys. Rev. B **62**, 6241 (2000).
[34] E. Agoritsas, V. Lecomte, and T. Giamarchi, Phys. Rev. B **82**, 184207 (2010).
[35] P. Le Doussal, K. J. Wiese, S. Moulinet, and E. Rolley, Europhysics Letters **87**, 56001 (2009).
[36] P. Le Doussal, A. A. Middleton, and K. J. Wiese, Phys. Rev. E **79**, 050101 (2009).
[37] P. Le Doussal and K. J. Wiese, Phys. Rev. E **79**, 051106 (2009).
[38] S. Brazovskii and T. Nattermann, Advances in Physics **53**, 177 (2004).
[39] T. Alberts, K. Khanin, and J. Quastel, "The continuum directed random polymer," arXiv:1202.4403v1 [math.PR] (2012).
[40] T. Halpin-Healy, Phys. Rev. A **44**, R3415 (1991).
[41] G. Zumofen, J. Klafter, and A. Blumen, Phys. Rev. A **45**, 7624 (1992).
[42] Y. Y. Goldschmidt and T. Blum, Phys. Rev. E **47**, R2979 (1993).
[43] Y. Y. Goldschmidt and T. Blum, Phys. Rev. E **48**, 161

(1993).

[44] A. I. Larkin, Sov. Phys. JETP **31**, 784 (1970).

[45] M. Mézard and G. Parisi, Journal de Physique I **2**, 2231 (1992).

[46] E. Agoritsas, S. Bustingorry, V. Lecomte, G. Schehr, and T. Giamarchi, "Finite-temperature and finite-time scaling of the directed polymer free-energy with respect to its geometrical fluctuations," (accepted for publication in Phys. Rev. E) (2012).

[47] P. Le Doussal and K. J. Wiese, Phys. Rev. E **72**, 035101 (2005).

[48] K. J. Wiese and P. L. Doussal, Markov Processes Relat. Fields **13**, 777 (2007).

[49] R. P. Feynman, Rev. Mod. Phys. **20**, 367 (1948).

[50] M. Kac, Trans. Amer. Math. Soc. **65**, 1 (1949).

[51] M. Kardar, *Statistical Physics of Fields* (Cambridge University Press, 2007).

[52] L. Bertini and N. Cancrini, Journal of Statistical Physics **78**, 1377 (1995).

[53] L. Bertini and G. Giacomin, Comm. Math. Phys **183**, 571 (1997).

[54] P. Calabrese, P. Le Doussal, and A. Rosso, Europhysics Letters **90**, 20002 (2010).

[55] V. Dotsenko and B. Klumov, Journal of Statistical Mechanics: Theory and Experiment , P03022 (2010).

[56] T. Sasamoto and H. Spohn, Nuclear Physics B **834**, 523 (2010).

[57] V. Dotsenko, Europhysics Letters **90**, 20003 (2010).

[58] C. A. Tracy and H. Widom, Communications in Mathematical Physics **159**, 151 (1994).

[59] M. Prähofer and H. Spohn, Journal of Statistical Physics **108**, 1071 (2002).

[60] T. Nattermann and W. Renz, Phys. Rev. B **38**, 5184 (1988).

[61] M. Kardar, Phys. Rev. Lett. **55**, 2923 (1985).

[62] A. B. Kolton, A. Rosso, and T. Giamarchi, Phys. Rev. Lett. **94**, 047002 (2005).

[63] Mathematica tutorial for the numerical integration of differential equations: http://reference.wolfram.com/mathematica/tutorial/NDSolvePDE.html.

[64] D. S. Fisher, Phys. Rev. Lett. **56**, 1964 (1986).

[65] T. Gueudré, P. L. Doussal, A. Rosso, A. Henry, and P. Calabrese, "Short time growth of a KPZ interface with flat initial conditions," arXiv:1207.7305v1 [cond-mat.stat-mech] (2012).

[66] K. A. Takeuchi and M. Sano, Phys. Rev. Lett. **104**, 230601 (2010).

[67] K. A. Takeuchi, M. Sano, T. Sasamoto, and H. Spohn, Scientific Reports **1**, 34 (2011).

[68] K. A. Takeuchi and M. Sano, Journal of Statistical Physics **147**, 853 (2012).

[69] S. Bustingorry, A. B. Kolton, and T. Giamarchi, Phys. Rev. B **85**, 214416 (2012).

[70] J. Candia and E. V. Albano, "Far-from-equilibrium growth of thin films in a temperature gradient," arXiv:1207.3559v1 [cond-mat.stat-mech] (2012).

[71] M. Mézard and G. Parisi, Journal de Physique I **1**, 809 (1991).

[72] D. S. Fisher and D. A. Huse, Phys. Rev. B **43**, 10728 (1991).

[73] T. Hwa and D. S. Fisher, Phys. Rev. B **49**, 3136 (1994).

[74] P. Le Doussal and C. Monthus, Physica A **317**, 140 (2003).

[75] A. Vasiliev, *Functional methods in quantum field theory and statistical physics* (Gordon and Breach Science Publishers, Amsterdam, 1998).

[76] This means that one can replace in averages *every* $\eta(-y)$ by $-\eta(y)$, simultaneously with every $\eta'(-y)$ by $\eta'(y)$, ... every $\eta^{(k)}(-y)$ by $(-1)^{k+1}\eta^{(k)}(y)$, ... without changing the result.

[77] Again, the equivalent is logarithmic: $\log \frac{p!}{p^{p+1}} \stackrel{p\to\infty}{\sim} -p$. The real equivalent $p! \stackrel{p\to\infty}{\sim} \sqrt{2\pi p}\,(p/e)^p$ is obtained after integration of fluctuations around the saddle.